Portland State University

PDXScholar

Compositional and mineralogical relationships between mafic inclusions and host lavas as key to andesite petrogenesis at Mount Hood Volcano, Oregon

Melinda Michelle Woods
Portland State University

THESIS APPROVAL
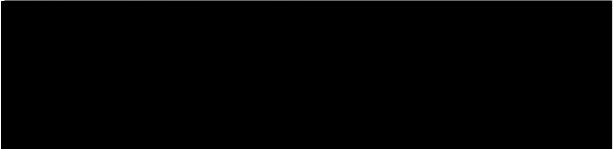
The abstract and thesis of Melinda Michelle Woods for the Master of Science in Geology were presented July 7, 2004, and accepted by the thesis committee and the department.

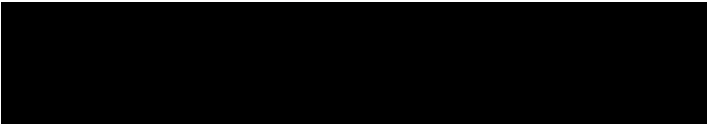COMMITTEE APPROVALS:

Martin J. Streck, Chair

Alex M. Ruzicka

Cynthia A. Gardner

Dirk Iwata-Reuyl
Representative of the Office of Graduate Studies

DEPARTMENT APPROVAL

Michael L. Cummings, Chair
Department of Geology

ABSTRACT

An abstract of the thesis of Melinda Michelle Woods for the Master of Science in Geology presented July 7, 2004.

Title: Compositional and Mineralogical Relationships Between Mafic Inclusions and Host Lavas as Key to Andesite Petrogenesis at Mount Hood Volcano, Oregon.

Throughout its eruptive history, Mount Hood has produced compositionally similar calc-alkaline andesite as lava flows and domes near the summit and basaltic andesitic flows from flank vents. Found within the andesite are slightly more mafic inclusions that are compositionally similar to the host andesite (or host lavas); no inclusions were found in the flank lavas. Host lavas and inclusions have the following mineral assemblage: plag + opx ± cpx ± amp + oxides. Flank lava mineralogy is similar to the inclusions and host lavas, but since they are more mafic they contain olivine instead of amphibole. Average silica content among samples analyzed ranges from 57.6 to 62.7 weight percent; however the incompatible trace element composition is more variable at lower silica contents and becomes less variable at higher silica contents. In terms of incompatible trace element composition, the host lavas and inclusions are either depleted (no amp) or enriched (amp ± cpx).

Mineralogy and composition of samples analyzed were used to construct petrogenetic chemical models to determine the origin of the andesites and inclusions. Major petrogenic processes modeled were crystal fractionation, magma mixing, and assimilation fractional crystallization (AFC). Fractional crystallization accounts for

the presence of the phenocrysts; however, the degree of enrichment does not correlate with increasing silica content. Likewise, the AFC process fails to account for the variability of enrichment of incompatible trace elements and most likely provides a negligible role in petrogenesis. However, magma mixing ascertains that the variability in incompatible trace element enrichment may be due to variability in trace element concentration among possible mafic end members. Scatter plots of mafic and silicic lavas erupted during the Pliocene at or in the vicinity of Mount Hood are comparable to the calculated mafic and silicic end members used in the magma mixing model, and mafic lavas erupted during the Pliocene show more variability in incompatible trace element composition than the silicic lavas of the same age. Therefore, formation of Mount Hood andesites and their inclusions is a combination crystal fractionation and magma mixing

COMPOSITIONAL AND MINERALOGICAL RELATIONSHIPS BETWEEN

MAFIC INCLUSIONS AND HOST LAVAS AS KEY TO ANDESITE

PETROGENESIS AT MOUNT HOOD VOLCANO, OREGON

by

MELINDA MICHELLE WOODS

A thesis submitted in partial fulfillment of the
requirements for the degree of

MASTER OF SCIENCE
in
GEOLOGY

Portland State University
2004

TABLE OF CONTENTS

LIST OF TABLES

LIST OF FIGURES

CHAPTER 1 – INTRODUCTION

Geographic and Geologic Background

The Cascade Range is located in the Pacific Northwest region of the United States and it is a volcanic province that has been periodically active since the Middle Eocene. The volcanic province, also known as the Cascades Volcanic Arc, is comprised of the older Western Cascades (Oligocene to Miocene) and to the east and lying parallel to the Western Cascades, the High Cascades (Quaternary). The active volcanic province is approximately 75 km wide in the central portion, narrowing to the north and south and stretches over 1100 km from Mount Meager, British Columbia (Canada) in the north to Mount Lassen, California (USA) in the south (McBirney, 1978; Blakely and Jachens, 1990; Priest, 1990) (Figure 1). The Cascade Volcanic Arc is a continental arc system formed by the
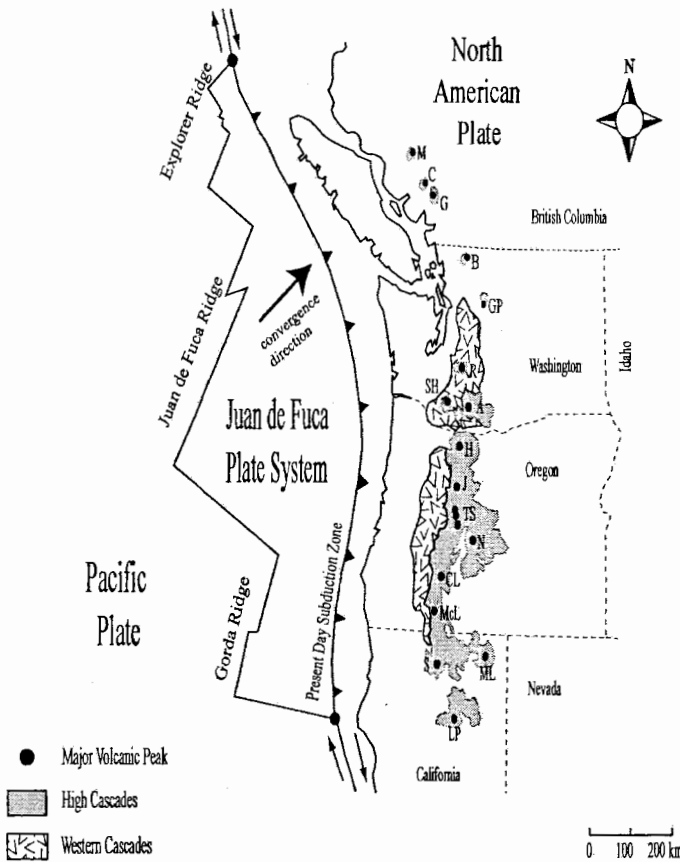
M = Mount Meager; C = Mount Cayley; G = Mount Girabaldi; B = Mount Baker; GP = Glacier Peak; R = Mount Rainier; SH = Mount St. Helens; A = Mount Adams; H = Mount Hood; J = Mount Jefferson; TS = Three Sisters (North Sister, Middle Sister, South Sister); N = Newberry; CL = Crater Lake (Mount Mazama); McL = Mount McLaughlin; S = Mount Shasta; ML = Medicine Lake; LP = Lassen Peak

Figure 1 - Map of the Cascade Volcanic Arc (modified after Winter, 2001).

1

subduction of the Juan de Fuca Plate beneath the North American Plate. The rate of subduction of this micro-plate varies from 3.8 cm/yr to 4.6 cm/yr. The subduction rate is up to 20% faster along British Columbia than along Oregon, and combined with oblique subduction, causes Oregon to rotate in a clockwise direction. The rotation of the region has resulted in the extension in the central Cascade Volcanic Arc and the compression along Washington and British Columbia (Rogers, 1985; Priest, 1990; Wells, 1990).

Sparse evidence of the calc-alkaline volcanism began to appear about 35 to 40 Ma. Outcrops of shallow sub-volcanic intrusions and associated pyroclastic units are found in Washington near the present day High Cascade Range. Outcrops in Oregon extend from the Coast Range well into Central Oregon. The outcrops in the Coast Range are marked by sub-volcanic intrusions, while in the Western Cascades and central Oregon, lava flows, tuffs and volcanic sediments are associated with vent complexes and shallow stocks, sills and dikes (McBirney, 1978). It is presumed that early volcanism was associated with the subduction of the Farallon Plate beneath the North American Plate. Approximately 30 Ma the Farallon Plate was consumed along the coast of California causing the San Andreas Fault to form. The fault progressively grew as more of the Farallon Plate was consumed. The remaining northern part of the Farallon Plate is called the Juan de Fuca Plate and the remaining southern part of the Farallon Plate is called the Cocos Plate. The intensity of calc-alkaline volcanism began to increase 30-20 Ma (McBirney, 1978; Rogers, 1985; Priest, 1990; Wells, 1990). The Western Cascades were at their pinnacle about 20 Ma erupting tholeiitic and calc-alkaline lava flows along with the emplacement of intrusions ranging in

2

composition from basalt to rhyolite and gabbro to granodiorite, respectively. This older volcanic arc may have resembled the High Cascades, although lower in elevation. The Middle to Late Miocene is characterized by sharply decreasing igneous activity in the volcanic province. The activity began to wane as a result of regional tectonic uplift and folding of the volcanic arc. The tectonic activity may have lasted as long as 4 my, and for a period of 10 my there was essentially very little volcanic activity (McBirney, 1978; Priest, 1990; Taylor, 1990). It was during the Late Miocene to Early Pliocene (~5 Ma) that an insurgence of volcanic activity began, with the axis of volcanism parallel and to the east of the axis for the Western Cascades. Coinciding with the onslaught of renewed volcanism, a graben in the central part of the arc began to open up as a result of the

SH = Mount St. Helens; A = Mount Adams; H = Mount Hood;
J = Mount Jefferson; TS = The Three Sisters

Figure 2 - Map view of the Central Cascades Graben showing associated volcanism (modified after Conrey et al., 1997).
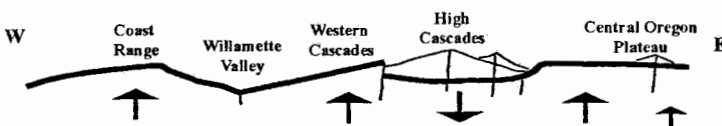
Figure 3 - Cross-section of the Cascade Range showing the tectonic down drop associated with the graben (modified after McBirney, 1978).

3

extension associated with the oblique subduction of the Juan de Fuca Plate (Blakely and Jachens, 1990). The maximum depth of the graben is located in the north central Cascades between Three Sisters and Mount Jefferson, and has had a direct influence on the types and amounts of lava erupted. There is a concentration of volcanic vents within the graben and the andesite volcanoes here are underlain by basaltic shield volcanoes, whereas the volcanoes in northern Washington and British Columbia are not underlain by basaltic outpourings and are fewer in number (Rogers, 1985). Since the Pliocene, there has been continuous volcanic activity in the Cascades Volcanic Arc, and it was during the Quaternary Era that the High Cascades or the modern day volcanic province began to produce the peaks were see today. Volcanic products of the High Cascades are generally calc-alkaline basaltic andesites to dacite with infrequent rhyolite. Several major eruptions have occurred during the Holocene, including the cataclysmic eruption of Mount Mazama (~7000 years BP) leading to the formation of Crater Lake, Mount Rainier (2300 years BP and 1000 years BP), Mount Hood (~ 200 years BP (Old Maid Eruption)) and Mount Saint Helens (~200 BP and May 18, 1980).

Geologic Background of Mount Hood

Mount Hood is located in the central region of the Cascade Volcanic Arc and is the highest and northernmost peak in Oregon. The volcano is built on top of lavas ranging in age from Miocene (Columbia River Basalt group, ~17-15 Ma) to Pliocene (~4.5-2 Ma). In comparison to the Middle to Late Miocene during which volcanic activity appears sporadic due to tectonic uplift, there was a major pulse of mafic

4

activity during the Pleistocene in the central region of the volcanic arc. The outpouring of these lavas is generally believed to be associated with extensional forces responsible for the graben formation. It is believed that the construction of the cone began no later than ~730 ka ago (Conrey et al., 1996; Gray et al., 1996).

Mount Hood consists of compositionally similar calc-alkaline andesites (SiO_2=57-63 wt %) which mostly erupted during dome building and dome collapse events emanating from the central vent. Concurrently with the eruption of the andesites, several satellite flank vents erupted basaltic andesites (SiO_2=52-57 wt %) (White, 1980; Wise, 1980; Cribb and Barton, 1997; Scott et al., 1997). The eruptive history has been divided into five eruptive periods; Main Stage period (~700-29 ka), Polallie period (15-12 ka), Timberline period (1.8-1.5 ka), Old Maid period (~200 years BP) and the Pumice Eruption (1859-1865 AD and possibly 1907 AD) (Wise, 1969; White, 1980; Cribb and Barton, 1997; Scott et al., 1997, 2003). The Main Stage period encompasses the bulk of the eruptive history of the volcano.` Recently, scientists at the United States Geological Survey (USGS) have leaned towards abandoning the term "Main Stage" as an eruptive period (C. Gardner, 2003 personal communication); instead they prefer to refer to the time $\geq$ 15 ka as the pre-Polallie or pre-glacial period. The hiatus between the Main Stage and Polallie periods has been defined as the Fraser Glaciation which occurred during the last global ice age reaching a maximum at about 18 ka (Wise, 1969; Crandell, 1980; White, 1980). Both the Polallie and Timberline eruptive periods are characterized by lava domes, pyroclastic flows, tephra and lahar deposits (Wise, 1969; Scott et al., 1997, 2003). The most recent eruptive periods of Mount Hood have occurred during historical times. The

5

Old Maid Eruption occurred about 200 years before present followed by the Pumice Eruption ~60-70 years later. Both eruptions were from the central vent. The Old Maid Eruption was a series of dome building and dome collapse events triggering several lahars flows down the Sandy River. Crater Rock, located on the south flank of the volcano, is the remnant of the dome from that eruption. The Pumice Eruption was very small and the pumice produced during the eruption was localized to the summit area.

Statement of Problem

The lavas flows of Mount Hood are generally light to medium gray and are porphyritic with large plagioclase phenocrysts and typically non-vesicular. In a few cases, the lava flows are reddish in color as seen at Site 0205 (top of the blue chair lift at Mount Hood Meadows Ski Resort) and at Site 0212 (~200-300 meters behind Timberline Lodge), and thus have experienced some oxidation. Many andesitic lava flows from Mount Hood contain magmatic inclusions that are slightly more mafic than the andesitic flows (host lavas), whereas the basaltic andesitic flows (satellite flank flow or flank lavas) do not contain inclusions. The abundance of the inclusions within a lava flow range from ~0.5 to ~ 5 % by volume (visual estimation at outcrop) and are spherical to elliptical ranging in size from ~2 cm to ~15 cm in diameter, light gray to red, aphyric to porphyritic and vesicular. The color of the inclusions is independent of the color of the host lava. In other words, gray host lavas will not contain only gray inclusions, nor would red host lavas contain only red inclusions. Gray inclusions have been observed in red lavas and vice versa.

Mafic inclusions may either represent chilled blobs of magma that were chilled when hotter magma came into contact with cooler magma, or the inclusions could represent cumulates. Cumulates form as minerals are fractionated out of the melt and accumulate along the walls and floor of the magma chamber. Cumulates are characterized by having well defined crystals with little or no interstitial material (e.g. Wiebe et al., 1997). During an eruption, cumulates can be plucked from the chamber walls and floor and are in this way incorporated into the magma. On the other hand, if inclusions are quenched blobs of magma, then they record magma mixing. Magma mixing, the mixing of two magmas, can occur either when a magma chamber experiences influx of a new magma or the chamber undergoes convection. If recharging magma is hotter then inclusions can form by quenching. Inclusions formed by this process are characterized by interstitial glass, quenched crystals, crenulated rims and disequilibrium mineral assemblages (Bacon, 1986). Regardless of their origin, mafic inclusions provide additional petrological data that is typically not provided by the magmas in which the inclusions are found. The existence of mafic inclusions in Mount Hood andesitic lavas has previously been noted (i.e. Trimble, 1963; Wise, 1969; Crandell, 1980; White, 1980; Cribb and Barton, 1997), but they have not been systematically studied, although they may provide important constraints for andesite magma genesis at Mount Hood. Thus a systematic investigation of mafic inclusions from selected sites is the focus of this study.

7

CHAPTER 2 – METHODS

Sample Collection

Samples of andesitic lava flows and their mafic inclusion were collected at six locations around the volcano. In addition, samples of satellite flows that were erupted from vents on the flanks of the main cone were also collected. Flank lavas were sampled with the purpose to compare their mineralogy and chemistry with those of the inclusions and host lavas, and to determine if they play a significant role in the petrogenesis of the inclusions and subsequently that of the host lavas.

Sample locations for inclusion bearing sites include a
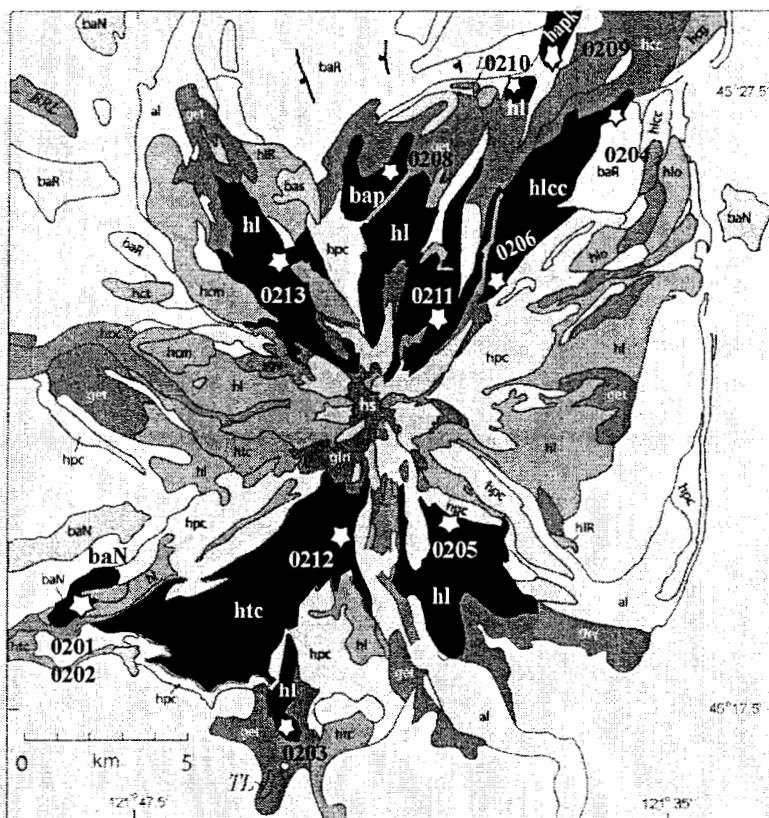
htc - andesite of the Timberline eruptive period (1.5 ka)
bapk - basaltic andesite of Parkdale (7.7 ka)
hpc - andesite of the Polallie eruptive period (13-20 ka)
hl - andesite of main cone (42-44 ka), sites 0205, 0210, 0211, 0213
baN - basaltic andesite of normal polarity (51 ka)
hl - andesite of main cone (121 ka), site 0203
bap - basaltic andesite of Pinnacle Peak (129 ka)
hlcc - basaltic andesite of Cloud Cap (424 ka)

Figure 4 - Geologic map of Mount Hood. The solid black areas indicate the geologic units from which the samples were collected. Sample locations within each geologic unit are designated by the stars and sample site numbers (i.e. 0201). See text for more details on the rock types at the sites. Map used with permission, Scott et al., 2003).

8

road cut along US Highway 26, behind Timberline Lodge (~200-300 m), and Mount Hood Meadows Ski Resort on the southern side of the volcano, and Laurence Lake, Compass Creek and Cathedral Ridge on the northern side. Flank lavas were collected from one site on the south side (Lady Creek) and the remaining flank lavas were collected from the north side of the volcano (Cloud Cap, Pinnacle Peak and the Parkdale Flow).
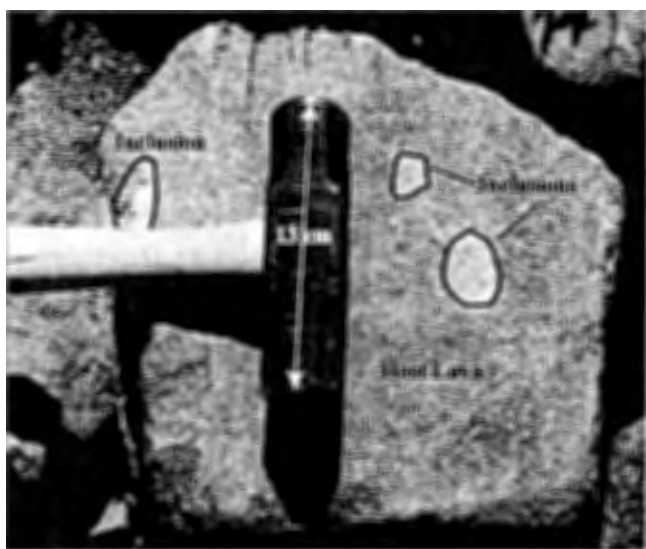
Figure 5 - Inclusions as they appear in host lava. The picture was taken at Laurence Lake (site 0210) by author.

Inclusions were selected based on size, and had to be at least 4-5 cm in diameter and with minimal evidence of weathering. Using a hammer and a chisel, the inclusions were dug out of the host lavas obtaining about 60 grams or more of rock containing little or no weathering surfaces. Samples of the host lavas and flank lavas were collected and the bulk of the weathering surfaces were cleaned off in the field. Field sampling yielded typically a minimum of five inclusions and two host lava. Exceptions were two of the sites which yielded three useable inclusions and one site yielded only two inclusions for analysis. Samples at each inclusion bearing site, along with one representative sample from each of the six flank lavas sampled, were petrographically and chemically analyzed.

Preparation of Samples

Rock samples that were selected for analysis included a clean (without any weathered surfaces) fragment measuring approximately 2 cm by 4 cm set aside for petrographic analysis. The remaining samples were broken down into chips roughly 0.5 cm to 1 cm in diameter. The chips were hand picked, and all pieces containing any weathered surfaces or showed any other unusual signs were discarded. The clean chips were ground into powders for chemical analysis.

Petrography

Inclusion samples were embedded in epoxy, and were sawed in half to expose the desired thin section surface. At this stage, samples were sent to Petrographic International in Canada, and prepared as "polished thin sections". These slides were ready for petrographic analysis and microprobe work. Flank lavas and host lavas samples were cut into billets and were sent to Spectrum Petrographics in Oregon. These samples were prepared as "end user polish" thin sections, and required extra polishing to obtain microprobe-grade thin sections. I started out by using a 6 μm grit compound, and polished the thin section for ten minutes on a piece of felt affixed to a glass plate. The second step was to repeat the first step with a 3 μm grit compound for five minutes. The final step was to polish the slides using a 1 μm grit compound on a disc polisher for five minutes.

The thin sections were analyzed on Leica petrographic microscopes. Detailed assessments of phenocryst to groundmass ratios, textures and mineral assemblages were made. Mineral proportions were estimated by counting the number of phenocrysts per mineral phase, and each mineral phase normalized to the total number

of phenocrysts counted. Grains were considered to be phenocrysts if they were approximately 300 μm in two dimensions. Grain sizes of phenocryst phases are discussed in Chapter 3.

Chemical Analysis

X-ray Fluorescence (XRF)

X-ray fluorescence was conducted at Washington State University (WSU), Pullman, Washington. I prepared the glass beads, and the GeoAnalytical Laboratory at WSU conducted the analysis. Approximately 30 grams of rock chips were ground in a tungsten carbide swing mill for two minutes. Three and a half grams (3.5 g) of the sample was weighed in a plastic mixing jar with 7.0 g of dilithium tetraborate ($Li_2B_4O_7$). A plastic ball was also placed in the jar to assist in mixing of the sample and dilithium tetraborate, which was mixed for ten minutes. The mixed powders were placed into graphite crucibles. The crucibles were then placed into a 1000 °C furnace; fusion took about five minutes. After cooling, the beads were re-ground in a tungsten carbide mill for 35 seconds, and then refused. Excess graphite was cleaned off the flat side of the bead by polishing with 600 grit alumina powder with alcohol. The glass beads were analyzed on a Rigaku 3370 XRF spectrometer with a rhodium (Rh) target run at 50kV/50mA with full vacuum and a 25 mm mask for all elements. Precision of instrumental analysis is presented in Table 1.

Table 1 – Analytical precision for XRF analysis, sample GSP-1, dacite.

Element	Std Dev (Wt %)	Element	Std Dev (ppm)
SiO_2	0.180	Ni	1
Al_2O_3	0.110	Cr	2
TiO_2	0.004	Sc	2
FeO*	0.010	V	5
MnO	0.001	Ba	9
CaO	0.010	Rb	1
MgO	0.100	Sr	1
K_2O	0.090	Zr	1
Na_2O	0.050	Y	1
P_2O_5	0.003	Nb	0.5
		Ga	1
		Cu	2
		Zn	2
		Pb	2
		La	10
		Ce	10
		Th	2

Inductively Coupled Plasma Mass Spectrometry

Inductively Coupled Plasma Mass Spectrometry (ICPMS) was conducted at WSU. I prepared the glass beads, and the GeoAnalytical Laboratory at WSU conducted the analysis. Approximately 15 grams of rock chips were ground in a iron swing mill for two minutes. Two grams (2.0 g) of the sample was weighed in a plastic mixing jar with an equal amount of dilithium tetraborate. A plastic ball was also placed in the jar to assist in mixing of the sample and dilithium tetraborate, which was mixed for ten minutes. The mixed powders are placed into graphite crucibles. The crucibles are placed into a 1000 °C furnace; fusion took about five minutes. Excess graphite is cleaned off the flat side of the bead by polishing with 600 grit alumina powder with alcohol. The Geo Analytical Laboratory staff carried out the remaining portion of the procedure per Knaack et al. (1994). The samples were analyzed on a Sciex Elan model 250 ICP-MS equipped with a Babington nebulizer, water cooled

spray chamber and Brooks mass flow controllers. Samples were introduced into argon

plasma at 1.0 ml/min and plasma power is at 1500 Watts. Analytical precision is

presented in Table 2.

Table 2 –Analytical precision for ICP-MS analysis, Sample AGV-1, andesite.

Element	Std Dev (ppm)	Element	Std Dev (ppm)
Ba	13	Yb	0.03
La	0.49	Lu	0.01
Ce	0.62	Rb	0.7
Pr	0.06	Y	0.29
Nd	0.48	Nb	0.29
Sm	0.15	Cs	0.03
Eu	0.05	Hf	0.07
Gd	0.08	Ta	0.02
Tb	0.01	Pb	0.29
Dy	0.10	Th	0.30
Ho	0.02	U	0..49
Er	0.06	Sr	0.11
Tm	0.01		

Instrumental Neutron Activation Analysis (INNA)

The analysis was conducted by myself at Portland State University (PSU).

Sample powders milled in an iron swing mill (left from WSU) were used for analysis.

Approximately 0.5 to 0.7 g of powder was placed in a small plastic vial and each vial

was sealed shut using a heat source. Samples were irradiated with neutrons for five

hours at a power level of 250 kW in nuclear reactor located at Reed College, Portland,

Oregon. Samples were brought back to PSU for analysis on a EG&G Ortec 92X

Spectrum Master Gamma Ray Detector. Three counting schemes were conducted as

follows: one week after irradiation each sample was counted for 4,000 seconds; two

week after irradiation each sample was counted for 5,000 seconds and four weeks after

irradiation each sample was counted for 30,000 seconds. Analytical precision for the

instrument is listed in Table 3.

13

Table 3 – Analytical precision for INAA analysis, Sample JA2, andesite.

Element	Std Dev%	Element	Std Dev%
Na_2O	1.1	La	1.9
FeO*	3.3	Ce	2.5
Sc	1.7	Nd	6.2
Cr	2.4	Sm	7.6
Co	2.0	Eu	1.1
Ni	8.7	Tb	5.6
Zn	5.6	Yb	7.9
Sb	29.2	Lu	6.0
Rb	92.1	Hf	4.6
Cs	5.7	Ta	3.9
Sr	92.1	Th	3.2
Ba	13.9	U	15.6

Electron Microprobe Analysis

Analysis was conducted by me at Oregon State University, Corvallis, Oregon. Three mineral phases (plagioclase, pyroxene, and amphibole) were analyzed on a Cameca SX50 microprobe with a 1 μm beam. Current levels for each analysis are as follows: plagioclase was analyzed with a sample current of 30 nA at 15 kV; pyroxene was analyzed with a sample current of 50 nA at 15 kV; and amphibole was analyzed with a sample current of 50 nA at 15 kV.

CHAPTER 3 – RESULTS

Lithology and Petrography

Flank Lavas

All of the six collected flank lavas are medium to dark gray, nearly aphyric, with few phenocrysts observable in hand samples, and non-vesicular. Samples 0201 and 0202 were collected in the Lady Creek area of Zigzag Canyon (Figure 4), on the southwestern flanks of Mount Hood. The sample from site 0201 is very dense, dark gray, aphyric, and exhibits flow banding, whereas sample from site 0202 is medium gray and contains about 10% by volume (visual estimation) phenocrysts of plagioclase and pyroxene. Samples from sites 0204 (road cut along Cooper Spur Road) and 0206 (Cloud Cap Inn) are samples of the Cloud Cap flow (northeastern flank, Figure 4) collected at roughly the opposite ends of the flow. Both of the samples are medium gray and non vesicular. Both samples contain about 7-10% by volume phenocrysts, but they differ in that the sample from site 0204 is olivine rich, whereas the sample from site 0206 does not contain phenocrystic olivine. The sample from site 0208 is from a flow that erupted at Pinnacle Peak, a vent located on the northern flank of the main cone. Site 0209 is the Parkdale Flow, which is also on the northern flank (Figure 4) of the main cone, but at a lower elevation in comparison to Pinnacle Peak. The lithology of both of these flows is comparable except that the Pinnacle Peak sample contains about 5% phenocrysts and the Parkdale flow 1-2% phenocrysts.

Microscopic observations of the flank lavas show that they are micro-vesicular and contain small phenocrysts (20-25 vol %), even though they appear nearly aphyric

15

in hand sample, with plagioclase being the dominant phenocryst phase (Figure 6). The phenocryst assemblage was found to be plagioclase (plag) + orthopyroxene (opx) + clinopyroxene (cpx) + oxides (ox) ± olivine (ol). The oxides could belong to minerals either of the magnetite series or the ilmenite series. For the purposes of this study they will be herein referred to as oxides. The groundmass is comprised of plagioclase laths along with small crystals (<200 μm) of either olivine or clinopyroxene. Both minerals have high birefringence, but the crystals were too small for accurate identification.

Although sample 0201 and sample 0202 were collected in the same location (differing outcrops) they may be representatives of two flows. The flow sampled at site 0202 is not a typical flank lava, but rather appears as a possible Mount Hood andesite of undetermined age (personal communication, C. Gardner, 2003). Petrographically, the sample from site 0202 does not resemble samples of the other five flank lavas collected, but closely resembles that of the host lava samples in terms of texture and mineral assemblage (Figure 6).
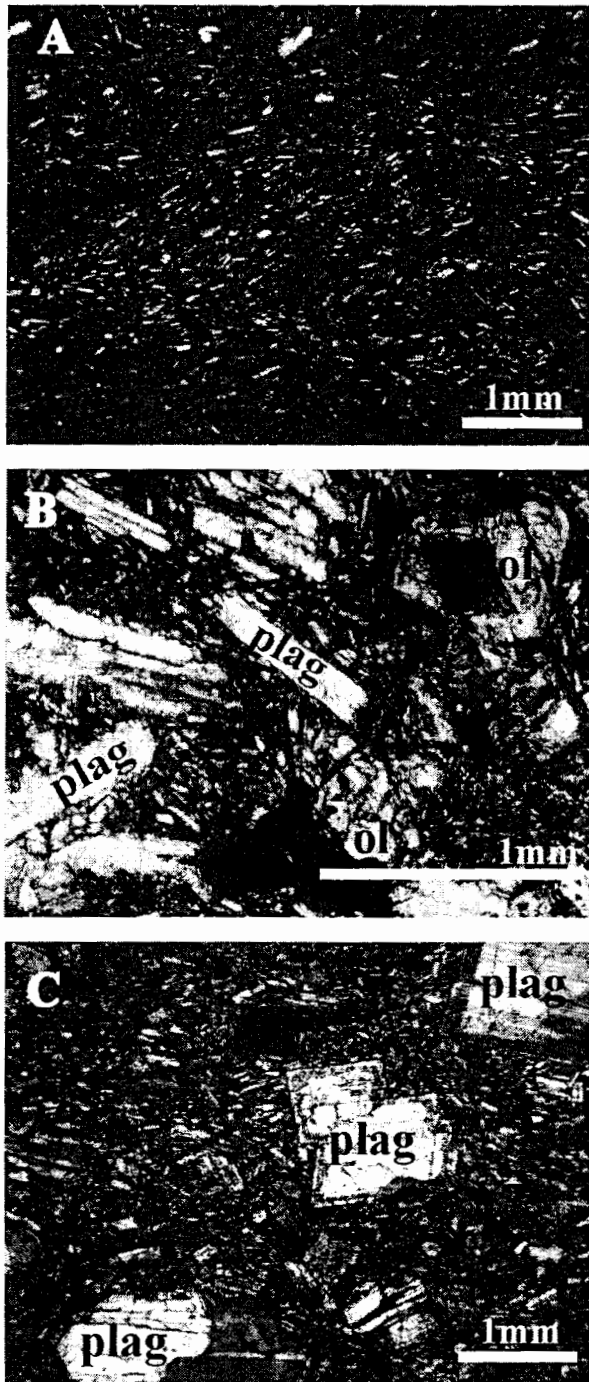
Figure 6 – Examples of flank lavas. (A) The sample from site 0201, a dark dense groundmass with micro-phenocrysts of plagioclase. (B) Sample of site 0204, the texture of this site is typical for the flank lavas. (C) Sample of site 0202, the sample contains fewer phenocrysts, and the groundmass has larger, easily identifiable plagioclase phenocrysts, as opposed to the other flank lavas in which the groundmass is denser, and not easily identifiable. All pictures were taken under crossed polarized light.

17

Host Lavas

The andesitic lava flows which host the mafic inclusions are called the host lavas. The host andesites are light to medium gray, sometimes red, non-vesicular and porphyritic containing approximately 20 vol% phenocrysts (plag + opx ± cpx ± oxides ± amphibole (amp)). The host lavas appear lithologically similar at each sample location.

Host lavas have the following general phenocryst assemblage: plagioclase + orthopyroxene + clinopyroxene + oxides ± amphibole. Based on the absence (or presence) of amphibole, the inclusion-bearing sites can be divided into two groups. In sites 0203 (U.S. Highway 26) and 0205 (Mount Hood Meadows) samples do not contain amphibole, either as phenocrysts nor as groundmass crystals. The groundmass is comprised mostly of plagioclase laths and oxides as well as intermittent clinopyroxene crystals. The groundmass of the host lavas in the other inclusion-bearing sites contain plagioclase laths, oxides, and needle-shaped amphibole crystals. In addition, these sites may also contain amphibole phenocrysts and have very low proportion of clinopryoxene phenocrysts (Table 4).

Inclusions

Inclusions are either gray or red and can be found in many andesitic lavas that are either of the same color or oppositely colored (i.e. a red inclusion in gray host lava and vice versa). Furthermore, inclusions are generally lighter in color than their host lavas due to their high degree of vesicularity. They are phenocryst-poor containing approximately 2-3 vol% phenocrysts (plag + opx ± cpx ± oxides ± amp) and finely

18

vesicular. Regardless of the sample location, all inclusions appear lithologically similar and thus indicate they may have originated in the same manner.

Inclusions have the same phenocryst mineral assemblage as their respective host lavas. Inclusions that are found in samples from sites 0203 and 0203 do not contain any amphibole just as their host lavas do not contain amphibole. Samples of the inclusions from the other inclusion-bearing sites contain varying amounts of amphibole like that of their respective host lavas (Table 4). The inclusion groundmass bears the same mineral composition as the host lavas.

Texturally, the mafic inclusions range from being vesicular to microvesicular with diktytaxitic texture. The degree of porosity is directly related to the mineralogy of the sample. The least vesicular sites, 0203 (U.S. Highway 26) and 0205 (Mount Hood Meadows) are those that do not contain amphibole while the most amphibole-rich site (Laurence Lake) is the most vesicular site (with diktytaxitic texture). The other sites that contain amphibole have degrees of vesicularity that are intermediate. In contrast, the host lavas are non-vesicular (Figure 7).
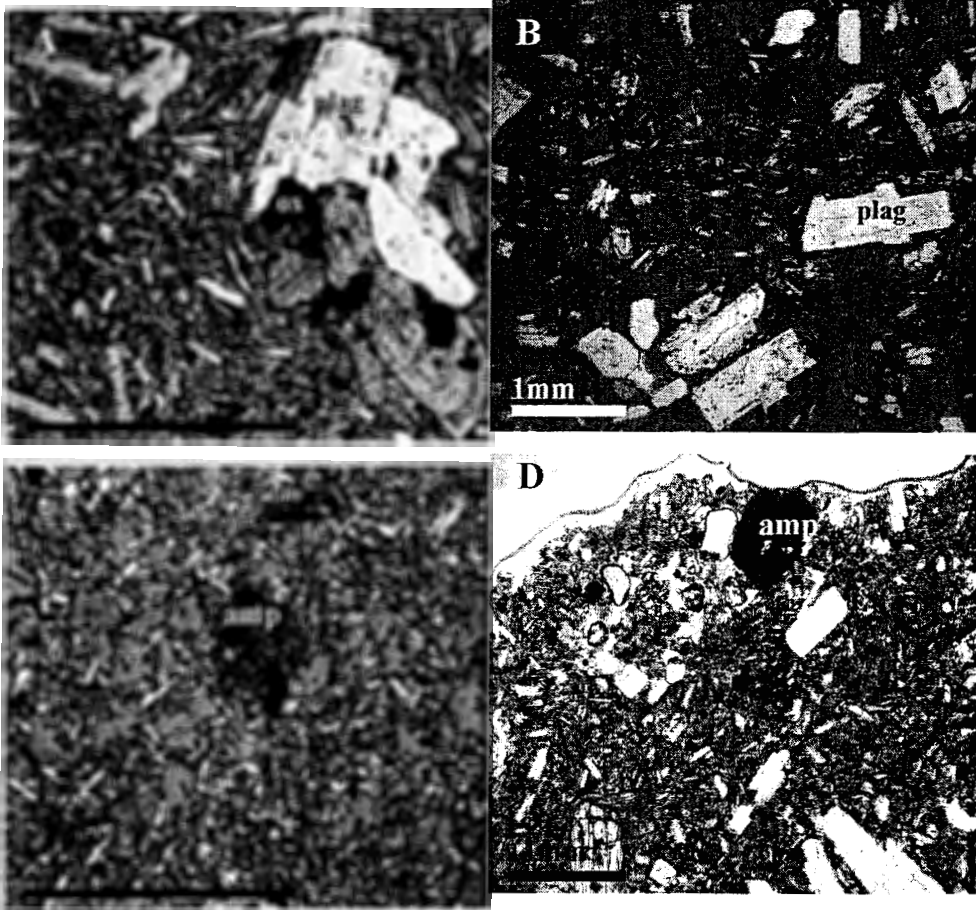
Figure 7 – Examples of inclusion and host lava pairs. (A) An inclusion from site 0205 (Mount Hood Meadows) contains large phenocrysts of plagioclase, pyroxene and oxides within a groundmass of mostly plagioclase laths. (B) A sample of host lava from site 0205, it also contains the same phenocrysts, although the picture above only depicts plagioclase. (C) An inclusion from site 0210, Laurence Lake. The inclusion exhibits diktytaxitic texture, the most extreme vesicularity seen in the samples (v = vesicle). (D) Host lava from site 0210 is similar to that of picture B. Shown in both C and D are large amphibole phenocrysts (amp). All pictures were taken under partially crossed polarized light.

20

Table 4 - Summary of estimated normalized modal phenocryst proportions; for mafic inclusions and host lavas, modal percentages represent averages. # = number of samples. P:GR = phenocryst to groundmass ratio.

Site #	Location	#	P:GR	SiO$_2$ (wt %)	Plag	Opx	Cpx	Amp	Ol	Ox
FLANK LAVAS										
0201	Lady Creek	1	2:98	56.9	65%	2%	2%	0%	0%	31%
0202	Lady Creek	1	15:85	59.8	56%	9%	18%	0%	1%	16%
0204	Cooper Spur Rd	1	15:85	55.8	69%	3%	9%	0%	12%	7%
0206	Cloud Cap Inn	1	35:65	59.0	77%	3%	8%	0%	0%	12%
0208	Pinnacle Peak	1	30:70	56.0	74%	2%	4%	0%	8%	12%
0209	Parkdale Flow	1	20:80	58.1	63%	1%	10%	0%	7%	18%
MAFIC INCLUSIONS										
0203	U.S. Highway 26	4	5:95	58.1	62%	14%	8%	0%	0%	16%
0205	Mt Hood Meadows	6	7:93	58.3	62%	14%	7%	0%	0%	17%
0210	Laurence Lake	5	4:96	57.7	36%	18%	2%	31%	0%	13%
0211	Compass Creek	3	7:93	59.5	40%	35%	2%	13%	0%	11%
0212	Timberline Lodge	3	6:94	59.4	40%	29%	1%	24%	0%	7%
0213	Cathedral Ridge	2	5:95	60.2	38%	25%	6%	15%	0%	16%
HOST LAVAS										
0203	U.S. Highway 26	3	25:75	61.5	68%	10%	8%	0%	0%	14%
0205	Mt Hood Meadows	4	28:72	60.6	74%	6%	4%	0%	0%	16%
0210	Laurence Lake	2	23:77	62.0	58%	19%	0%	17%	0%	5%
0211	Compass Creek	2	25:75	61.7	51%	22%	0%	16%	0%	11%
0212	Timberline Lodge	2	26:74	63.4	55%	17%	0%	18%	0%	11%
0213	Cathedral Ridge	2	27:73	62.3	50%	29%	0%	7%	0%	13%

Origin of the Inclusions

The origin of the inclusions is of paramount importance if we want to better understand the petrogenesis of the andesite. The inclusions in the andesitic lava flows of Mount Hood represent a more mafic magmatic component, yet the mineralogy between the inclusions and the host lavas are similar. The inclusions may either be cumulates or represent a magma of a differing composition interacting with the andesitic magmas resulting in chilled blobs of magma. If the inclusions were cumulates they could give us a detailed looked into the mineralogy and composition of

21

crystals fractionated from the melt to yield andesites whereas if the inclusions were a magma at the time of entrainment in the andesitic magma, the inclusions would preserve a record of magma mixing, then this would give us details about mixing processes associated with mafic recharge.

Cumulates are aggregates of crystals that were formed by separation of crystals and melt, and are generated near the cooling margins of a crystallizing magma. The accumulation may occur by several means. The crystals could have formed *in situ*, were transported by gravitational settling processes (or by flotation if the density is less than that of the melt), or were transported and deposited on the floor of magma chamber by density currents (Hess, 1989; McBirney, 1993). Cumulus minerals may trap small amounts of the melt between the crystals. The trapped liquid may crystallize to form small inter-cumulus crystals. A cumulate with trapped liquid will have large subhedral to euhedral crystals with small amounts of interstitial material (Figure 8a). However if the cumulus crystals continue to grow or no melt is trapped between the crystals, then no interstitial material is present in the cumulate resulting in subhedral to anhedral crystals that have grown together (Figure 8b) (Williams et al., 1982; McBirney, 1993). When the inclusions were examined petrographically, the texture observed were not those of cumulates, but instead they are porphyritic, ranging from 1-10% phenocrysts by volume (Figures 8a, 8c, 9).

A   B   C
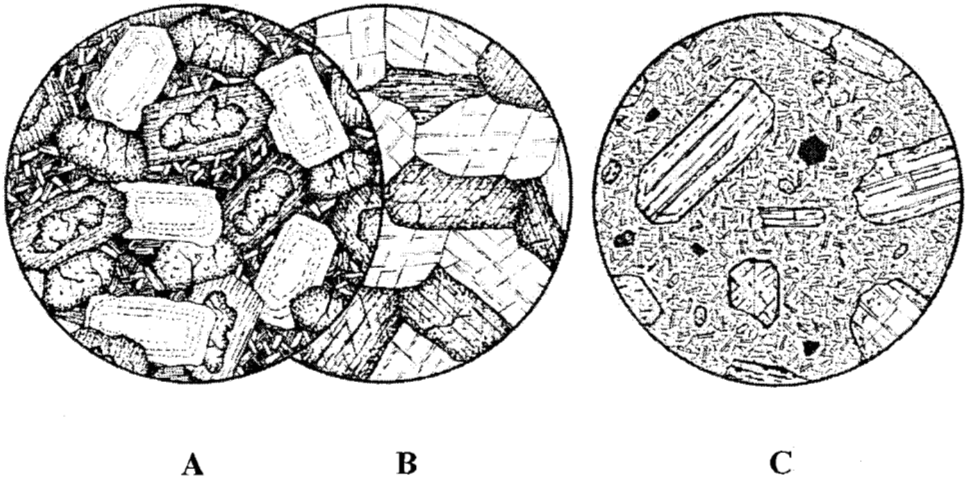
Figure 8 - The drawings on the left (A and B) are typical cumulate textures. The far left (A) is an example of a crystallized interstitial material between the cumulus crystals, whereas the center drawing (B) has no interstitial material. The drawing on the far right (C) is typical for porphyritic texture and it is this texture that was observed in the inclusions. (Figures taken from McBirney, 1993).

dark patch = interstitial glass

glass

Vesicle
glass

quenched amphibole

Figure 9 – An example of an (amphibole rich) inclusion. Take note of the dark gray patchy areas of interstitial glass as indicated by the arrows. The interstitial glass formed upon quenching of the inclusion. The large amphibole crystals that are visible are also quenched. V= vesicle.

23

I will also show that inclusions are also not incorporated country rocks pieces but represent blobs of more mafic magma that were chilled upon contact with the host lava. When mafic and silicic magma come into contact, thermal equilibration occurs quickly between the inclusions and the host. During the equilibration the mafic magma is cooled causing crystallization while the silicic magma is heated. The rapid cooling of the more mafic magmas leads to quenching resulting in interstitial glass between phenocrysts and groundmass crystals as well as quenched (skeletal) crystals (Bacon, 1986). This cooling and crystallization cause a rapid increase in the viscosity of the inclusion magma further preventing complete homogenization of the two magmas. Glass and quenched crystals are found in all inclusions (Figure 10). Furthermore, upon incorporation into the cooler host lava, partial crystallization of the inclusion leads to saturation with a vapor phase producing a vesicular to a highly porous texture, also something that is typical for investigated inclusions (Figure 9). The porosity arises as the volatiles try to escape the inclusion but instead are entrapped by the chilled margin. The inclusions becomes buoyant within the hybrid magma and remains suspended, thus inclusions have often a spheriodal shape (Bacon, 1986; Thomas and Tait, 1997; Blake and Fink, 2000). Another textural phenomenon that occurs is the alignment of groundmass crystals (usually plagioclase laths) along the inner side of the inclusion rim. It seems that given the rigidity of the rim and the inclusion ballooning out due to increased volatile pressure, the elongated plagioclase crystals tend to arrange themselves into a preferred orientation. Crenulated rims are also a characteristic rim feature found in most magmatic inclusions (Bacon, 1986). Crenulated margins, aligned plagioclase laths near margins and a vesicular

24

groundmass are all features observed among inclusions (Figure 10). According to Clynne (1999) and Landi et al. (2004) and references herein, disequilibrium characteristics such as sieved textures and mineral overgrowths arise through magma mixing, and thus are commonly associated with mafic inclusions. If thorough mixing has occurred leading to an absence of inclusions then mineralogical disequilibrium features are the only evidence indicating magma mixing. In summary, based on the porphyritic texture, disequilibrium characteristics (sieved textures and mineral overgrowths), see also below, and all of the above petrographic evidence, I have concluded that the inclusions were magma (liquid + crystals) shortly before entrainment and their existence is due to mixing of the host andesitic magma with the inclusion magma that was quenched at contact.

Figure 10 – Interface between the host lava (below the white line) and the inclusion.

Individual Mineral Phases

Plagioclase

Plagioclase is the most abundant mineral phase of all sites sampled. It comprises about 64-70% of all phenocrysts. Seventy six plagioclase phenocrysts from both the inclusions and host lavas were analyzed using the electron microprobe yielding 640 analysis points. Most (72) phenocrysts were analyzed with three points placed in the center, at the rim and about half way between center and rim of the grains, and a few phenocrysts were analyzed along analysis traverses from center to rim of grains with step spacings of 4.0 μm to 5.7 μm. The composition of plagioclase was determined to be An_{30-74} in host lavas and An_{33-80} in inclusions (Figure 11). There is essentially no difference in the plagioclase composition between the host lavas and the inclusions, although the inclusions contain some plagioclase that are (barely) more Ca-rich as would be expected for the more mafic composition compared to andesitic host lavas. Plagioclase crystals, both phenocrysts and groundmass laths, are strongly euhedral; however, in a few instances they are subhedral. The groundmass laths are on average <200 μm in length and approximately 50 μm in width, whereas the phenocrysts are on average 1-3 mm long and 0.5 to 1.5 mm in wide.
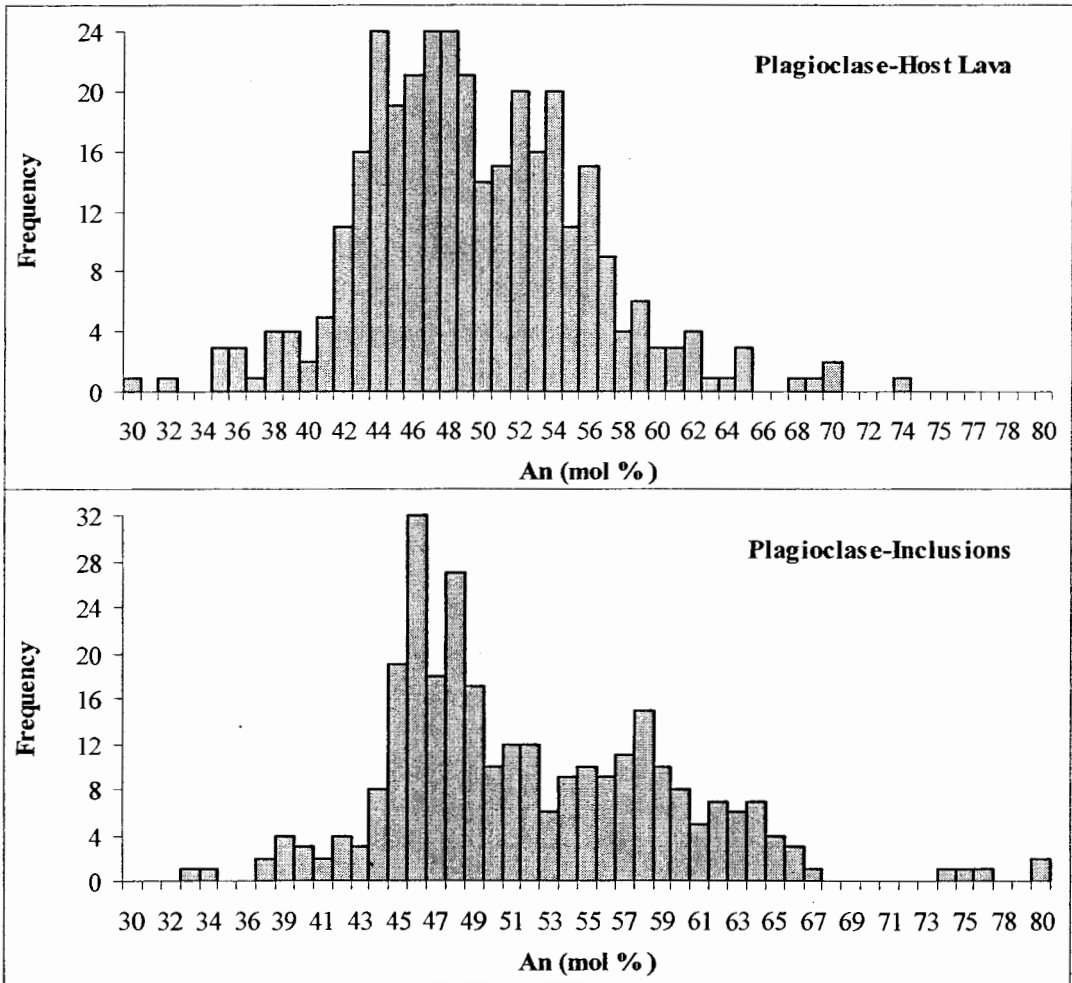
Figure 11 – Histograms of the microprobe analyses of plagioclase, illustrating the distribution of the anorthite content among the 76 (total) phenocrysts analyzed.
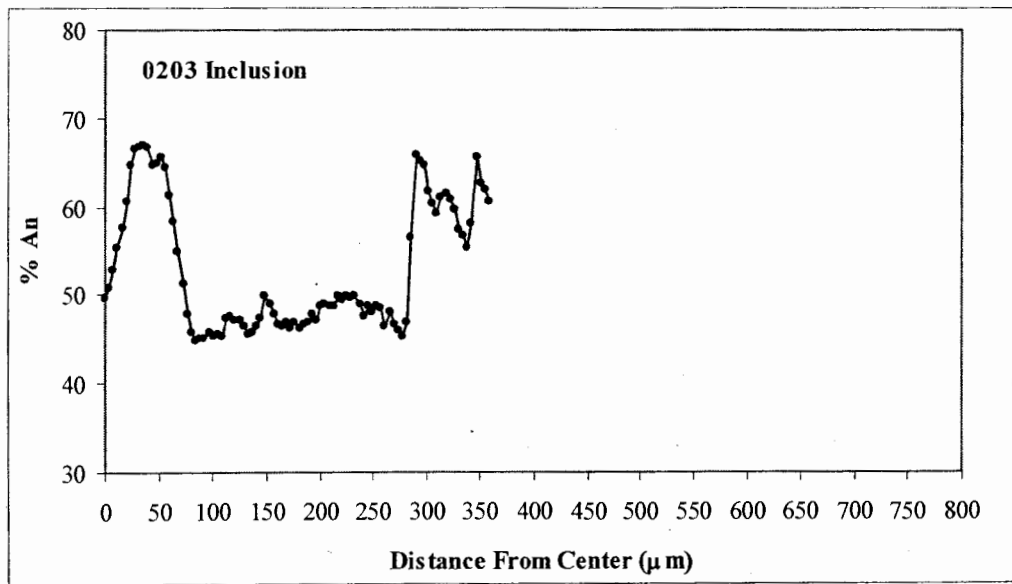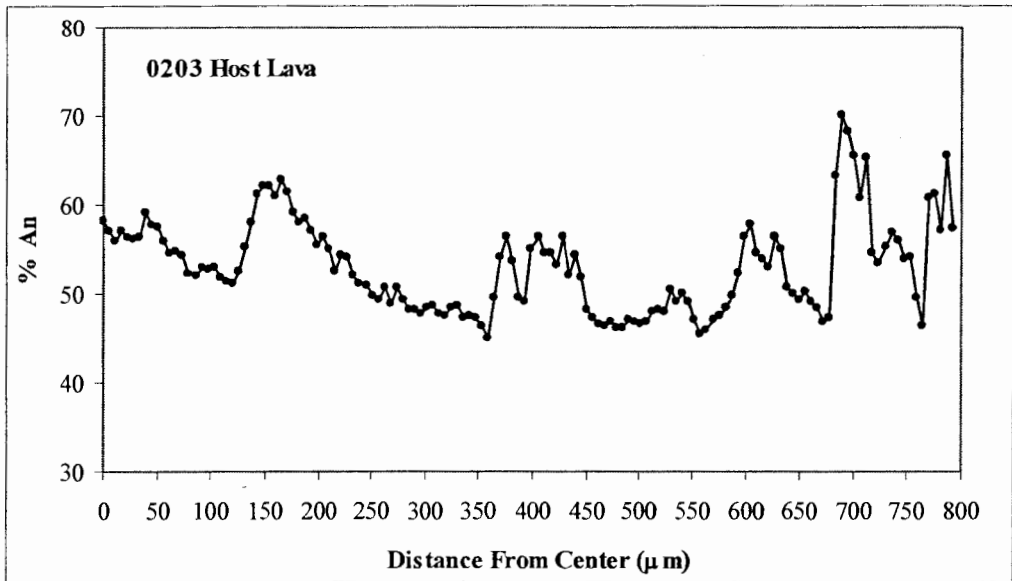
Figure 12 – Line traverses for the host lava (above) and inclusion (below) for site 0203, the road cut along US Highway 26. The patterns show strong alternations of calcium rich and sodium rich bands reflecting complicated crystallization histories. Traverse location shown in Figure 13.

The four selected plagioclases for analysis traverses represent two sites, U.S. Highway 26 (0203) and Mount Hood Meadows (0205), and represent typical phenocrysts of host lavas and inclusions (Figures 12, 13, 14, 15). In each case, the line traverses began at the center of the phenocryst and ended at the rim.

The crystallization history of the phenocryst in the host lava (site 0203) is more complicated than the phenocryst in the inclusion (Figure 12) as illustrated by the several episodes (or cycles) of increase and decease in the anorthite content. The composition of the core of the host lava phenocryst is An_{57-58} and progresses through several cycles prior to the composition peaking at An_{70} (~775 mm) and at the rim (~800 mm) the composition is An_{56-57}. Although the composition of the phenocryst is approximately the same at the core and rim, the mineral chemistry illustrates that it underwent several episodes of alternating normal and reverse zoning prior to being erupted. The composition of the phenocryst from the inclusion at the core is An_{50}; it too underwent periods of normal and reverse zoning, where at the rim the composition is An_{60}.
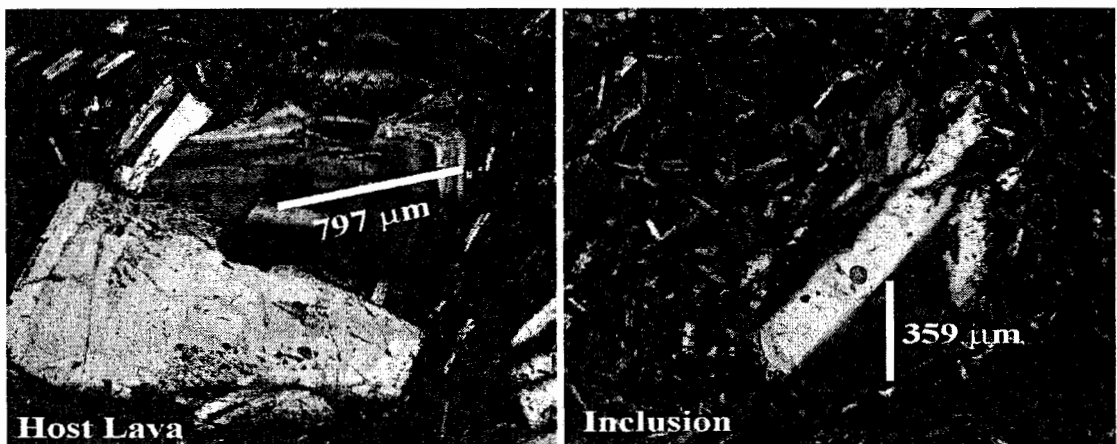
Figure 13 – Traverses conducted by electron microprobe of a representative plagioclase phenocrysts from host lava (left) and inclusion (right) for site 0203. Oscillatory zoning is prevalent. Electron microprobe profiles are shown in Figure 12.

29
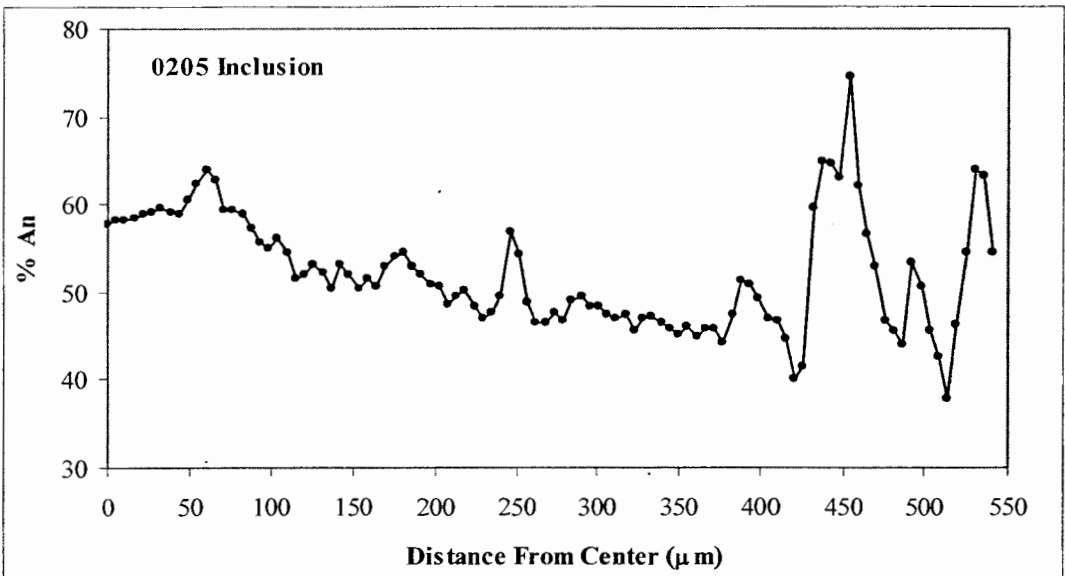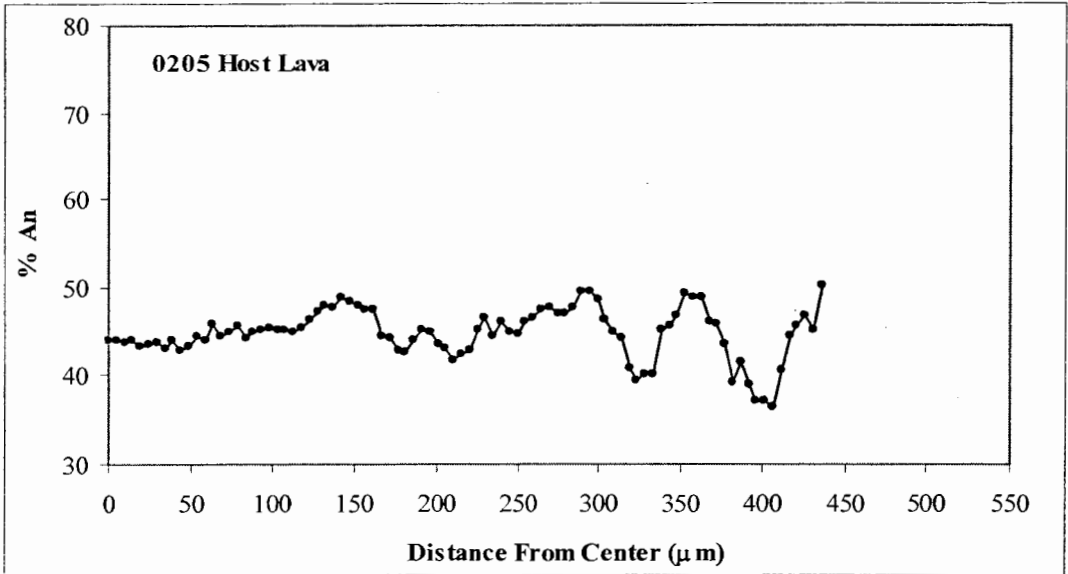
Figure 14 – Line traverses for the host lava (above) and inclusion (below) for site 0205, Mount Hood Meadows Ski Resort. The patterns show strong alternations of calcium rich and sodium rich bands reflecting complicated crystallization histories. Traverse location shown in Figure 15.

The crystallization history of the phenocryst in the host lava from Mount Hood Meadows (site 0205) and the phenocryst in the inclusion are similar, although the crystallization history of the host lava phenocryst is more subtle (Figure 14). The composition of the core of the host lava phenocryst is An_{45} and progresses through several cycles prior to the composition peaking at An_{50} at the rim. The composition of

the inclusion phenocryst is An_{58-59} and peaks at An_{65} and at the rim the composition is An_{55}. However the inclusion phenocryst underwent several episodes of normal and reverse zoning and the changes in composition between bands is more dramatic than it is in the host lava.

Most phenocrysts exhibit oscillatory zoning (Figures 13, 15), whereas the groundmass crystals apparently do not. Oscillatory zoning reflects alternating Ca- and Na-rich bands. In addition to oscillatory zoning, a variety of other textures are found among phenocrysts of all samples. Phenocrysts can be grouped into one of the following three groups, non-sieved, sieved rim and sieved core (Figure 16). Formation of sieved textures will be discussed later. Proportionality among these vary but the most abundant type is always the non-sieved texture except for inclusion sample 0211 (Table 5).

Figure 15 – Traverses conducted by electron microprobe of a representative plagioclase phenocrysts from host lava (left) and inclusion (right) for site 0205. Oscillatory zoning is prevalent. Electron microprobe profiles are shown in Figure 14.

31
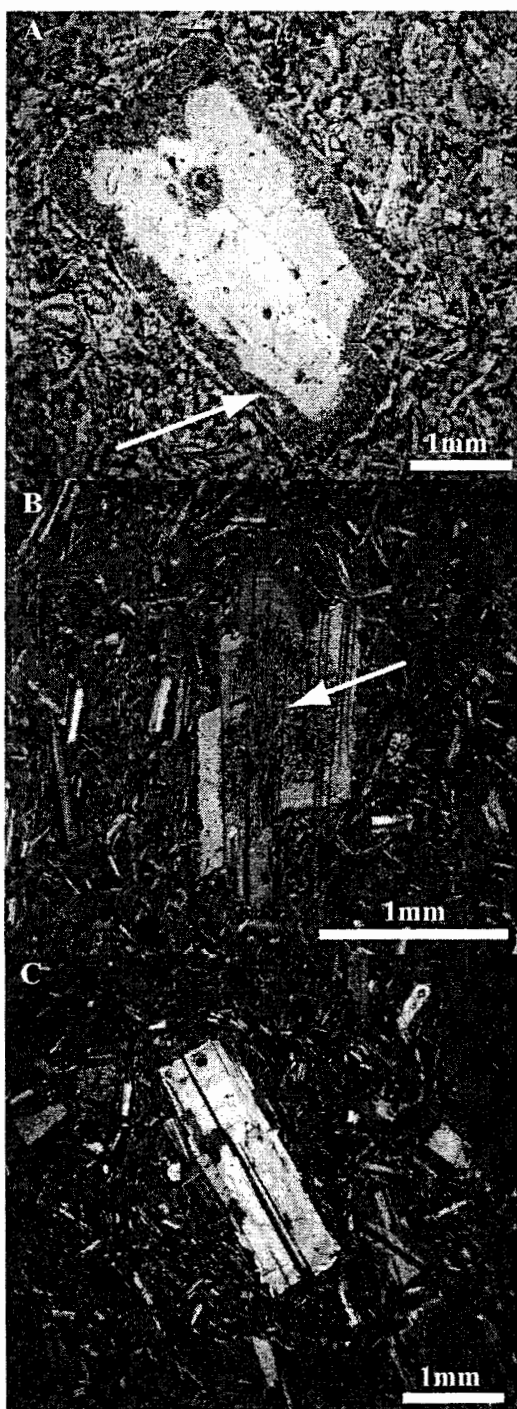
Figure 16 – The three groups of plagioclase based on texture; (A) plagioclase with a sieved rim, as shown by the white arrow (Site 0211), (B) plagioclase with a sieved core, also shown by the white arrow (Site 0203), and (C) an euhedral, non sieved plagioclase (Site 0205). (A) and (B) under plane light and (C) under partially crossed polarized light.

Table 5 – Distribution of textures among plagioclase phenocrysts. The values for the mafic inclusions and host lavas are average percentages for each site.

Site Number	Location	Number of Samples	% Sieved Rim	% Sieved Core	% Non-Sieved
FLANK LAVAS					
0201	Lady Creek	1	0%	1%	99%
0202	Lady Creek	1	23%	8%	69%
0204	Cooper Spur Rd	1	0%	1%	99%
0206	Cloud Cap Inn	1	0%	22%	78%
0208	Pinnacle Peak	1	16%	36%	47%
0209	Parkdale Flow	1	2%	12%	86%
MAFIC INCLUSIONS					
0203	U.S. Highway 26	4	0%	1%	99%
0205	Mt Hood Meadows	6	23%	8%	69%
0210	Laurence Lake	5	0%	1%	99%
0211	Compass Creek	3	0%	22%	78%
0212	Timberline Lodge	3	16%	36%	47%
0213	Cathedral Ridge	2	2%	12%	86%
HOST LAVAS					
0203	U.S. Highway 26	3	9%	13%	78%
0205	Mt Hood Meadows	4	3%	13%	84%
0210	Laurence Lake	2	8%	12%	79%
0211	Compass Creek	2	13%	16%	70%
0212	Timberline Lodge	2	15%	13%	72%
0213	Cathedral Ridge	2	9%	8%	82%

Orthopyroxene

This mineral is present at all sites as phenocrysts with sporadic micro-phenocrysts (<200 μm) in the groundmass, and comprises 3-12% of all phenocrysts. On average, orthopyroxene phenocrysts measure in size from ~500 μm to 1500 μm (1.5 mm). The phenocrysts are approximately one half to three quarters the size of the plagioclase although there are some crystals that rival the plagioclase. Associated with the orthopyroxene (and clinopyroxene, see below) there are clumps of oxide minerals within or adjacent to the phenocrysts. Microprobe analysis of 46 phenocrysts (138 points) shows that the composition of orthopyroxene in host lavas is $En_{56-74}Fs_{23-43}Wo_{1-3}$ and the composition in inclusions is $En_{57-76}Fs_{21-41}Wo_{1-5}$ (Figure 17), although

33

there are 3 analyses (2 host lava analyses and 1 inclusion analysis) where the composition is at or above En_{80}. Furthermore, four analyses yielded Wo contents above 5% and this would be pigeonites (Figure 17). Orthopyroxene, as plagioclase, also shows negligible differences in composition between whether found in host lavas and inclusions. Some orthopyroxene phenocrysts have a subhedral to euhedral shape in which the rims appear frayed, thus indicating the rims have been partially resorbed (Figure 18). One orthopyroxene phenocryst from Laurence Lake also indicates strong resorption but in addition shows being overgrown with clinopryoxene (Figure 19). Reverse zoning is apparent in several of the orthopyroxene analyzed by electron microprobe (Figures 20, 21).
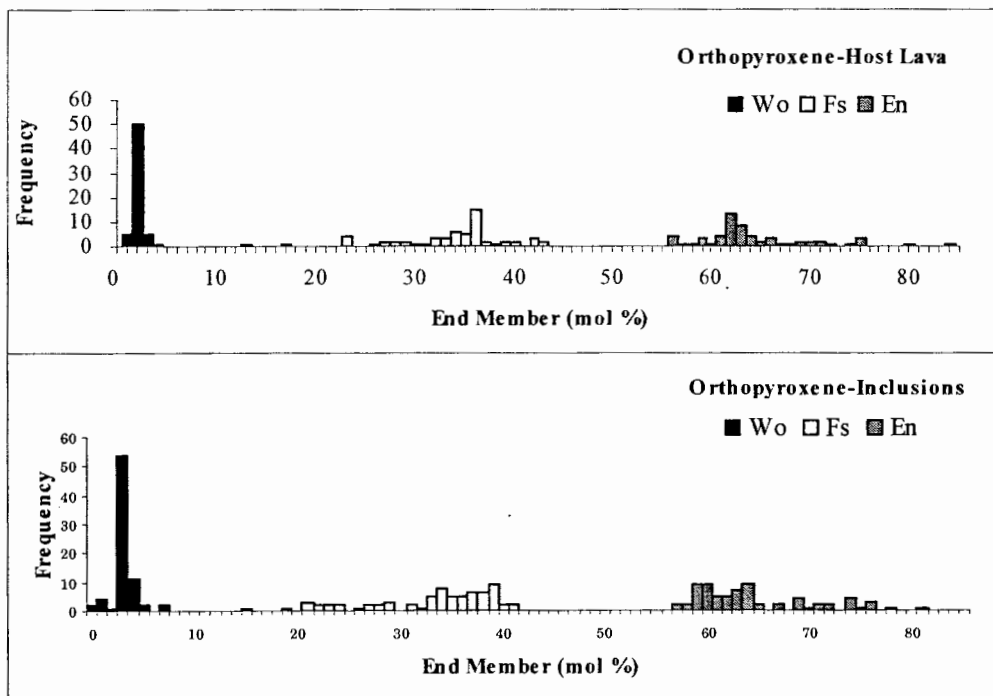
Figure 17 – Histograms of the microprobe analysis of orthopyroxene, illustrating the distribution of the end member content among the phenocrysts analyzed.
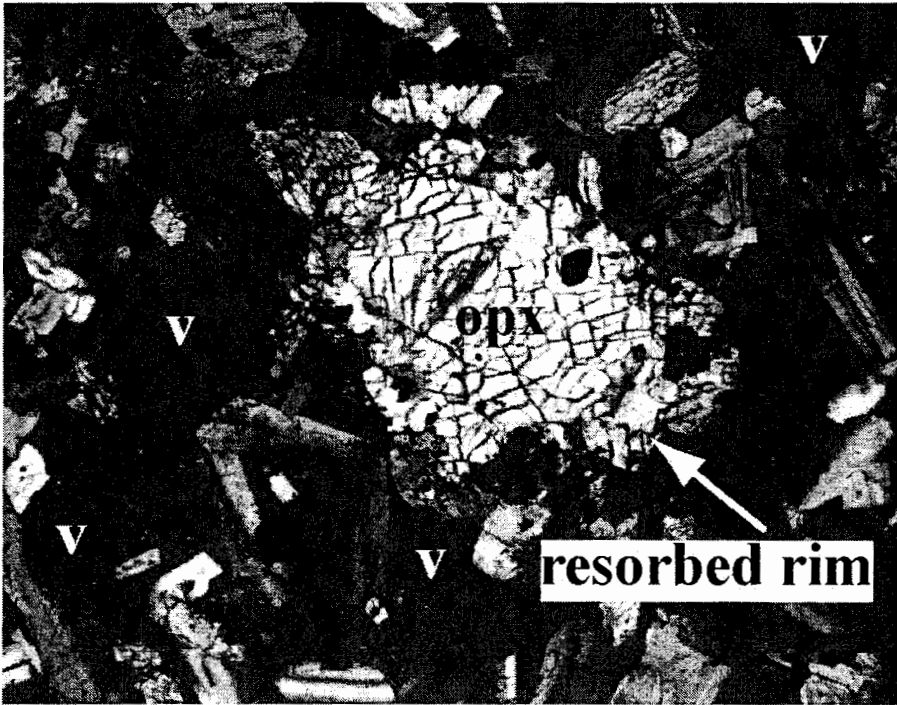
Figure 18 – An orthopyroxene with a resorbed rim found in an inclusion sample from Laurence Lake (Site 0210). Picture was taken at 100x magnification under crossed polarized light. V = vesicle.
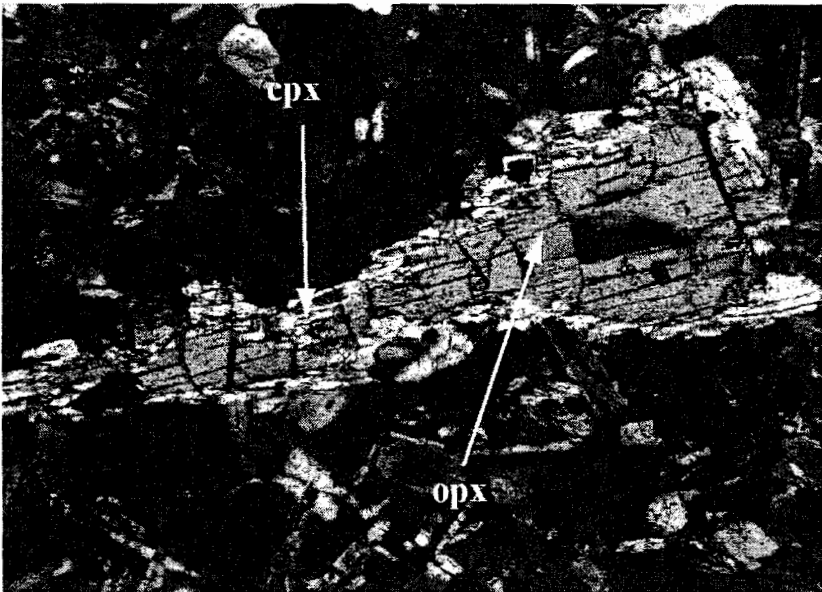
Figure 19 – An orthopyroxene phenocryst with an overgrowth of clinopyroxene, found in sample 0210B, an inclusion from Laurence Lake. Picture was taken at 100x magnification, polarized light.

35
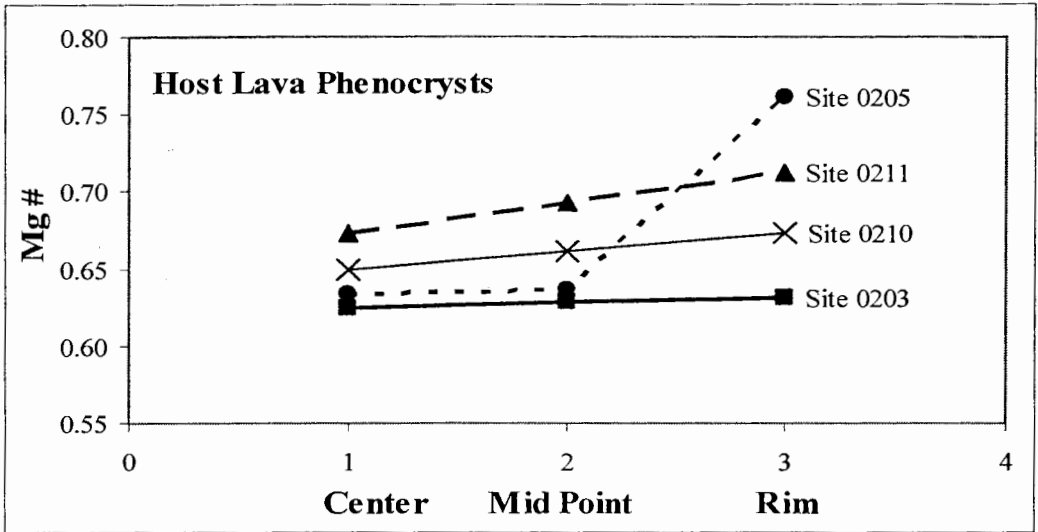
Figure 20 –Graph illustrating the reverse zoning of selected orthopyroxene host lava phenocrysts. The Mg# number increases as progression from the core to the rim, opposite of normal zoning where Mg# decreases towards rim.
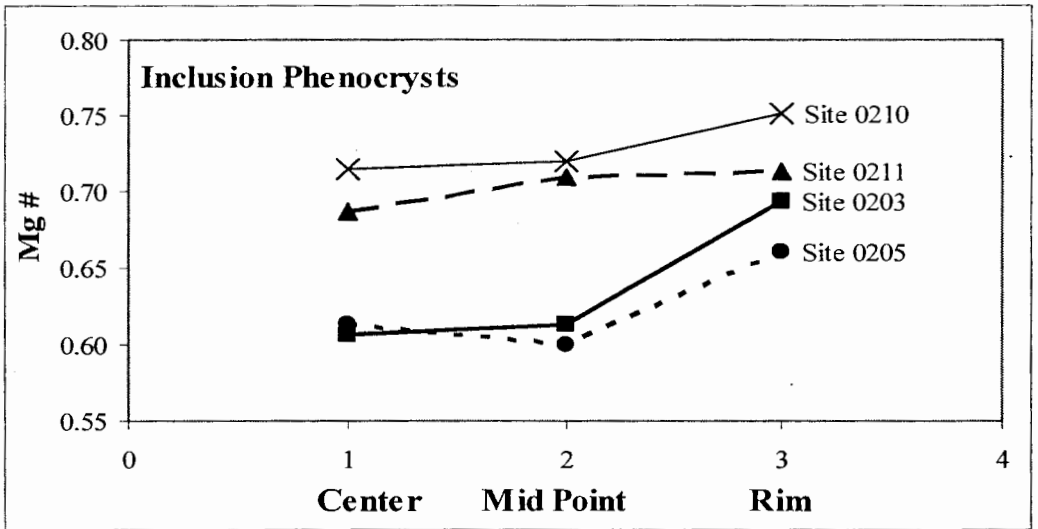
Figure 21 –Graph illustrating the reverse zoning of selected orthopyroxene inclusion phenocrysts. The Mg# number increases as progression from the core to the rim, opposite of normal zoning where Mg# decreases towards rim. $Mg\# = {}_{mol}(Mg/Fe^{total} + Mg)*100$.

36

Clinopyroxene

This mineral is present at sites that do not contain amphibole, as phenocrysts and intermittent micro-phenocrysts (<200 µm) in the groundmass, but also appears occasionally at sites that contain amphibole (Table 4). The phenocrysts are of the same size as the orthopyroxene. Only limited phenocrysts of clinopyroxene were analyzed (2 crystals); the acquired data do not allow a detailed survey. The average composition of the six points (3 points per crystal) is $En_{45}Fs_{13}Wo_{42}$, but of those analysis points two analyses have a Cr_2O_3 content > 0.1%, indicating that these clinopyroxene crystals grew likely from basaltic magmas. Clinopyroxene phenocrysts have no apparent zoning.

Amphibole

Amphibole is *not* present at all sites, it only occurs at Laurence Lake (0210), Compass Creek (02011), Cathedral Ridge (0213) and to a lesser degree at Timberline Lodge (0212). Furthermore, amphibole from these sites consitutes approximately 17% of all the phenocrysts, and it is a large component of the groundmass (25-30% by volume, visual estimate). Phenocrysts are subhedral to anhedral and are typically elongated with spiky ends indicating growth during rapid cooling. Quite a few euhedral crystals show typical two directions of cleavage at 56° and 124°, and many have dark (black) rims that are reaction rims. A scatter plot of Si atoms (T site) verses the sum of Na + K atoms in the A site (Deer et al., 1992) indicates that the amphiboles present at Mount Hood are calcic amphibole, specifically, hornblende, pargasite and tshermakite (Figure 22). Electron microprobe analysis shows that a few of the

37

amphibole phenocrysts are reversely zoned as demonstrated by increasing trends in Mg# from core to rim (Figures 23, 24)
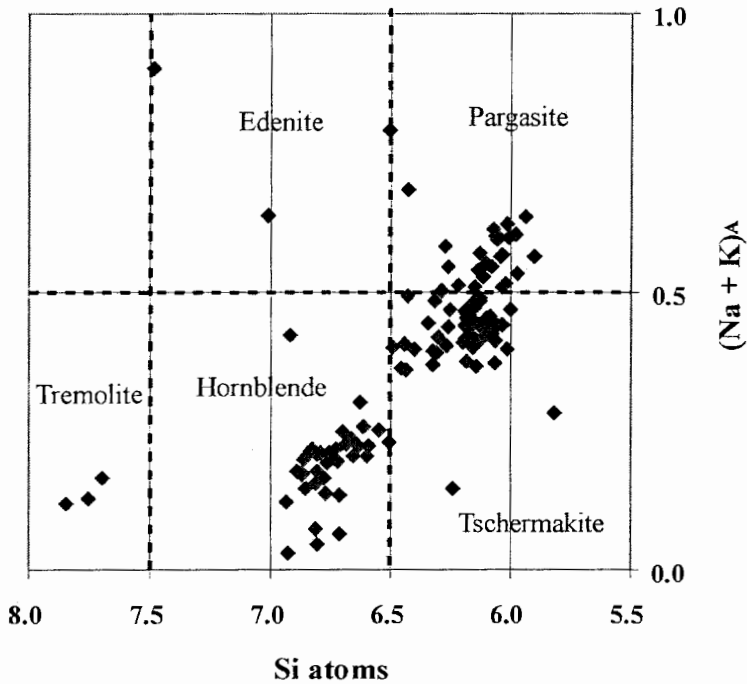
Figure 22 – Electron microprobe analysis of amphiboles show that Mount Hood has produced hornblende, pargasite and tschermakite (outliers no considered).
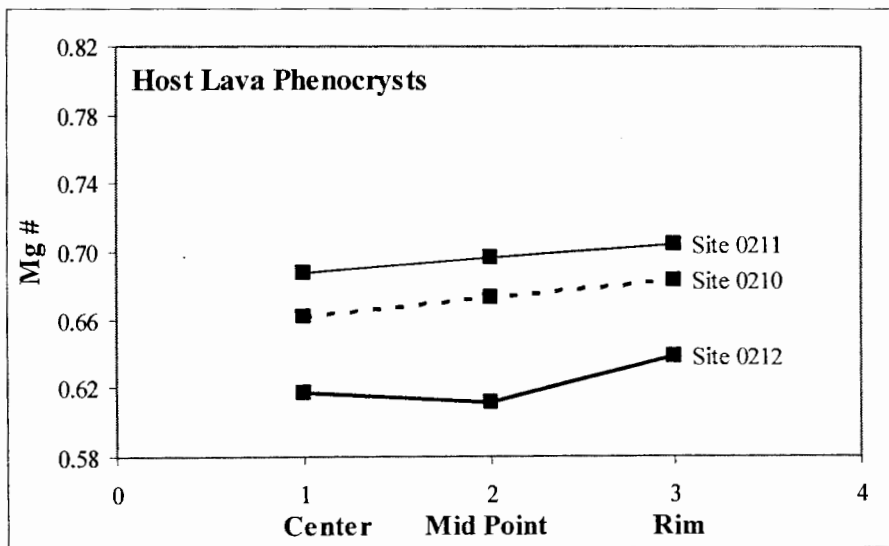
Figure 23 –Graph illustrating the reverse zoning of selected amphibole host lava phenocrysts in which the Mg# number increases as progression from the core to the rim.
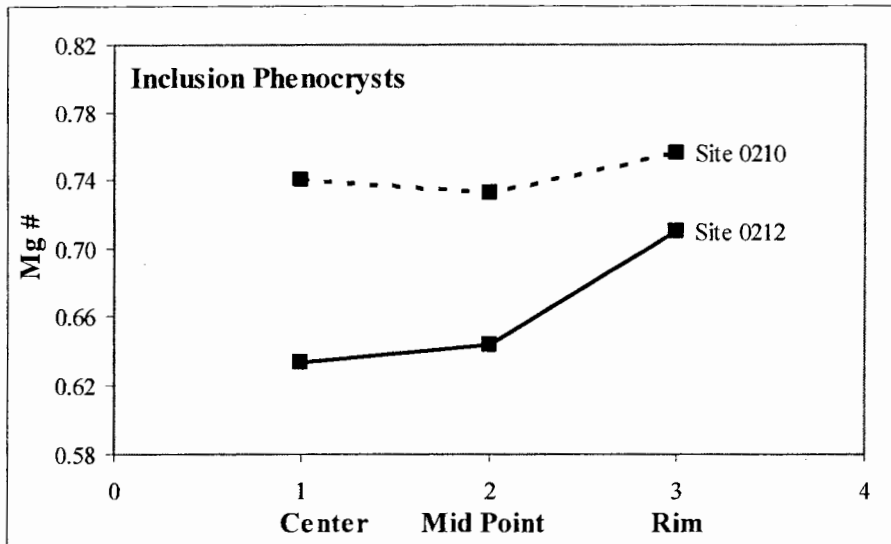
Figure 24 –Graph illustrating the reverse zoning of selected amphibole inclusion phenocrysts in which the Mg# number increases as progression from the core to the rim.

Olivine

This mineral is present only in the (slightly) more mafic flank lavas, however it is absent at two locations (0202, Lady Creek and 0206, Cloud Cap Inn). The mineral comprises about 4-5% of the phenocrysts present. The phenocrysts have an average size of about 1 mm, they are heavily fractured, and the rims have been altered to iddingsite. Olivine was not chemically analyzed.

Oxides

The oxides are ubiquitous at all sites, both as phenocrysts (about 15% of the population) and in the groundmass. Phenocrysts range in size from about 0.5 mm to 1 mm, whereas the groundmass crystals are less than 100 μm. Oxide phenocrysts are most often found in association with the pyroxenes forming oxides-pyroxene

39
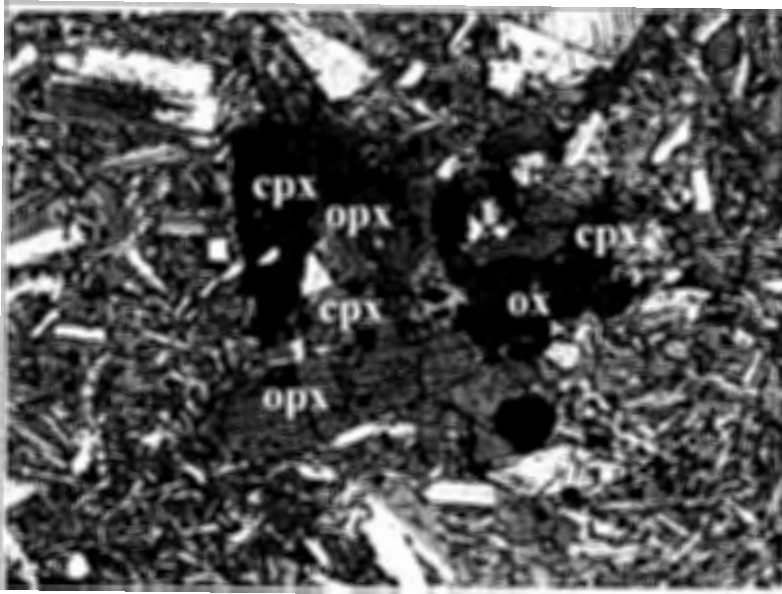
Figure 25 – An oxide-pyroxene glomerocryst from an inclusion collected at site 0203 (U.S. Highway 26).

glomerocrysts (Figure 25). In the clumps are several crystals of both of the pyroxenes and several crystals of the oxides, and as mentioned above, the volume assumed by both the pyroxenes and oxides are equal. They are most likely a combination of minerals from the magnetite and ilmenite series. A definite identification can not be determined as these minerals were not analyzed using the electron microprobe.

Petrographic Evidence for Petrogenesis

Type, proportion and composition of minerals are dependent on magma composition and physical parameters such as temperature and pressure of crystallization (e.g. Coombs et al., 2002). Furthermore, minerals are sensitive recorders of growth environments (i.e. quenched crystals) and conditions of equilibrium (Hibbard, 1995). Several mineral features observed in inclusions are distinctive and point to specific petrogenetic scenarios that must have played a role in generating magmas as preserved in mafic inclusions and andesite host lavas. Mineral features of interest are compositional variations, oscillatory zoning, sieved textures,

40

and resorption. Furthermore, disequilibrium is evident mineral textures (sieved or resorption features) and complicated crystallization histories as expressed by zonation. The host lavas and inclusions (and flank lavas as well) are intermediate igneous rocks (52-63 SiO_2 wt %) (LeMaitre et al., 2002). Based on the documented general mineral assemblage for both the inclusions and the host lavas one may not necessarily suspect that the inclusions and host lavas are *not* in a state of equilibrium. However, the textural features among the phenocrysts, especially plagioclase, and the chemical zoning of the major mineral phases (plagioclase, orthopyroxene and amphibole) lavas exemplify disequilibrium, and/or variable and repetious conditions during growth

Plagioclase is a solid solution of anorthite (Ca-rich end member) and albite (Na-rich end member), and plagioclase crystals often contain alternating zones of Ca-rich or Na-rich compositions. Since, anorthite-rich plagioclase crystallizes at higher temperatures than albite-rich plagioclase, 1553 °C and 1118 °C (end member temperatures in a pure two component system) respectively (McBirney, 1993), plagioclase phenocrysts may record the heating and cooling cycles in addition to chemical changes that take place concurrently with heating or cooling within a magma chamber. Periods of heating may occur by either recharge events or when the top of the chamber experiences upwelling of deeper seated hotter magma during a convection cycle. Conversely, periods of cooling would occur in between recharge events or decent towards the chamber floor during a convection cycle.

The plagioclase phenocrysts in both host lavas and inclusions bear strong chemical evidence of complicated crystallization histories as recorded by the chemical zoning within the phenocrysts (Figures 12, 14). In order to get a better understanding

41

of the crystallization history of the plagioclase phenocrysts, line traverses were conducted on selected phenocrysts, two each from host lava and inclusion samples. The four phenocrysts that were selected represent lava flows that outcrop at U.S. Highway 26 (0203) and at the top of the Blue Chair Lift at Mount Hood Meadows Ski Resort (0205) (Figure 4 for location).

Figure 12 graphically illustrates the analysis traverses for a host lava plagioclase phenocryst and an inclusion plagioclase phenocryst in terms of anorthite content verses the point location of analysis. Initial observation indicates that the crystallization history of the host lava phenocryst appears to be more complicated than the crystallization history of the inclusion phenocryst. However, Figure 13 illustrates that the traverse for the inclusion phenocryst is shorter than the traverse for the host lava phenocryst. On the other hand there is a general similarity between the zonation of the inclusion phenocryst and the host lava phenocryst from its core to rim. Both phenocrysts have lower An contents near the beginning of their traverses followed by a zone of strong (Δ ~15% An) reverse zonation followed by a middle line of lower An and experiencing another zone of strong reverse zonation near the rim with ending An that is ~10 mol% higher than core or mid points (Figure 12). Based on this similarity of the An-profile, both phenocrysts could have a similar origin, albeit one phenocryst is located in the host lava and the other in the inclusion. Furthermore, the core of the plagioclase in the inclusion has lower anorthite content than the core of the plagioclase of the host lavas suggesting lower temperature of crystallization and/or Ca/Na of the melt at the onset of crystallization of this phenocryst. This suggests that the

phenocrysts may have originated from the more evolved host lava as observed by Clynne (1999) at Mount Lassen, Cascade Range, California.

Figure 14 graphically illustrates the chemical zoning of a host lava phenocryst and an inclusion phenocryst found in a sample collected at site 0205, and the traverses are shown in Figure 15. The composition of the core for the host lava phenocryst is An_{45} whereas the for the inclusion phenocryst it is An_{58-59}. Both sets of traverses (Figures 13, 15) indicate that plagioclase is compositionally complexly zoned and that similarities among plagioclase from inclusions and host lavas suggest not a simple crystallization scenario led to the observed phenocrysts. At least, this is preliminary suggestions and would require more analyses particularly from the other sites.

Plagioclase phenocrysts also present strong textural evidence for disequilibrium. All plagioclase phenocrysts can be grouped into three textural types, crystals with sieved rim, crystals with sieved core and non-sieved crystals (Figure 16). These textures are represented by plagioclase phenocrysts from all sites including the flank lavas. The crystals that have sieved textures may or may not show oscillatory zoning. The sieved or spongy texture forms when part of the crystal has been resorbed back into the melt. This process can occur when there is an increase in the environmental temperature (Hibbard, 1995), usually when a cooler magma comes into contact with a hotter magma either through recharge events or through convective mixing of the magma chamber contents. Plagioclase was not the only mineral phase to undergo resorption; there are examples of orthopyroxene that have been partially resorbed. The resorbed orthopyroxenes are more often found in the host lavas than in

the inclusions, whereas many examples of resorbed plagioclase are found in both host lavas and inclusions.

Another textural feature that may illustrate disequilibrium is the overgrowth of one mineral by another resulting in the original mineral to be completely enclosed by the secondary mineral growth. Mineral overgrowths were observed with only the pyroxenes, in which clinopyroxene formed the overgrowth on orthopyroxene (refer to Figure 19).
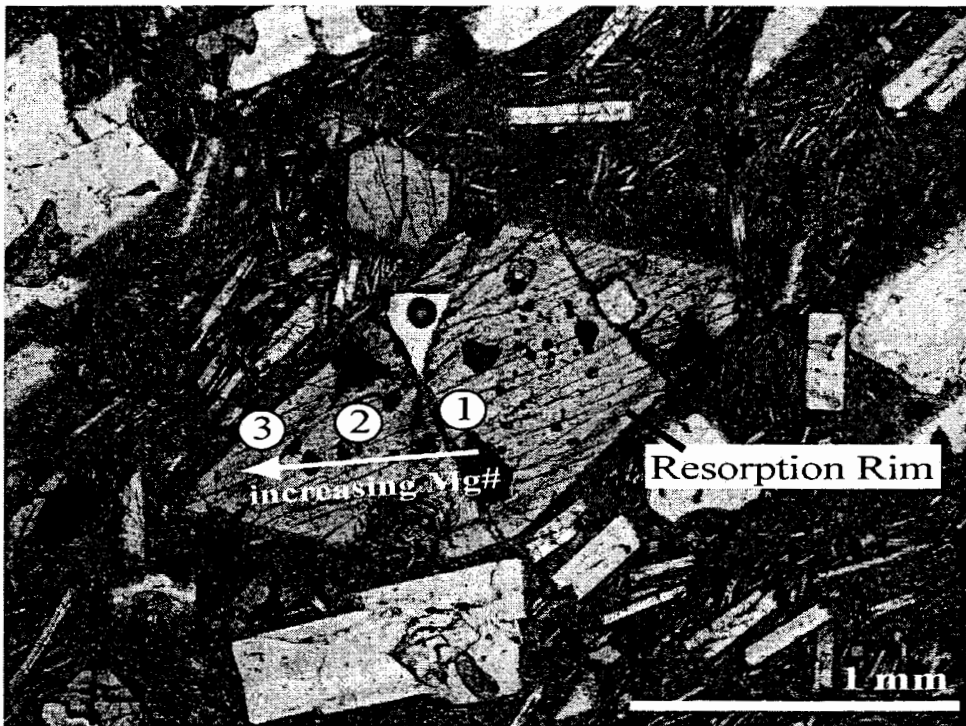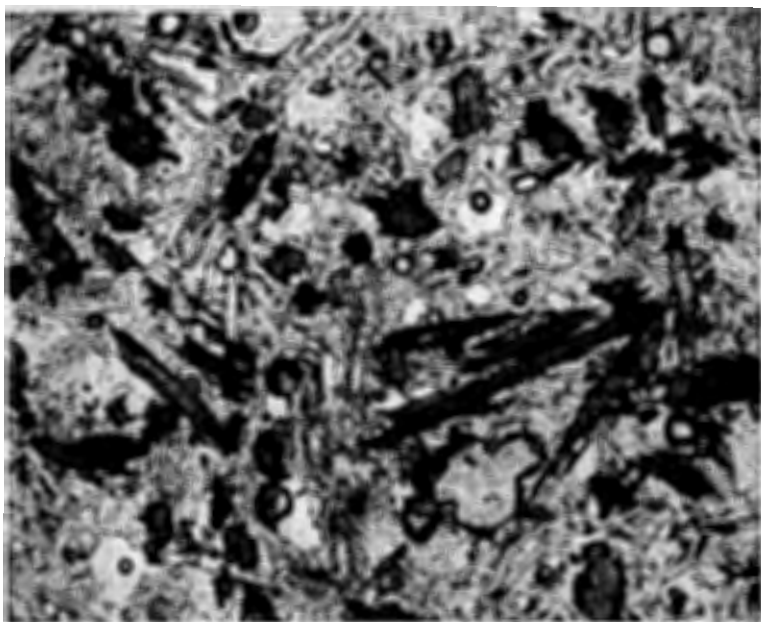

Figure 26 – An orthopyroxene from a sample of host lava from site 0205. Point locations are indicated by the white circles, and the (single) arrow points in the direction of increasing Mg#. The short black line points to a rim of partially resorbed material. Points 1 and 2 have Mg#'s of 0.63 and 0.64 respectively, are located within the area inside of the resorption rim. The Mg# for point 3 is 0.76 and this point lies outside the resorption rim. Chemical data is shown in Figure 16.

Microprobe analysis of orthopyroxenes in both host lava and inclusion samples indicate that from core to rim, there is a general trend of increasing magnesium number (Mg#), which may be also thought of an increase in enstatite, the Mg-rich end

44

member. The data reflect that as the enstatite content increases, the ferrosilite (Fe-rich end member) content decreases, in spite of this, the wollastonite (Ca-rich end member) content remains unchanged, at about 2% of the overall composition. If magma were allowed to cool on its own accord and undergo crystallization, the resulting orthopyroxene, would indicate a decreasing Mg# from core to rim generating a normally zoned crystal. This would be mostly a combined temperature-composition effect. However, the trend is opposite for the orthopyroxenes found in lavas erupted at Mount Hood. Orthopyroxene phenocrysts in both host lavas and inclusions are in general reversely zoned (Figure 26). Reverse zoning is an indication that later crystallization occurred from a more Mg-rich melt that was likely also hotter. Later growth from a more mafic melt is in essence a sign of magma mixing (Streck et al., 2002).

Figure 27 – An example of a quenched amphibole. The outer rim (black) is where the amphibole has reacted to an reaction rim.

Amphibole, as mentioned earlier, is not present in all sites, only those sites that are chemically enriched (in terms of incompatible trace elements) (see below). Many of the amphibole needles as well as a few of the phenocrysts have a skeletal crystal

45

morphology, which is characterized by sharp, spiky ends (Figure 27) or even swallow tailed. This texture is an indication that the amphibole crystals grew rapidly under conditions of undercooling, i.e. were quenched. Many of the amphibole phenocrysts have undergone a reaction (in cross-section appear as a black outer rim) to form a reaction rim (Figure 27). Reaction rims on amphibole can have several origins, most commonly are formed during magma ascent or during magma mixing, but in general indicate that melt conditions changed so that amphibole is no longer stable.

Figure 28 – An amphibole from a sample of an inclusion collected at site 0212. The white dots represent the location of the microprobe analysis. Points 1 and 2 have a Mg# of 0.63 and 0.64 respectively, and both points are located in the darker interior region of the crystal. Point 3 is located in the lighter rim area and its Mg# is 0.71. The arrow indicates the direction of increasing Mg#. Chemical data is shown in Figure 20.

Amphibole phenocrysts were analyzed using the electron microscope, and calculation of the magnesium number indicates the Mg# increases from the core to the rim in those phenocrysts that petrographically appear zoned (Figure 28). As with the

46

orthopyroxenes, a normally zoned amphibole would have the magnesium number decrease from core to rim. Therefore, the reversely zoned amphiboles could indicate growth from more mafic and hotter melt prior to eruption.

Disequilibrium textures found in the major mineral phases have been observed in both the inclusions and the host lavas, indicating that some mixing did occur prior inclusion formation which prevented further hybridization.

Geochemistry

Using the major element composition, I was able to classify the type of rock for each site/sample following the International Union of Geological Sciences (IUGS) guidelines, in particular in the application of the total alkali silica (TAS) diagram (Figure 29). The flank lavas at sites 0201 (Lady Creek), 0204 (Cloud Cap, Cooper Spur Road) and 0208 (Pinnacle Peak) plotted as basaltic andesite, whereas the remaining three flank lavas (0202, Lady Creek; 0206, Cloud Cap at Cloud Cap Inn; and 0209, Parkdale Flow) plotted as andesites with a couple of exceptions. One inclusion from site 0203 (road cut along US Highway 26) plotted as a basaltic andesite, and four of the five inclusions from Laurence Lake plotted at the junction of the basaltic andesite, basaltic trachyandesite, andesite and trachyandesite. The host lavas plotted as andesites, although two of the samples are in the dacite field. For simplicity, I will refer to all of the host lavas as andesite (see Scott et al., 1997, 2003). The general trend is that the most mafic sites are the flank lavas with the inclusions overlapping, while the host lavas sit on the right of the plot reflecting more silicic compositions. There is no compositional overlap between the host lavas and

47

inclusions (Figure 29). Chemical trends of major elements and selected trace elements indicate trends compatible with that reflect crystal fractionation; however, the incompatible elements are more variable at lower SiO_2 content and less variable at higher SiO_2 content (Figure 30) requiring other petrogenetic scenarios.

Taking only the inclusion-bearing sites into consideration, the sample sites can be divided into enriched and depleted sites. The depleted sites are those that have at a given SiO_2 (wt %) concentration, lower concentrations of incompatible trace elements. These site are 0203 (Highway 26) and 0205 (Mount Hood Meadows). The other sites or enriched sites have higher incompatible trace element concentrations, at a given SiO_2. The two sites that represent the extremes are U.S. Highway 26, site 0203 (most depleted) and Laurence Lake, site 0210 (most enriched). The enrichment of Laurence Lake (0210) is apparent on the TAS diagram (Figure 29). The four circles that plot at a higher alkali content represent four of the five inclusions that were sampled from this location. The elevated alkali content in these four inclusions is also mirrored by extremely elevated concentrations of Rb and Ba (Figure 30). Other trace elements in these samples are also elevated, but not to the extreme of Rb and Ba. These two elements range from 50% to 100% higher than the other sites. All of the other sites fall into a relatively narrow range for each of the trace elements. Those sites that have a relatively low concentration of incompatible element do not contain amphibole, whereas the enriched sites contain amphibole and little to no clinopyroxene.
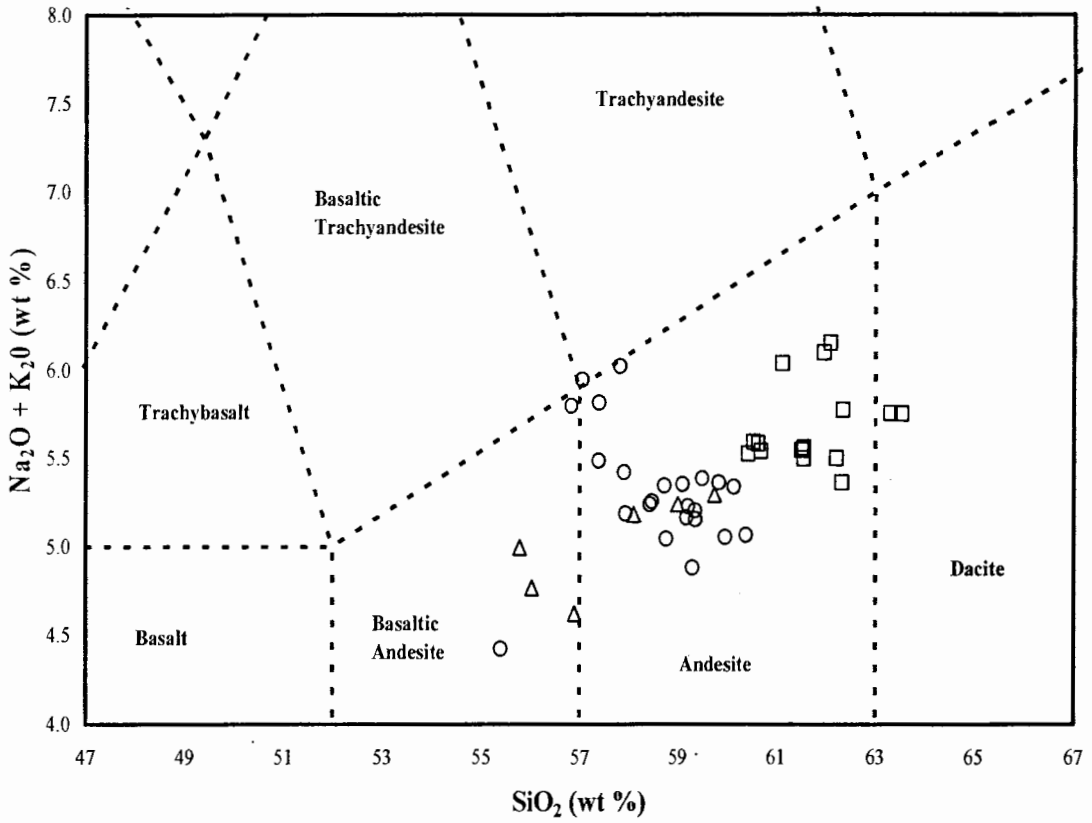
Figure 29 – TAS diagram of the samples collected. The flank lavas are represented by triangles, inclusions by circles and host lavas by squares.
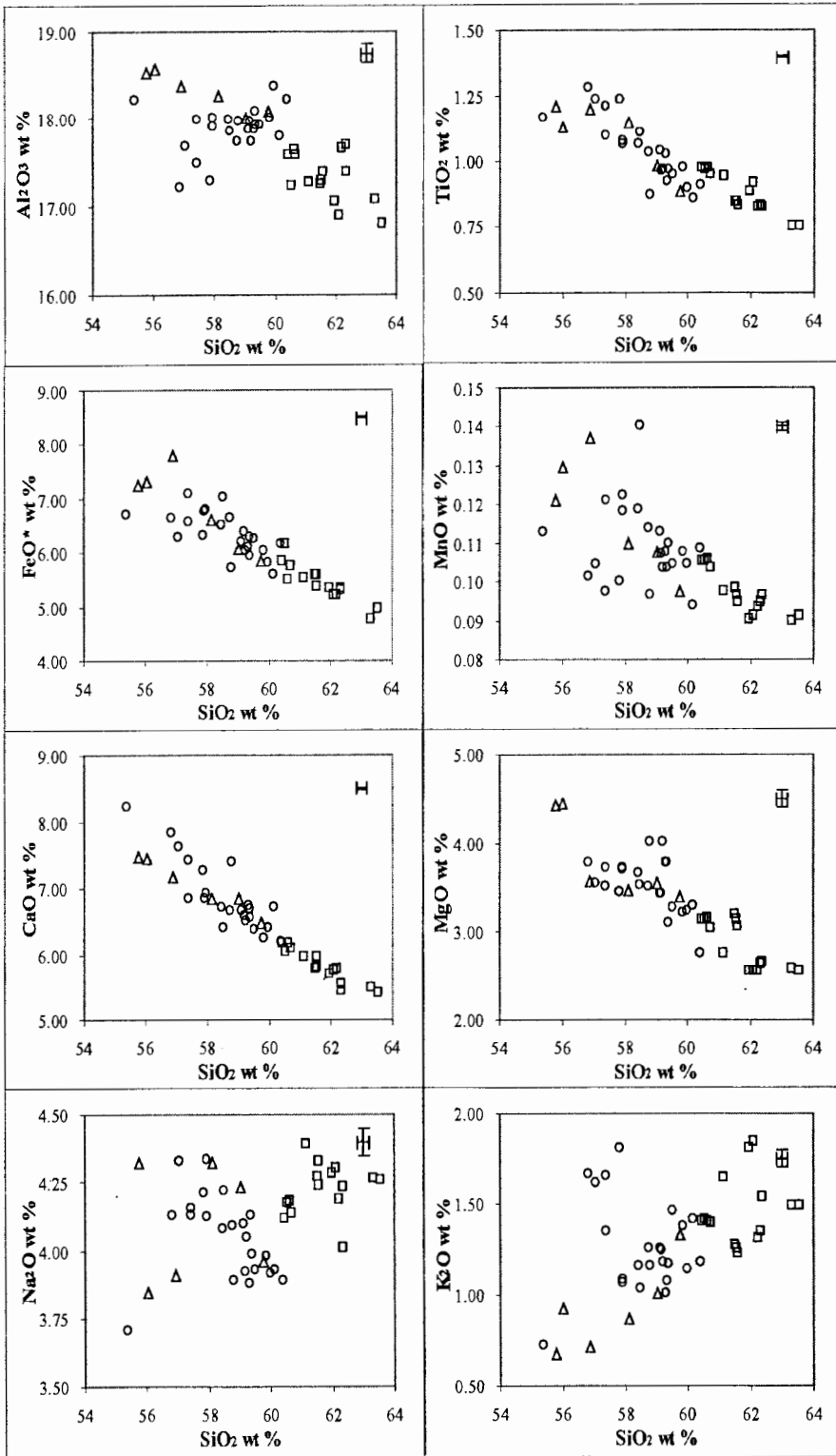
Figure 30 - Scatter plots of major elements and selected trace elements used in subsequent chemical modeling. The flank lavas are represented by triangles, inclusions by circles and host lavas by squares. Analytical error designated by the crosses in the upper right corner of each scatter plot.
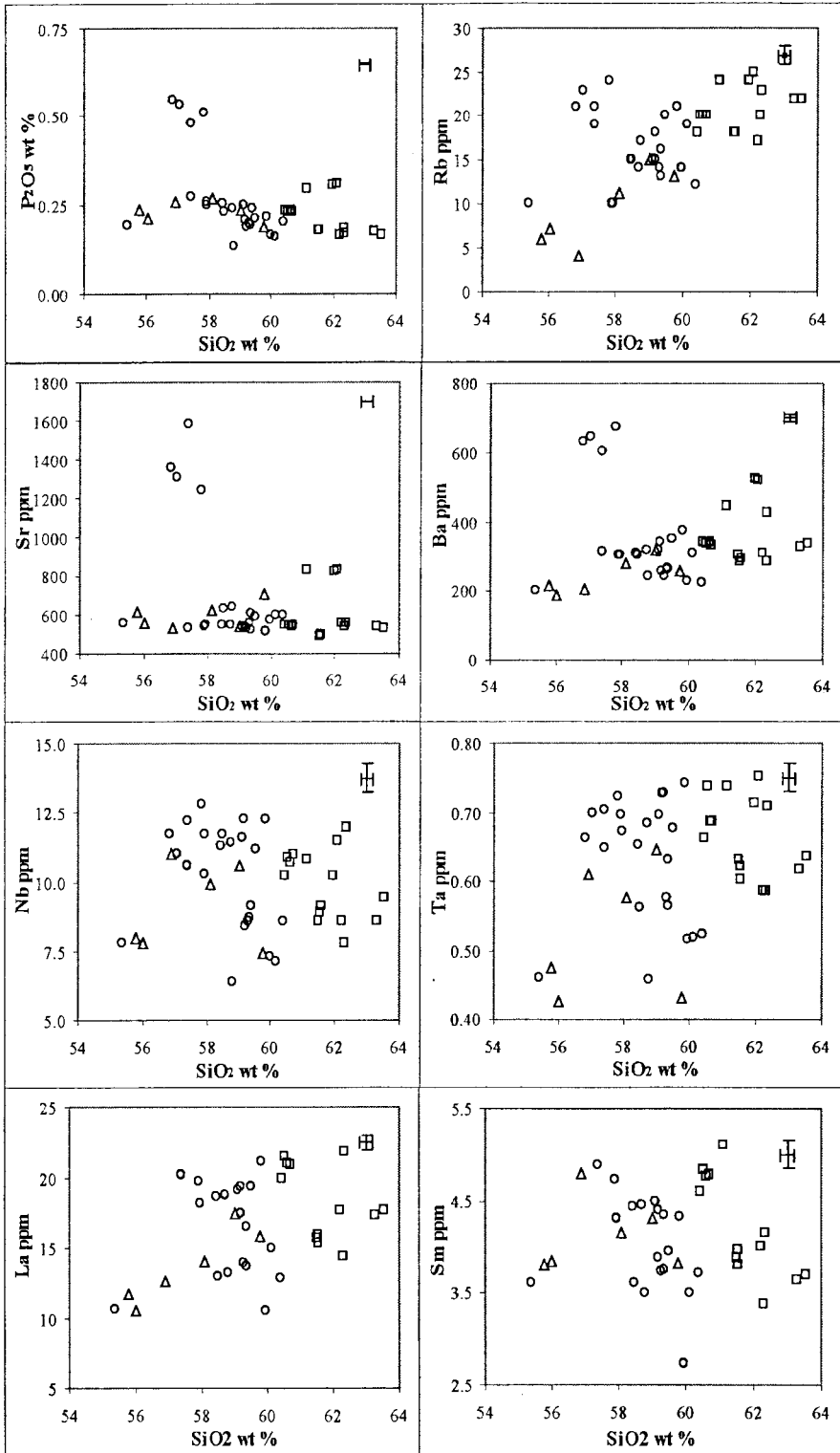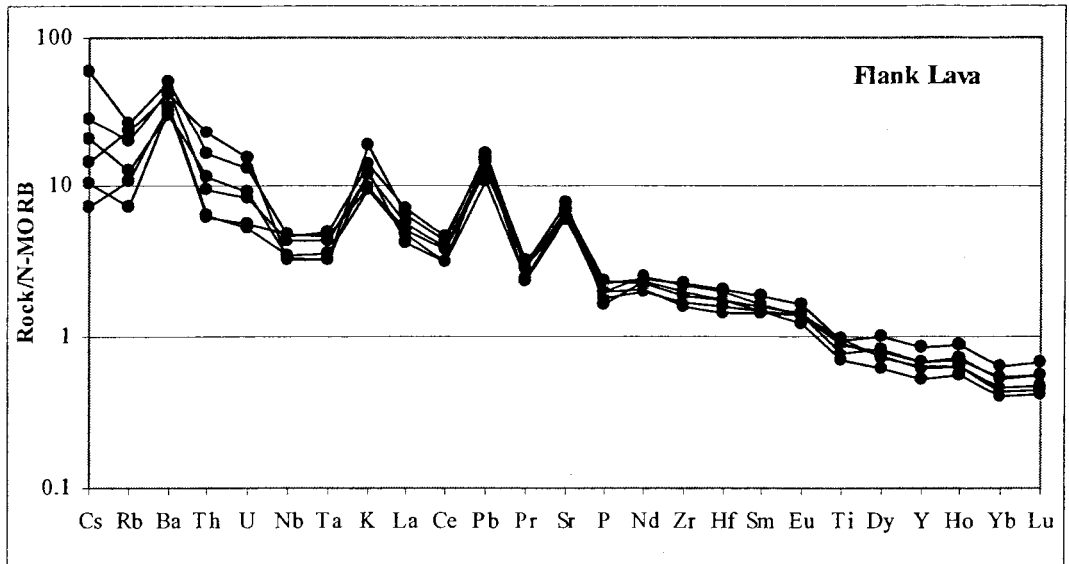
50

Figure 30 cont. -

51

Figure 31 – Spiderdiagram of the flank lavas normalized to N-MORM after Sun and McDonough, 1989.
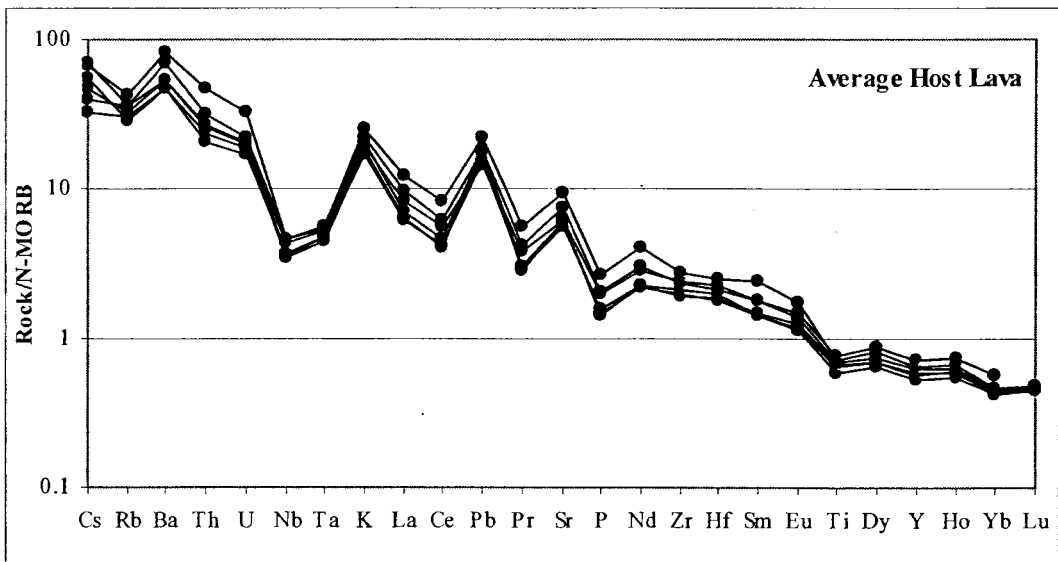
Figure 32 – Spiderdiagram of the average host lava composition at each site normalized to N-MORM after Sun and McDonough, 1989.
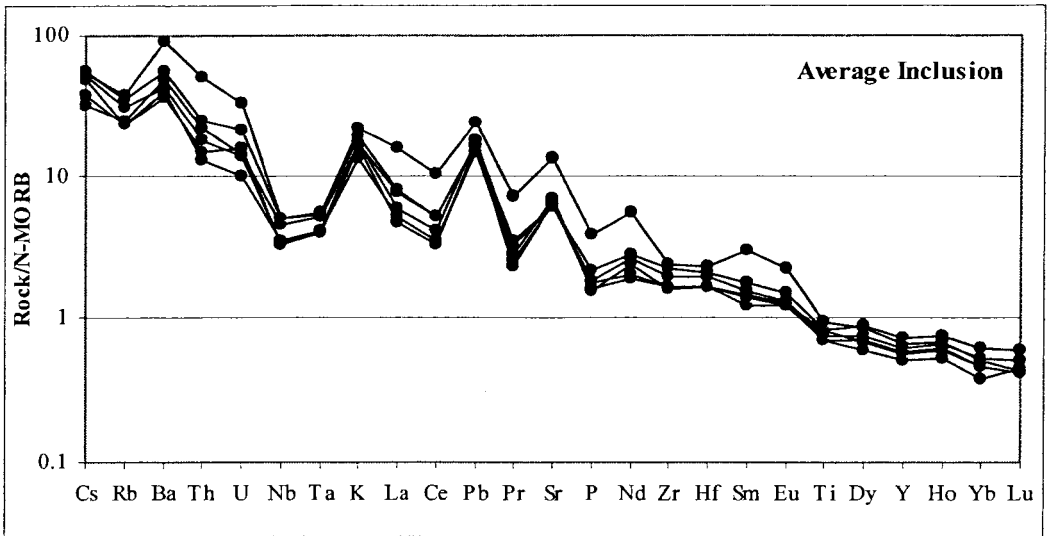
Figure 33 – Spiderdiagram of the average host lava composition at each site normalized to N-MORM after Sun and McDonough, 1989.

Figures 31, 32 and 33 are spiderdiagrams of the flank lavas, average host lava composition and average inclusion composition normalized to chondrite values presented by Sun and McDonough (1989). The trace elements on the x-axis are from left to right, most incompatible to least incompatible (Sun and McDonough, 1989). All three spiderdiagram illustrate a typical subduction zone signature in that they show enrichment in large ion lithophile elements (LILE), such as Rb, Ba, K, Pb, and Sr, and depletion in the high field strength elements (HFSE) such as Nb and Ta (Wilson, 1989). The top most line in Figure 32 represents site 0210, Laurence Lake, which is the most enriched site in terms of incompatible elements. Most often four of the five inclusion samples that were analyzed are easily identifiable on various scatter plots. For example, a review of the Harker diagrams presented in Figure 30 show that there are at least four points that are grouped together and lie above the remaining points. This is seen for most of the Harker diagrams. The cluster of four points represents four of the five inclusion samples that were analyzed from this site. They are also

53

easily identified in the TAS diagram (Figure 29). It shows that the average composition of the Laurence Lake inclusions is more enriched in incompatible elements in comparison to the average host lavas, indicating that the degree of enrichment must originate from the inclusions themselves and is not an artifact of the analyzing part of the host lavas. Reasons as to why this site has a higher concentration of trace elements will be discussed further in conjunction with chemical modeling

Compositional Relationships among Host Lavas and Inclusions

To illustrate the differences among the inclusions compared to the host lava within each site, I normalized the composition of each inclusion to the one of the host lava. The inclusions of each site generally are compositionally alike. Exceptions are two inclusion at site 0203 (U.S. Highway 26) and one inclusion at site 0210 (Laurence Lake). The two inclusions at site 0203 show a depletion of U in comparison to the other inclusions and the one inclusion is markedly depleted in comparison to the other four inclusions analyzed. Each of the spiderdiagrams also exemplifies the degree of enrichment of incompatible trace elements. Figures 34 and 35 are for sites 0203 and 0205 respectively, and the plots indicates that for most of the trace elements shown, they are either similar or slightly greater that the average composition for their respective host lavas.
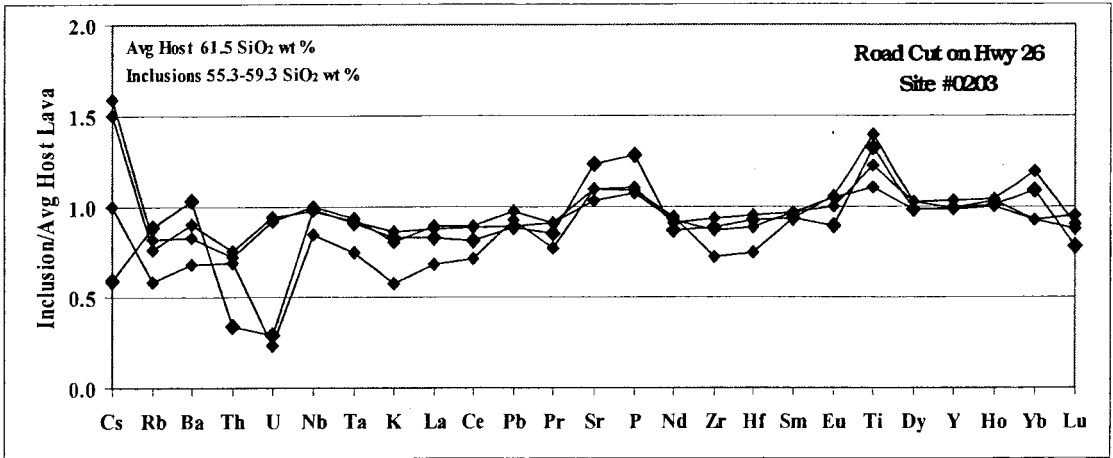
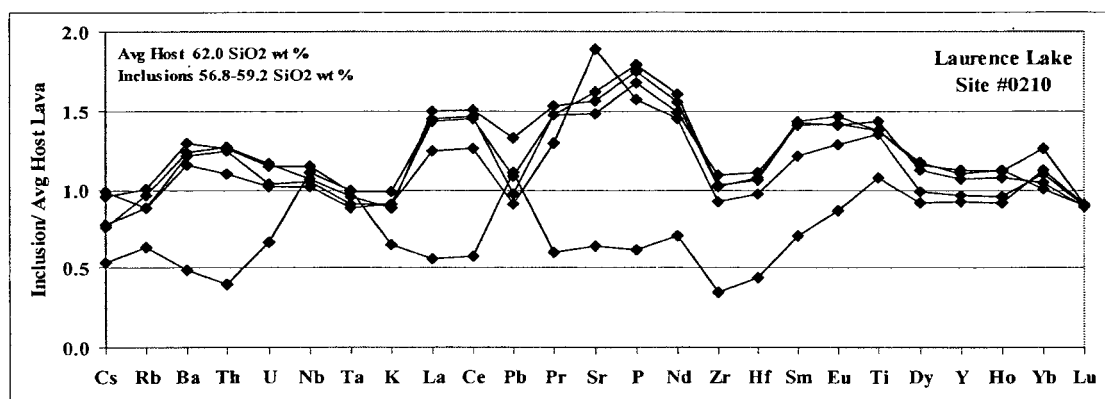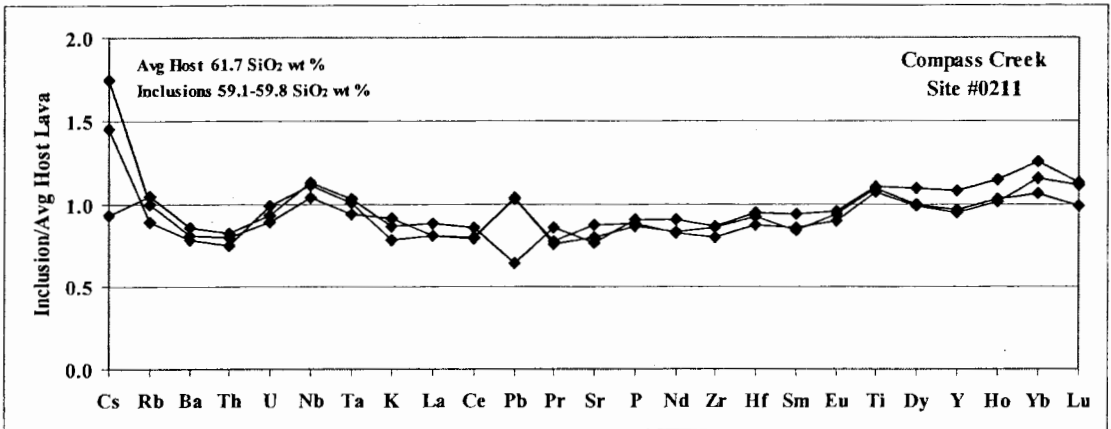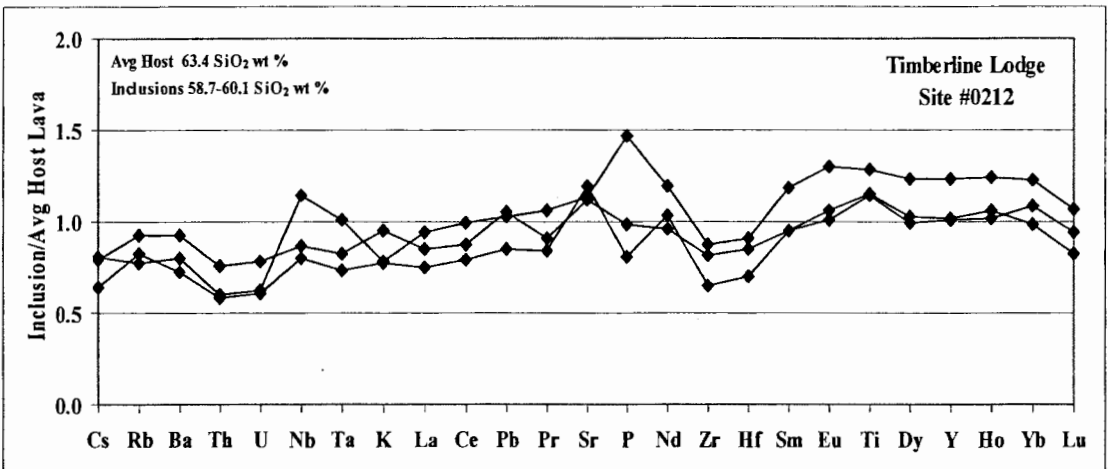Figure 34 – Spiderdiagram of the four analyzed inclusions from site 0203 normalized to the average host lava.
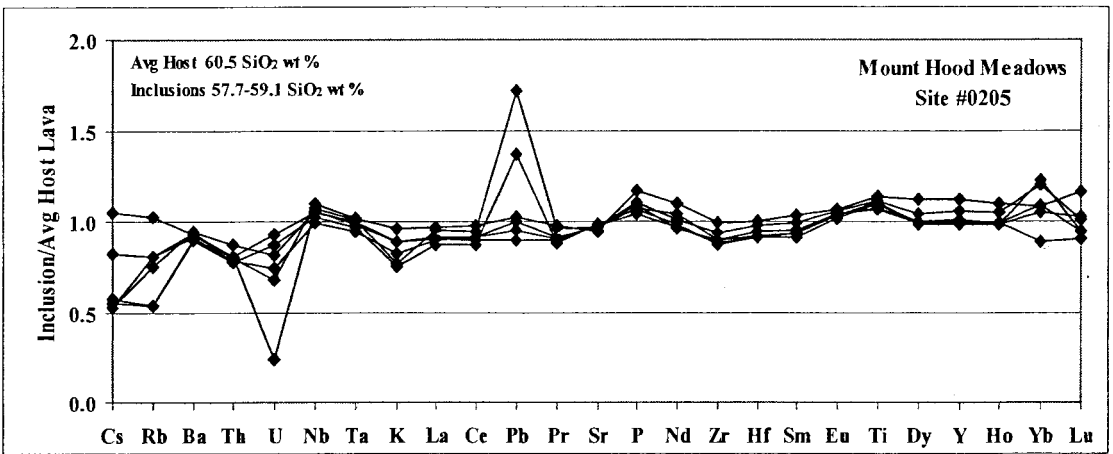
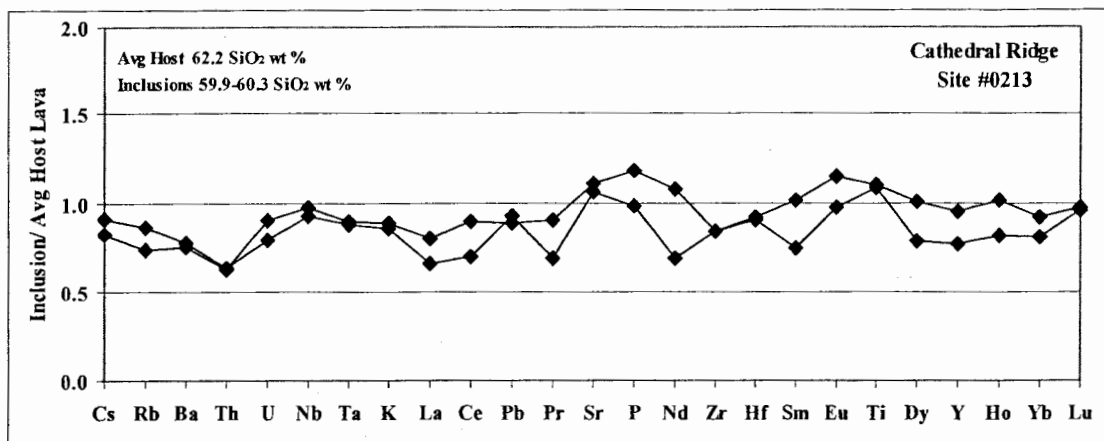Figure 35 – Spiderdiagram of the six analyzed inclusions from site 0205 normalized to the average host lava.

Figure 36 is the spiderdiagram for Laurence Lake; this site is the most enriched site that was sampled. Five of the sampled inclusions were analyzed. Four of the inclusions exhibit the same pattern in the spiderdiagram, but pattern produced by the fifth inclusion reflects the opposite pattern. The fifth inclusion shows that its incompatible trace element composition is less than the average host lava composition;

55

whereas the compositions of the other four inclusions show that they are much higher than the average host lava. The differences in concentration of trace elements may be due to the differences in the sizes of the inclusions. Filter pressing is a mechanism that can further modify the chemical composition of the magmatic inclusions (Sisson and Bacon, 1999). Interstitial melt is driven out of the inclusions into the host melt when the magmatic inclusions crystallize as they approach thermal equilibrium with the host, which in turn forces H_2O-rich gas to exsolve leading to an increase in the pressure within the inclusions. This way a pressure gradient towards the inclusion surroundings is created causing the melt to migrate out of the inclusion (Bacon, 1986; Sisson and Bacon, 1999). When the melt is squeezed out of the inclusion it carries with it incompatible elements that have not been partitioned into mineral crystals, thus an inclusion that has undergone filter pressing will show a marked depletion in the concentration of incompatible trace elements in comparison to other inclusions that have not undergone this process. The abnormal chemical composition of one of the five Laurence Lake inclusions (0210F) is interpreted as having undergone this filter pressing process leading to the observed depletion in incompatible elements compared to the other inclusions from this site.

Figure 36 – Spiderdiagram of the five analyzed inclusions from site 0210 normalized to the average host lava.

56

Figures 37, 38 and 39 illustrate the behavior of the trace elements in sites 0211, 0212 and 0213. The spiderdiagrams indicated that in these three sites, the trace element concentration in the inclusions is often greater than their respective host lava.

Figure 37 – Spiderdiagram of the three analyzed inclusions from site 0211 normalized to the average host lava.

Figure 38 – Spiderdiagram of the three analyzed inclusions from site 0212 normalized to the average host lava.

Figure 39 – Spiderdiagram of the two analyzed inclusions from site 0213 normalized to the average host lava.

In general, within each site there are examples where one or two inclusions differ from the remaining samples by being enriched or depleted in relation to other inclusions. The slight difference in comparison could possible reflect the difference in timing for inclusion formation.

Petrographic Features Correlating with Geochemistry

There are significant geochemical differences among flank lavas, mafic inclusions and host lavas (Figures 31-39). The most intriguing variations are those where samples with the same silica content vary strongly in incompatible major and trace elements. Furthermore, as silica increases the variability in incompatible element composition decreases. Along with these chemical signatures there are mineralogical characteristics that appear to correlate with the degree of enrichment at a given silica content. On the mafic silica end, depleted compositions as recorded by inclusions from sites 0203, U.S. Highway 26; 0205, Mount Hood Meadows; and two flank lavas (0201, Lady Creek and 0206, Cloud Cap Inn) contain only clinopyroxene

58

and orthopyroxene as mafic silicate phase. On the other end of the spectrum, inclusions from the most enriched site, 0210, Laurence Lake, have the highest proportion of amphibole and are generally poor in clinopyroxene. Inclusions from the other sites, 0211, Compass Creek; 0212, Timberline Lodge; and 0213, Cathedral Ridge, which are compositionally intermediate contain both amphibole and clinopryoxene in variable proportions. In other words, the amount of amphibole or amphibole to clinopryoxene ratio is larger with increasing degree of incompatible trace element enrichment at a given silica content.

Chemical Modeling of Inclusions and Host Lavas

In order to investigate further the petrogenesis of the inclusions and the host lavas three types of chemical models were constructed; crystal fractionation, magma mixing and assimilation fractional crystallization (AFC) models. Inclusion-bearing andesites at Mount Hood could have originated through any one of these processes or through any possible combination of these processes. The chemical modeling is based primarily on trace elements. I selected the following trace elements for chemical modeling: Rb, Sr, Ba, Th, Zr, Hf, Nb, Ta, Y, La, Ce, Eu, Tb, Yb, Cr and Sc. The selection of elements is based on a combination of the following: geochemical behavior (incompatible to compatible), geochemical affinity and analytical precision.

Crystal Fractionation

Crystal fractionation (or fractional crystallization) also known as Rayleigh fractionation quantifies the chemical effects to a magma composition if previously crystallized minerals are separated (removed) from the magma (Wilson, 1989; McBirney, 1993; Rollinson, 1993). Rayleigh fractionation is mathematically expressed by the following equation:

$$\frac{C_L}{C_O} = F^{(Dbulk-1)}$$

Equation 1

Where C_L = wt fraction of element in daughter
C_O = wt fraction of element in parent
F = amount (percentage) of melt remaining
D_{bulk} = bulk distribution (partition) coefficient

For this study, C_L was chosen to be the host lavas as they are the most silicic rocks, and C_O is either flank lava or inclusion material since both of these rock types are more mafic than the host lavas. The bulk distribution (partition) coefficient, D_{bulk}, is dependent on the composition of the melt (including temperature and pressure of crystallization), the modal proportion of the minerals present and the oxidation state of the trace element.

Since the bulk distribution (partition) coefficient is dependent on several factors, it was necessary to calculate a value for each trace element and for each inclusion site and for each flank lava that was chosen for the model. I used the modal proportions presented in Table 4 for the flank lavas, inclusions and host lavas. Partition coefficients were taken from Rollinson (1993), and were selected on the basis

of the type of igneous rock, whether or not the rock is basaltic andesite or andesite.

The bulk distribution coefficient was calculated using the following equation:

$$D_{bulk} = \Sigma x_i D_i$$

Equation 2

Where x_i =   modal proportion of mineral i
        D_i =   distribution coefficient of element for mineral i

The values of the D_{bulk} reflect the overall behavior of trace elements within the rocks sampled. If D_{bulk} has a value greater than 1, then it is said that the trace element is compatible; in other words, the element will be incorporated into a crystal lattice during crystallization, thus it will be preferentially removed from the melt. On the other hand, if D_{bulk} has a value less than 1, then it is said to be incompatible and prefers to remain in the melt.

Table 6 - Calculated bulk partition coefficients for the flank lava and inclusions.

	Flank Lava	Mafic Inclusions					
	Site 0204	Site 0203	Site 0205	Site 0210	Site 0211	Site 0212	Site 0213
SiO_2 Wt %	55.77	58.13	58.25	57.66	59.51	59.43	60.18
	Basaltic Andesite	Andesite	Andesite	Andesite	Andesite	Andesite	Andesite
Rb	0.054	0.039	0.039	0.037	0.036	0.038	0.035
Sr	1.271	1.011	1.005	0.675	0.698	0.713	0.671
Ba	0.163	0.102	0.101	0.091	0.081	0.089	0.080
Th	0.010	0.030	0.031	0.072	0.051	0.061	0.056
Zr	0.055	0.059	0.061	0.475	0.224	0.364	0.271
Hf	0.259	0.030	0.029	0.185	0.095	0.149	0.111
Nb	0.039	0.247	0.254	0.611	0.408	0.492	0.472
Ta	0.298	0.068	0.065	0.222	0.132	0.186	0.153
Y	0.124	0.299	0.292	0.973	0.575	0.791	0.681
La	0.285	0.268	0.270	0.328	0.245	0.279	0.274
Ce	0.228	0.180	0.181	0.276	0.189	0.235	0.209
Sm	0.200	0.146	0.146	0.738	0.356	0.568	0.436
Eu	0.353	0.866	0.857	1.078	0.781	0.960	0.845
Yb	0.204	0.151	0.149	0.617	0.351	0.502	0.406
Cr	13.602	9.286	9.316	16.471	12.204	13.374	14.615
Sc	0.282	0.974	0.985	3.956	2.578	3.398	2.768

61

There are several ways one can solve the Rayleigh fractionation equation (Equation 1). One way is to solve for C_L, the concentration of the trace element in the host lava. If C_L is our unknown, the other unknown is the amount of fractionation, "F". Thus, F was varied to see which fractionation amount could produce observed concentrations. In order to do this, the amount of melt remaining (F) was varied from F=1 (100% melt) to F=0.35 (35% melt remaining). Graphs were plotted to illustrate modeling results (Figures 40, 41, Appendix C). Figure 40 shows selected results for the most depleted site, 0203 (U.S. Highway 26), where Figure 41 shows selected results for the most enriched site, 0210 (Laurence Lake).

Equation 1 could also be solved for F assuming C_O is the average composition of the inclusions and C_L are the associated host lavas (Appendix A). Average values of the inclusions and host lavas for each site (Appendix A) were used in these calculations. Two scenarios of fractionation were modeled. In the first scenario, the parental magma was assumed to be equivalent to the inclusion magma. In the other, the parental magma was the most depleted flank lava sampled (sample 0204). The results are presented below in Tables 7 and 8. Ideal model fit would include the following for both modeling approaches: (1) F would fall between 0 and 1 (i.e. 100% to 0% crystallization if percent crystallization is equal to F-1), (2) values of F are in concordance with each other, and (3) C_L would model the observed concentration.

In general, results for modeling C_L (assuming the inclusions as parental magma) indicate that (a) if the concentration of an incompatible trace element is greater (vice versa for compatible elements) in the inclusion than in the host lava, then no amount of fractionation was able to produce observed values, (b) if the

62

concentration of the trace element in the host lava and inclusion are approximately the same (± within analytical uncertainty), then observed values could not be reproduced by the model, and (c) for some of the trace elements modeled, observed values could be modeled however typically yielding discordant fractionation amounts (Figures 39, 40). Similarly modeling F indicates (a) when the most depleted flank lava (sample 0204) is assumed to be the parental magma, most of the observed host lava compositions could be produced by fractionation, and (b) when the inclusions are the parental magma, fewer observed host lava compositions could be produced.
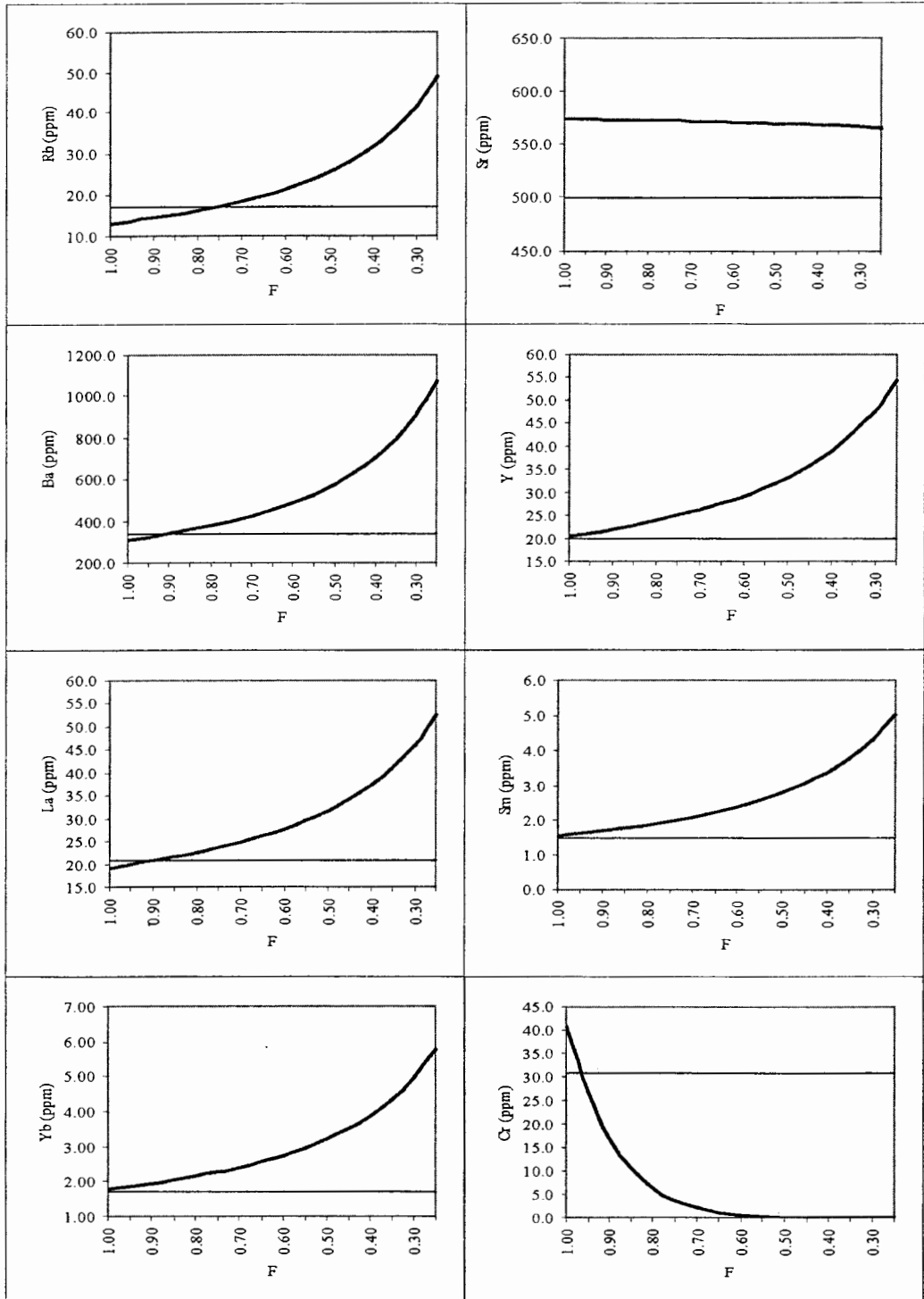
Figure 40 – Plots illustrating the behavior of selected trace elements for site 0203, road cut along U.S. Highway 26, the most depleted site. The solid horizonal lines indicate the modeled trace element concentration in the host lava. These plots were generated assuming that the inclusions were the parental magma (C_O). Models for Sr, Y Yb and Sm do not reproduce observed concentrations , while the other elements (Rb, Ba, La, Cr) yield strongly discordant amounts of fractionation.
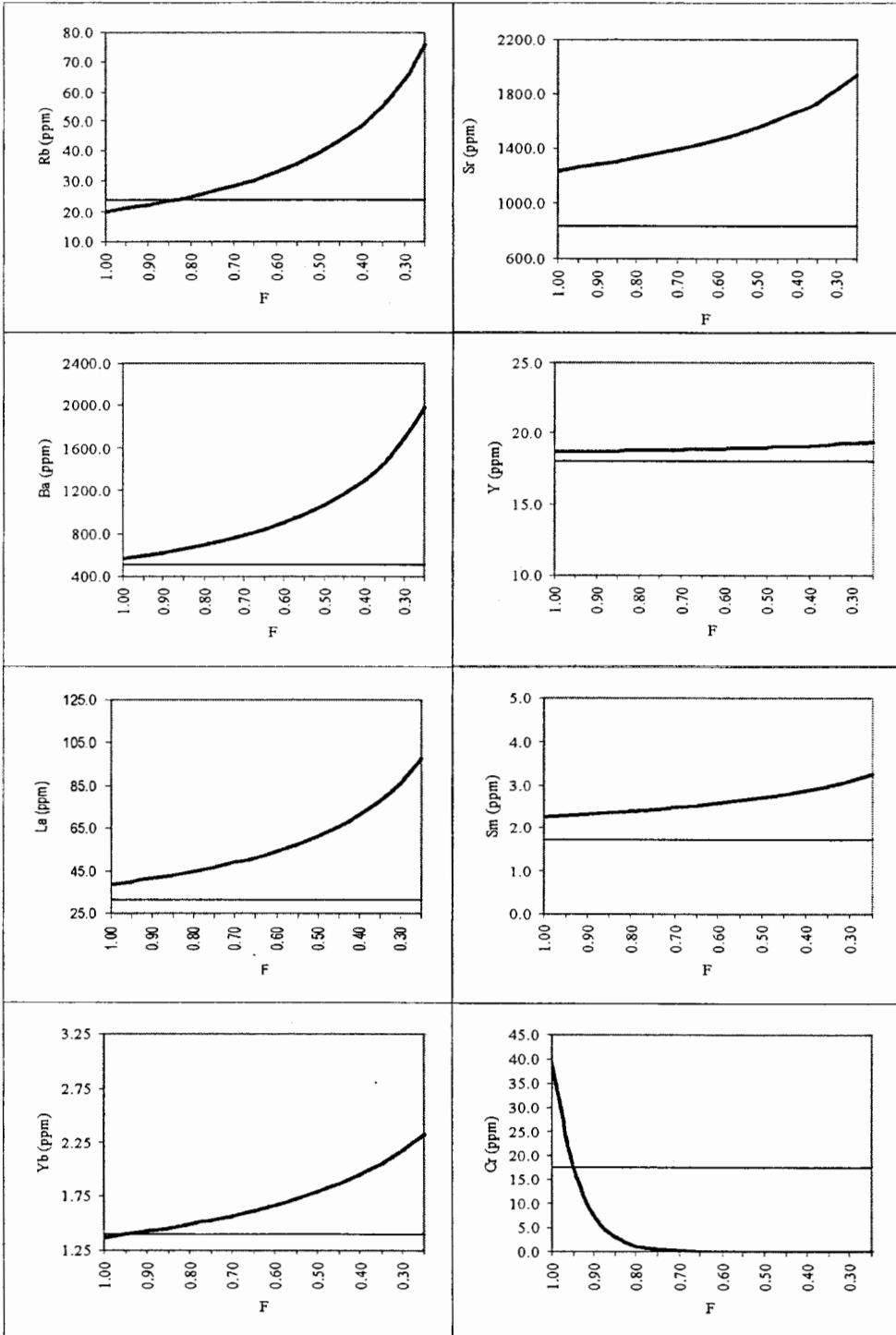
Figure 41 – Plots illustrating the behavior of selected trace elements for site 0210, Laurence Lake, the most enriched site. The solid horizonal lines indicate the modeled trace element concentration in the host lava. These plots were generated assuming that the inclusions were the parental magma (C_O). Model for Sr, Y, Ba, La, and Sm do not reproduce observed concentrations and the other elements (Rb, Yb, Cr) require 5-17% of fractionation.

65

Table 7 - Calculation of the amount of fraction of melt remaining using Equation 1. The results in this table were calculated using the most depleted flank lava (sample 0204) as the parental magma (C_O). Bold numbers indicate no model solution (of $F \leq 0$ or ≥ 1).

	Site 0203	Site 0205	Site 0210	Site 0211	Site 0212	Site 0213
Rb	0.33	0.30	0.23	0.27	0.27	0.34
Sr	0.44	0.61	**2.87**	0.60	0.58	0.62
Ba	0.67	0.58	0.35	0.43	0.60	0.72
Th	0.31	0.24	0.13	0.20	0.23	0.27
Zr	0.77	0.58	0.51	0.60	0.68	0.72
Hf	0.71	0.56	0.48	0.60	0.64	0.74
Nb	0.87	0.74	0.68	0.69	0.89	0.94
Ta	0.68	0.57	0.53	0.54	0.66	0.73
Y	**1.09**	0.87	0.97	**1.06**	**1.20**	**1.12**
La	0.67	0.45	0.25	0.37	0.57	0.64
Ce	0.69	0.48	0.29	0.41	0.62	0.86
Sm	0.28	0.22	0.15	0.22	0.30	0.30
Eu	0.30	0.24	0.18	0.25	0.34	0.33
Yb	0.97	0.72	0.93	0.93	**1.02**	0.98
Cr	0.96	0.93	0.89	0.91	0.90	0.91
Sc	**1.36**	**1.27**	**1.64**	**1.57**	**1.75**	**1.58**

Table 8 - Calculation of the amount of fraction of melt remaining using Equation 1. The results in this table were calculated using the average composition of inclusions from each site as the parental magma (C_O). Bold numbers indicate no model solution (of $F \leq 0$ or ≥ 1).

	Site 0203	Site 0205	Site 0210	Site 0211	Site 0212	Site 0213
Rb	0.75	0.71	0.83	0.90	0.78	0.80
Sr	**0.00**	**2.72**	**3.36**	**1.01**	**1.68**	**1.22**
Ba	0.78	0.90	**1.09**	0.78	0.80	0.77
Th	0.63	0.81	**1.13**	0.77	0.65	0.63
Zr	0.87	0.98	0.97	0.89	0.76	0.85
Hf	0.87	0.94	0.91	0.90	0.79	0.90
Nb	0.93	**1.06**	**1.23**	**1.15**	0.87	0.90
Ta	0.87	0.99	0.93	**1.04**	0.82	0.87
Y	0.97	**1.03**	**3.82**	**1.10**	**1.47**	0.71
La	0.76	0.89	1.37	0.78	0.80	0.65
Ce	0.79	0.90	1.37	0.78	0.85	0.89
Sm	0.94	0.95	**2.24**	0.82	**1.07**	0.79
Eu	0.97	**1.33**	0.04	0.72	**18.18**	**1.45**
Yb	0.96	**1.04**	0.94	**1.14**	**1.11**	0.83
Cr	0.95	0.97	0.95	0.95	0.97	0.99
Sc	**37808.28**	**18642.24**	0.91	0.87	0.88	0.94

Magma Mixing

Magma mixing involves mechanical mixing of magmas, and is governed by rheological and fluid dynamical properties. Magma mixing typically indicates open system processes and leads to chemical disequilibrium among phenocryst phases (Russell, 1990). Based on petrographic evidence all rocks sampled are to some extent hybrid lavas, having experienced magma mixing.

To evaluate mixing scenarios, I calculated various magma mixing models. The basic equation is expressed as:

$$C_h = C_s X_s + C_m (1 - X_s)$$ **Equation 3**

Where C_h = wt fraction of element in hybrid mixed lava
C_m = wt fraction of element in mafic end member
C_s = wt fraction of element in silicic end member
X_s = fraction of silicic end member
$(1-X_s)$ = fraction of mafic end member

The next question was how will I be able to devise mixing models in which observed data can be used as model constraints as much as possible. The following systematics were instrumental for setting up model approaches: existence of (1) inclusion-host lava pairs in which inclusion represents the more mafic composition and (2) wider trace element spread at lower silica contents and narrow spread at higher silica contents.

Mixing between two end members is expressed on element-element diagrams as straight lines between end members. In other words, mixed magmas at variable mixing proportions will all plot on a straight line between the silicic and mafic end members. If one knows one end member and one mixed product, one can construct a

vector on which the other end member must lie. If I take the inclusion as the mafic end member and the andesitic as mixed product then this gives me a vector towards the silicic end. Based on this, I was able to calculate the composition of a hypothetical silicic end member, by constructing scatter plots (Harker diagrams) of all major elements and the same trace elements used in the fractionation model (Figure 42, Appendix D). The composition of the hypothetical silicic end member is presented in Table 9.

Table 9 - Calculated hypothetical silicic end member (HSEM). For all elements, except SiO_2, the hypothetical value represents the amount of element (y axis) and the SiO_2 content is the amount of SiO_2 (x-axis). The value of SiO_2 marked by an asterisk is the average of SiO_2 values listed in the SiO_2 content column. Some values presented below (i.e. K) differ from those presented in Appendix F. Changes in values were based on the linear plots.

Major Element	Hypothetical Value	SiO_2 content	Trace Element	Hypothetical Value	SiO_2 content
SiO_2	66.37*	--	Rb	25	67.00
Al_2O_3	16.60	67.00	Sr	475	65.50
TiO_2	0.60	67.00	Ba	400	67.00
$FeO*$	4.00	67.50	Th	4	66.00
MnO	0.08	65.50	Zr	175	66.00
CaO	4.00	68.00	Hf	5	66.00
MgO	1.50	68.00	Nb	9	67.20
K_2O	1.80	69.00	Ta	0.7	66.00
Na_2O	4.50	67.00	Y	16	64.50
P_2O_5	0.18	65.50	La	20	64.50
			Ce	40	65.50
			Sm	2	65.00
			Eu	0.75	65.75
			Yb	1.2	66.25
			Cr	10	65.00
			Sc	8	67.50
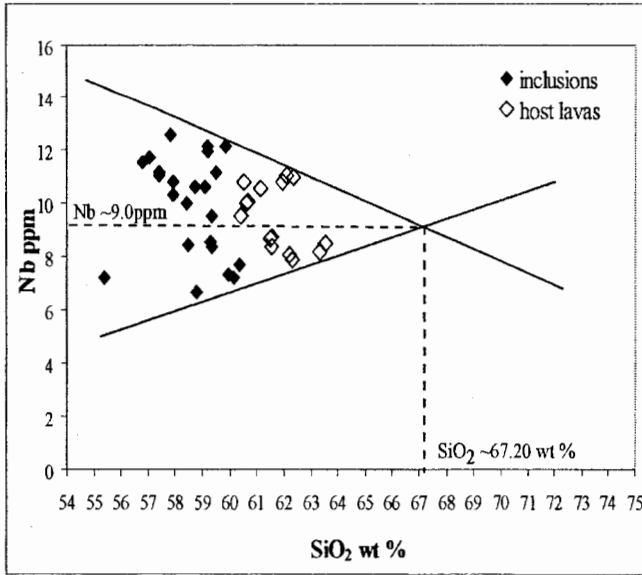
**Figure 42 – An example of how the composition of
the hypothetical silicic end member was calculated.**

The validity of the HSEM was tested by plotting the concentration of each
element on a corresponding Harker diagram of silicic lavas erupted during the
Pliocene in the vicinity of Mount Hood (Figure 43). It was found that the calculated
HSEM fell within the compositional range for historically erupted silicic lavas at or
near Mount Hood.

Now that the composition of a silicic end member is estimated, one is able to
calculate the mixing proportion between the inclusion and silicic end member using
the following equation:

$$C_{HL} = x\% C_I + (1 - x\%) C_{HSEM}$$ **Equation 4**

Where C_{HL} =   wt fraction of element in host lava
       C_I =   wt fraction of element in inclusion
     C_{HSEM} =   wt fraction of element is hypothetical
                       silicic end member
       $x\%$ =   fraction of mixing proportion

Solving Equation 4 for x% yields the amount of inclusion material that mixed with the HSEM to produce the host lava. There is no mixing solution if x% does not fall between 0 and 1. If a value was negative, the concentration of an element in the HSEM was greater than either the host lavas or the inclusion. If a value was greater than 1, then the difference between the host lava and HSEM was greater than that of the inclusion and the HSEM. For example, at site 0203, U.S. Highway 26, the result for Rb was 0.52, indicating that in order to produce a host lava containing an average concentration of 18.8 ppm Rb, a mixture of 52% inclusion (average concentration of 13 ppm) and 48% HSEM (25 ppm) was needed. The model worked well for the major elements, except for P_2O_5 and moderately well for the trace elements (Table 10).
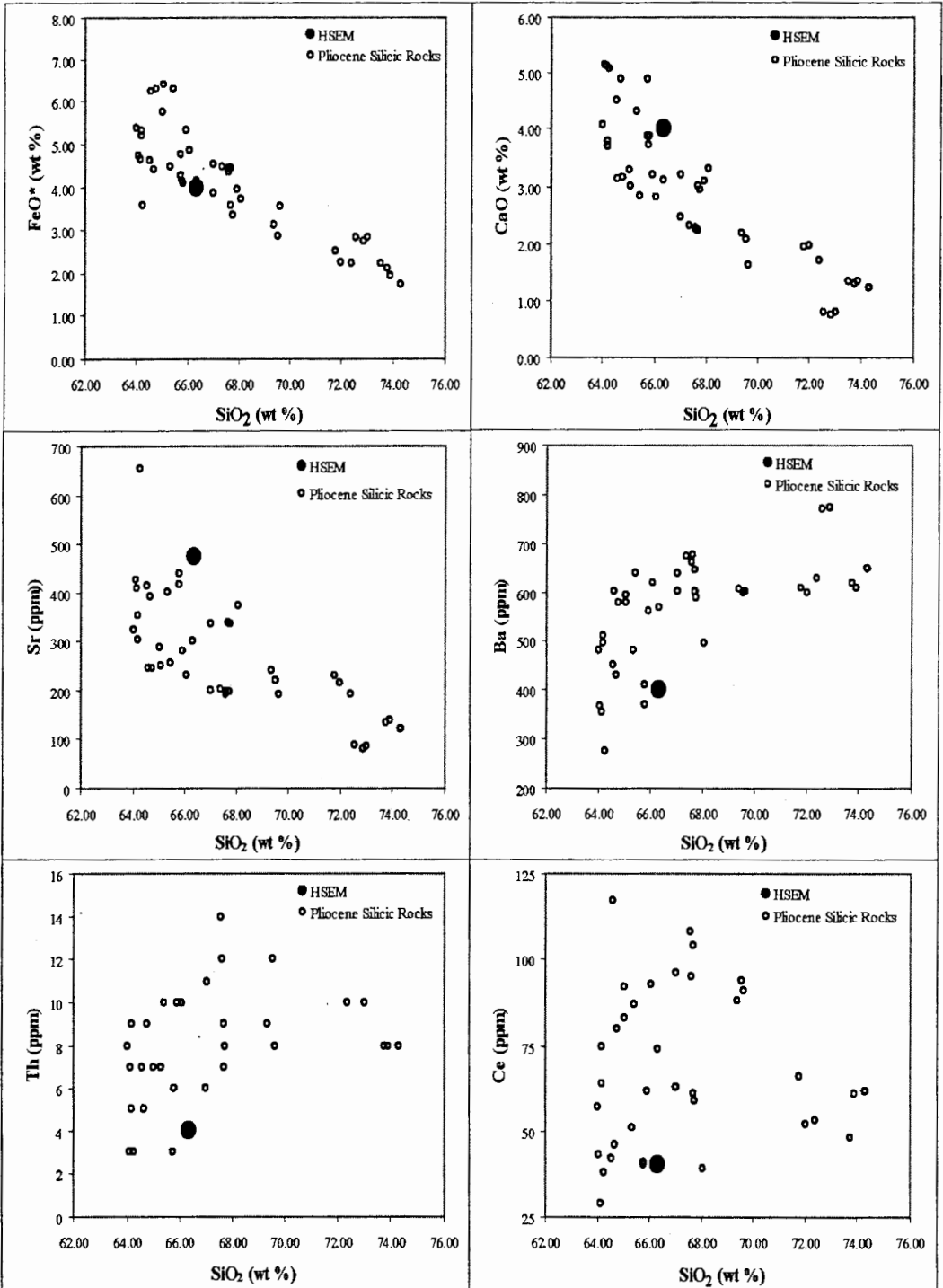
Figure 43 –Harker diagrams illustrating that the hypothetical silicic end member plots within silicic rocks erupted at or in the vicinity of Mount Hood during the Pliocene.

71

Table 10 - Amount of inclusion material (wt fraction) at each site required to mix with the hypothetical silicic end member to produce the host lava at each site. Bold values indicate mathematically invalid results.

	Site 0203 US Hwy 26	Site 0205 Mt. Hood Meadows	Site 0210 Laurence Lake	Site 0211 Compass Creek	Site 0212 Timberline Lodge	Site 0213 Cathedral Ridge
SiO2	0.71	0.71	0.50	0.67	0.42	0.66
Al2O3	0.65	0.69	0.43	0.53	0.24	0.63
TiO2	0.81	0.79	0.51	0.79	0.52	0.75
FeO*	0.78	0.71	0.58	0.67	0.53	0.68
MnO	0.75	0.70	0.60	0.70	0.61	0.60
CaO	0.71	0.76	0.52	0.71	0.50	0.72
MgO	0.68	0.81	0.59	0.74	0.63	0.81
K2O	0.64	0.79	0.60	0.72	0.74	0.83
Na2O	0.66	0.98	0.63	0.34	0.42	0.67
P2O5	**2.28**	0.73	0.47	**1.89**	**15.73**	**-2.87**
Rb	0.52	0.55	0.23	0.70	0.50	0.73
Sr	0.74	**1.04**	0.47	2.81	0.43	0.66
Ba	0.09	0.28	0.81	**-38.57**	0.21	0.53
Th	0.34	0.58	0.71	0.22	0.41	0.55
Zr	**-0.05**	**-21.00**	1.15	0.06	0.47	0.64
Hf	0.30	0.66	**-0.33**	0.65	0.56	0.80
Nb	**-0.45**	0.56	0.61	0.57	0.67	0.78
Ta	0.03	0.41	**-4.01**	0.47	0.44	0.63
Y	5.05	0.93	0.82	0.71	0.00	**-1.09**
La	**-0.91**	1.82	0.66	2.38	**-0.27**	0.17
Ce	**-0.94**	1.80	0.64	3.08	**-0.06**	0.76
Sm	1.12	1.07	0.74	1.27	0.94	1.38
Eu	1.46	0.92	0.66	1.17	0.74	0.86
Yb	2.25	0.92	1.09	0.76	0.81	1.69
Cr	0.33	0.68	0.26	0.43	0.49	0.76
Sc	0.68	0.78	0.60	0.66	0.56	0.82

Despite some inconsistencies (i.e. P_2O_5, Zr, La, Ce), Table 10 indicates the following results. Major elements largely indicate a very similar x%, although single elements (P or Na) may divert from this. Trace elements indicate a similar match but there are some sites (i.e. 0203) where trace elements yield poor concordance.

To take this modeling approach a step further, we can investigate what the mafic end member should look like if inclusion material and host lava are both treated as mixtures, although at different proportions and using the calculated HSEM as silicic

mixing member. Doing so is supported by the fact that inclusion and host lavas show petrographic evidence for being both hybrid lavas. For this purpose I redefined the variables in Equation 4 to construct the following equation:

$$C_{HL} = C_{HSEM}X + X_{HMEM}(1 - X_{HSEM})$$ **Equation 5**

Where C_{HL} = wt fraction of element in host lava
C_{HSEM} = wt fraction of element in silicic end member
C_{HMEM} = wt fraction of element in mafic end member
X_{HSEM} = fraction of mixing proportion

Instead of solving for X as in Table 6, I solved for C_{HMEM} in order to construct a composition for a hypothetical mafic end member. By varying the amount of X_{HSEM}, I was able to calculate the compositions of two hypothetical mafic end members, one being basaltic (49 wt % SiO_2) and one being basaltic andesitic (54 wt % SiO_2). Hypothetical mafic end members were calculated for each inclusion-bearing site (Table 11).

As with the calculated HSEM, I wanted to see if the compositions of the hypothetical mafic end members (HMEM's) largely reflect compositions of mafic lavas that had been erupted at or near Mount Hood, and thus supporting the existence of such magma for mixing to yield inclusions and host lavas. I tested the validity of the HMEM's in the same manner as I did for the HSEM. In this case, I plotted the two HMEM's (triangles and squares) from each inclusion-bearing site on Harker diagrams of primitive and mafic magmas that were erupted during the Pliocene and Quaternary in the vicinity of Mount Hood (Conrey, et al., 1997; Conrey, unpublished). Flank lavas collected during this study and flank lavas collected by C. Gardner (unpublished) were included on the Harker diagrams (Figure 44). It was found that the HMEM's do

plot within the range of erupted mafic magmas, and if mixing lines are drawn from the upper and lower boundaries of the HMEM, a mixing cone is formed which encompass the majority of the flank lavas indicating that the flank lavas may be hybrid lavas just as the inclusions and host lava.

Table 11 - Composition of hypothetical mafic end members for each inclusion-bearing site, both a basaltic mafic end member and a basaltic andesite end member.

|	Site 0203 U.S. Hwy 26		Site 0205 Mt Hood Meadows		Site 0210 Laurence Lake		Site 0211 Compass Creek		Site 0212 Timberline Lodge		Site 0213 Cathedral Ridge	
	B	BA	B	BA	B	BA	B	BA	B	BA	B	BA
SiO_2	49.01	54.00	48.99	54.00	49.01	54.01	49.01	54.02	49.03	54.01	48.99	54.02
Al_2O_3	19.15	18.42	19.34	18.54	18.12	17.68	19.31	18.53	19.65	18.77	21.20	19.86
TiO_2	1.45	1.21	1.69	1.38	1.79	1.45	1.66	1.36	1.52	1.26	1.55	1.28
FeO*	9.47	7.89	9.47	7.89	9.14	7.65	9.30	7.77	9.11	7.64	9.42	7.85
MnO	0.15	0.13	0.17	0.14	0.14	0.12	0.16	0.13	0.16	0.14	0.16	0.13
CaO	10.68	8.76	10.38	8.53	10.96	8.95	10.42	8.57	11.27	9.18	11.06	9.01
MgO	7.42	5.71	6.38	4.97	5.78	4.54	6.03	4.72	7.02	5.43	6.21	4.85
K_2O	-0.17	0.40	0.62	0.96	1.92	1.89	1.03	1.25	0.40	0.80	-0.18	0.39
Na_2O	3.70	3.93	3.45	3.76	3.67	3.91	3.79	3.99	3.25	3.61	2.79	3.28
P_2O_5	0.18	0.18	0.34	0.29	0.69	0.54	0.40	0.34	0.17	0.17	0.13	0.15
Rb	-3.77	4.51	5.73	11.30	20.38	21.71	6.77	12.03	3.08	9.39	-12.2	-1.44
Sr	562.6	5376	692.6	629.7	1908.7	1495	734.4	659.5	800.3	706.7	785.6	695.5
Ba	46.55	148.3	214.8	268.3	887.9	747.14	465.8	446.8	286.7	319.3	-97.3	46.91
Th	-1.52	0.07	1.55	2.26	10.81	8.84	3.12	3.38	0.35	1.40	-1.11	0.37
Zr	38.92	78.10	185.54	182.49	277.41	247.86	171.2	172.33	88.79	113.60	53.72	88.90
Hf	0.68	1.92	3.57	3.98	5.39	5.28	2.37	3.13	0.41	1.73	-0.68	0.97
Nb	6.21	7.16	11.29	10.77	15.14	13.51	14.27	12.89	9.93	9.80	2.97	4.87
Ta	0.41	0.49	0.70	0.70	0.83	0.79	0.78	0.76	0.52	0.57	0.21	0.35
Y	17.06	16.75	27.80	24.39	24.03	21.71	18.64	17.88	16.17	16.12	15.44	15.60
La	4.33	8.84	22.51	21.79	64.69	51.79	35.32	30.90	17.95	18.54	3.30	8.15
Ce	9.84	18.53	44.62	43.29	128.44	102.92	65.63	58.23	28.16	31.57	-17.4	-0.79
Sm	8.82	6.85	10.27	7.88	18.95	14.06	11.87	9.02	10.27	7.89	9.22	7.13
Eu	2.59	2.06	2.95	2.31	4.77	3.61	3.27	2.54	2.77	2.19	2.58	2.05
Yb	2.26	1.90	3.14	2.52	2.61	2.14	2.50	2.07	2.48	2.05	2.49	2.06
Cr	153.2	112.0	72.50	54.43	40.12	31.43	62.63	47.43	74.04	55.61	65.32	49.27
Sc	29.94	23.62	28.45	22.54	25.32	20.32	25.74	20.62	29.75	23.49	27.79	22.05
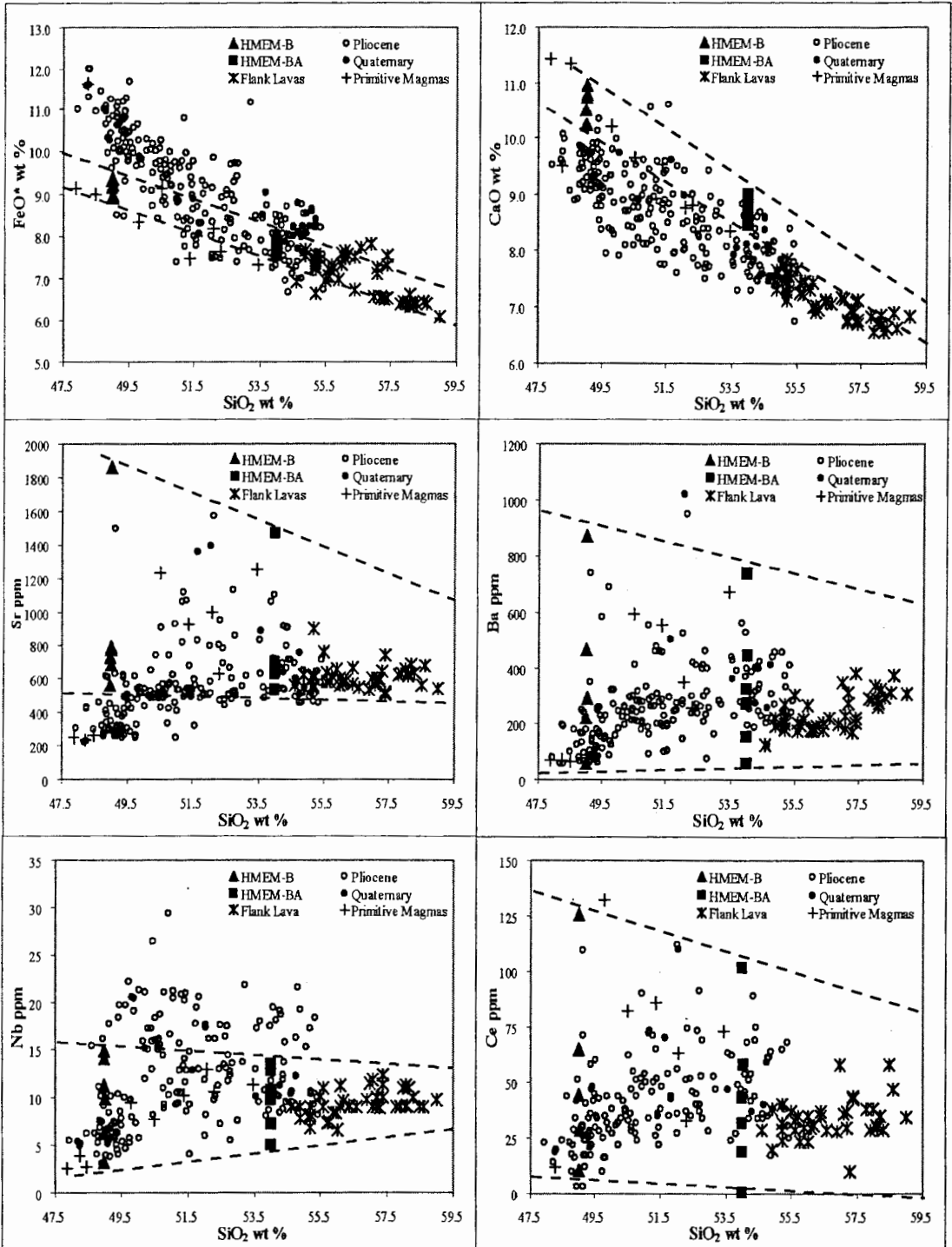
Figure 44 - Selected Harker diagrams illustrating that the hypothetical mafic end members plot within mafic and primitive rocks erupted in the vicinity of Mount Hood during the Pliocene and Quaternary. Flank lavas are plotted as well. The dashed lines represent the upper and lower "mixing" boundaries established by the HMEMs; note that the mixing lines encompass most of the flank lavas. Plots for Nb and Ce show a linear trend among the flank lavas, this is due to chemical analyses reported around the detection limits for analytical instrumentation (XRF at USGS Denver).

75

I have evaluated the composition of the HMEM further by constructing linear correlation plots for each element. Lines were drawn through the calculated end members and the host lava, which represent the mixing lines of the system. When the composition of HMEM, basalt or basaltic andesite, mixed with the HSEM, the host lava and inclusion should fall on the line connecting the two end members. Since I did not use the composition of the inclusions to calculate the HMEM, I can use the composition of the inclusion to check for internal consistencies for the hypothesis that inclusions and host lavas resulted from mixing of the same end members however at different proportions. In most cases, the inclusions were either on or close to the line (Figure 45, Appendix F). In some instances the inclusion is neither on nor close to the mixing line. This may reflect that the HMEM's was either depleted or enriched in comparison as to what the actual mafic mixing end member was at the time of mixing.
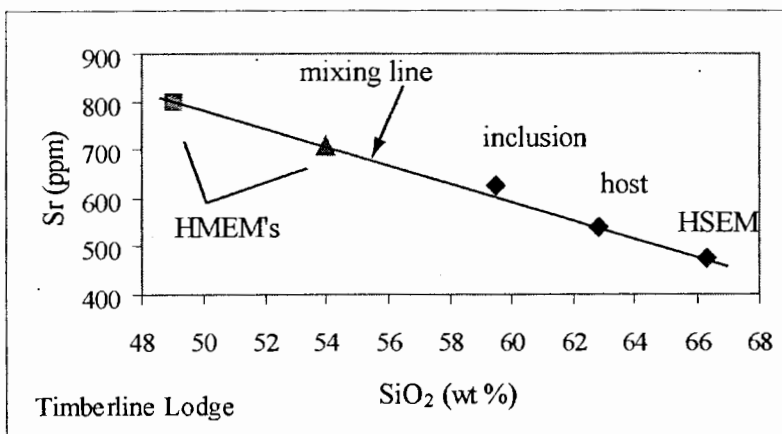
Figure 45 – Example of a linear correlation plot testing the validity of the magma mixing model.

Assimilation Fractionation Crystallization (AFC)

Assimilation fractionation crystallization is a process in which a magma is undergoing fractionation while concurrently assimilating the surrounding country rock and incorporating the foreign material into the melt, and according to Rollinson (1993) it is mathematically defined as:

$$\frac{C_L}{C_O} = f' + \frac{r}{(r-1+D_{bulk})} \bullet \frac{C_A}{C_O}(1-f')$$

Equation 6

and f' is defined as:

$$f' = F^{-(r-1+D_{bulk})(r-1)}$$

Equation 7

Where
C_L	=	wt fraction of element in the fractionating liquid
C_O	=	wt fraction of element in the originating liquid
C_A	=	wt fraction of element in the assimilating wall rock
r	=	ratio of the assimilation rate to the crystallizing rate
F	=	fraction of melt remaining
D_{bulk}	=	bulk partition coefficient

For the purposes of this model, C_L could be either the host lava or the HSEM and C_O could be inclusion material, flank lava material or the HMEM's. The variables r and F were set at multiple values, ranging from 0.1 to 0.99 for r and from 0.95 to 0.50 for F. If r =0, then Equation 6 reduces to the equation for Rayleigh fractionation (Equation 1) (Wilson, 1989). The D_{bulk} values are the same values used for the fractionation model, however the D_{bulk} values for the HMEMs had to be calculated. I first determined the CIPW normative values using the compositions of the HMEMs, which allowed me to determine a hypothetical mineral assemblage. The CIPW normative values were calculated by computing the major element composition in MAGMA, a freeware program distributed the Regents of the University of California.

Normalizing the amounts of each mineral to the total sum, I was able to determine a hypothetical modal proportion, which was then used in Equation 2 to calculate the D_{bulk} values. Equation 6 was algebraically rearranged to solve for C_A, the concentration of element in the wall rock

The goal of this model was to reproduce the reported concentrations of the inclusions. If the model calculations yielded a solution (i.e. an element concentration of a hypothetical contaminant) then this was called a successful model. On the other hand, if the calculation failed it means no concentration exists that could explain elemental budgets between HMEM and inclusion and between inclusions and host lavas. This approach, however, does not evaluate how geologically reasonable a certain assimilant concentration. The flank lava used in the modeling is sample 0204 as it is the most depleted. However, wanting to reproduce the values of the host lavas and inclusions it would be prudent not to include either one of these lavas into the equation, even though models involving flank lava-host lava, inclusion-HSEM, inclusion-host lava and HMEM-host lava interactions were constructed. All of these models with the exception of the flank lava-host lava model failed to model the host lavas and inclusions by producing negative values in the solution, and this occurred at a rate of 50% with respect to the number of modeled elements.

The flank lava –host lava model had a failure rate of 21%. The elements that failed to be modeled (negative solutions) developed three trends of failure among the inclusion-bearing sites. The most depleted sites, 0203 and 0205 had only one failed element each (Sc), the most enriched site (0210) had three failed elements (Sr, Y, Sc), and the moderately enriched sites had five failed elements each (Y, Sm, Eu, Yb, Sc).

78

The next successful model was the flank lava-HSEM model which had a failure rate of 20%. In all of the inclusion-bearing sites Y, Yb and Sc had failed to reproduce both host lava and inclusion concentrations, but Sr also failed at site 0210 only. The failure of Sr is due to it being strongly enriched in inclusions (average 1233 ppm) and host lavas (average 832 ppm), so it was not surprising that it failed to be modeled successfully.

The last model that yielded adequate results was the HMEM-HSEM model with a failure rate of 32%. As with the previous model (flank lava-HSEM) this model gave results that show the same elements fail among all of the inclusion-bearing sites. The elements that failed to be modeled are Y, Eu, Sm, Yb, and Sc. The behavior of Sr at site 0210 failed for both inclusion and host lava using the basaltic HMEM (49 wt % SiO_2), whereas only the inclusion failed to be modeled using the basaltic andesite HMEM (54 wt % SiO_2).

Comparing the AFC model to the fractionation model, the results varied depending on the fractionation model. Comparison of the two models, in which host lavas fractionated from the inclusion material, the AFC model appeared to be a marginally better model of the host lavas. However, comparison of the AFC model to the model that fractionated host lavas from the most depleted flank lava, it was found that the fractionation model was a better match.

CHAPTER 4 – DISCUSSION

Enriched vs. Depleted Sites

Ranking the host lavas by the (average) silica content, the sites from most mafic to most silicic are 0205 (Mount Hood Meadows), 0203 (U.S. Highway 26), 0211 (Compass Creek), 0210 (Laurence Lake), 0213 (Cathedral Ridge) and 0212 (Timberline Lodge). If the degree of enrichment of incompatible trace elements were dependent on silica content then it would be expected that site 0205 to be most depleted and site 0212 most enriched in incompatible elements because more silicic magmas that have experienced more fractionation would thusly be more enriched. The incompatible elements' tendency to accumulate in the melt results in their subsequent enrichment in the bulk composition (Blundy and Wood, 2003). In spite of this, it is site 0203 that is most depleted and site 0210 that is most enriched indicating that silica content has no direct influence on the degree of enrichment of incompatible elements in the samples analyzed from Mount Hood. Quantitative models of fractional crystallization confirm that fractional crystallization cannot be the main reason for inducing the variability in the degree of enrichment observed in incompatible elements. Thus, it appears that the enrichment was largely induced by mixing with compositionally variable mafic end members since there is a funneling effect towards higher silica, and AFC models suggest that assimilation cannot explain enriched patterns either (Figure 45, Appendix D). Spiderdiagrams illustrating the compositional relationship between individual inclusions and their host lavas (Figures 34-39) also support this theory by demonstrating that the relationship between the host

lava and inclusions point to the concentration of the incompatible trace elements being most often greater in the inclusions than the host lavas, thereby indicating that the source of enrichment is the mafic mixing end member

Scatter plots of selected major and trace elements in Figure 46 illustrate the relationship of mafic (basaltic) and silicic (dacitic to rhyolitic) lavas erupted and/or emplaced during the Pliocene and Quaternary within the vicinity of Mount Hood (Wise, 1969; Crandell, 1980; Conrey et al., 1997; Conrey unpublished). The mafic lavas, in general, exhibit a wider range of elemental concentration than the silicic lavas. If mixing lines were drawn to encompass the upper and lower values on each scatter plot, the result is funneling towards the silicic lavas for Al, Sr, and Ba, however there is no funneling seen in Na, Rb and Nb. Figure 47, shows the same scatter plots as in Figure 46, but with the addition of the flank lavas, host lavas and inclusions analyzed for this study (+'s). Both of these figures, especially Figure 46, clearly illustrate the funneling effect if mixing of variable mafic end member (as observed) with one dacite ($SiO_2 > 65$ wt %) is involved reproducing compositional range of calc-alkaline andesitic inclusions and host lavas of this study. The mixing trend is also seen in Figure 44 with the flank lavas and hypothetical mafic end members. Although, there is compositional variability among the silicic lavas as seen in Figures 46 and 47, it is for the most part that the enrichment of incompatible trace elements is from the mafic mixing end member and not the silicic end members because the host lavas vary much less than inclusions allowing for calculation of the hypothetical silicic end member.
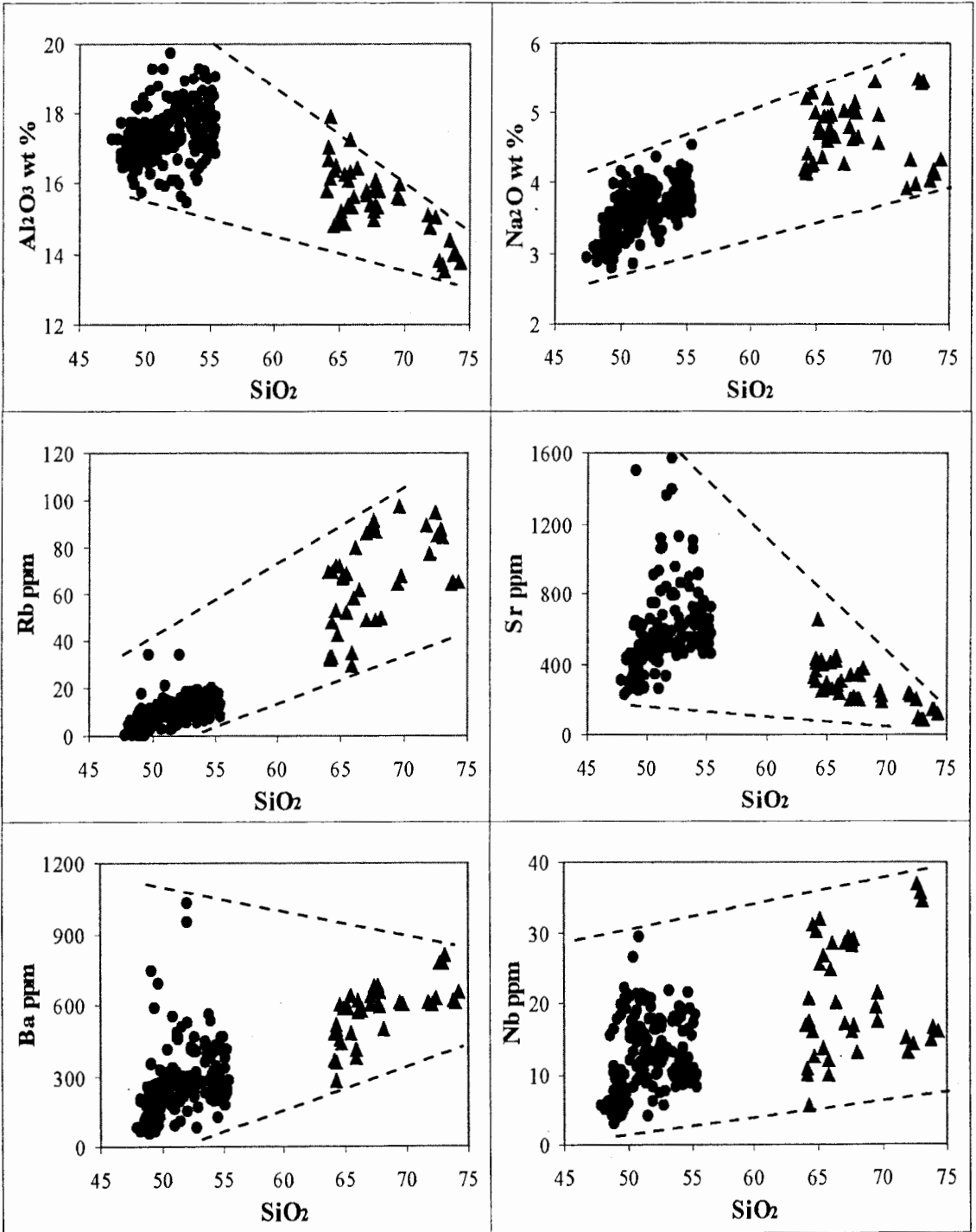
Figure 46 – Scatter plots of selected major and trace elements of mafic and silicic lavas from the vicinity of Mount Hood, both from the Pliocene (Conrey et al., 1997; Conrey unpublished). There is a general funneling effect that narrows toward the silicic lavas (Al, Sr, Ba). Circles represent the mafic lavas and the silicic lavas by the triangles. Pliocene andesites are not plotted.
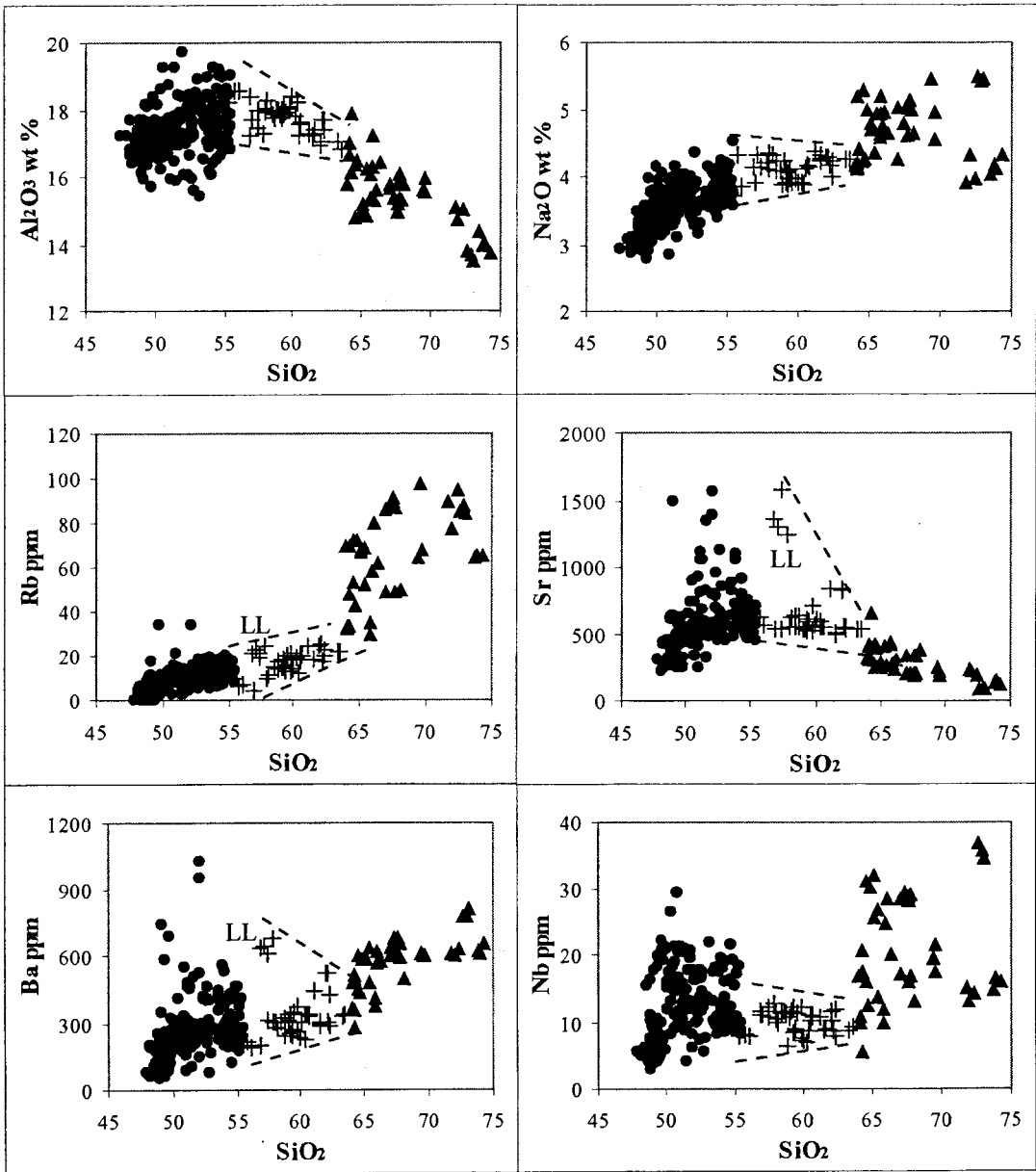
Figure 47 – The same scatter plots as the previous figure with the addition of all samples analyzed for this study (+'s). The scatter plots illustrate that the lavas erupted at Mount Hood fall in between the two possible mixing end members. "LL" represents the four highly enriched inclusions of from Laurence Lake, notice that the enrichment of these elements are due to the enrichment of the same elements in the mafic lavas. Pliocene andesites are not plotted.

Mineralogically, the main difference between the depleted sites and the enriched sites is the presence of amphibole found only in the enriched inclusion bearing sites. The concentration of amphibole is dependent on the degree of enrichment, and as this study demonstrates, White (1980) also found that the occurrence of clinopyroxene is inversely proportional to the occurrence of amphibole. Miniscule amounts of clinopyroxene have been found in samples of the enriched sites, however the clinopyroxene is found only in the inclusions and is absent in the host lavas. This implies that the clinopyroxene is a remnant of a mafic component that has been mixed with the contents of the magma chamber (Clynne, 1999).

The presence of amphibole can be attributed to either elevated bulk Na_2O concentrations and/or the presence of water in the magma. The bulk Na_2O concentrations for all samples analyzed do not indicate that there in an enrichment of Na_2O in the enriched sites in comparison to the depleted sites; instead all samples plot together (Figure 48). Therefore,
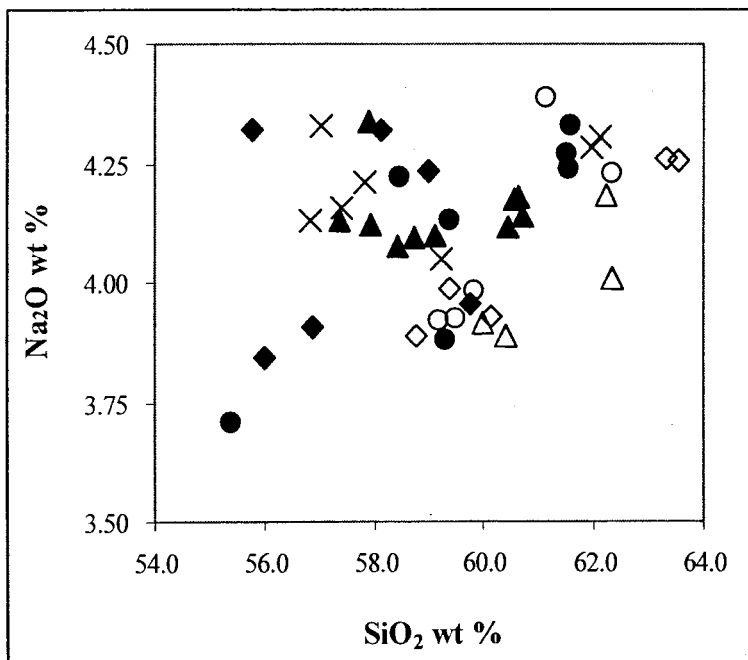
Figure 48 - Harker diagram illustrating the concentration of Na2O in the flank lavas (black diamonds) and the depleted (solid symbols) and enriched (open symbols and x's) inclusions bearing sites. All samples are found in a narrow range of Na2O (~1 wt %). Site 0203 = black circles; Site 0205 = black triangles; Site 0210 = x's; Site 0211 = open circles; Site 0212 = open diamonds; Site 0213 = open triangles

the presence of amphibole is thought to be due to the presence of water in the magma. According to Cribb and Barton (1997), calculations based on an H_2O dependent plagioclase hydrometer yielded H_2O values between 3.9-6.1 wt percent prior to eruption during the Pre-Polallie Period and White (1980) calculated a P_{H2O} range of 2.5-3.5 kbar based on the f_{O2} and plagioclase thermometry. These results are consistent for values calculated for Mount St Helens, which include 4.0 wt percent H_2O upon eruption for lavas erupted in the last 4,000 years (Gardner et al., 1995) and approximately 4-5 wt percent for the last 2,200 years (Smith and Lehman, 1993). Conditions had to have been at the correct criteria in order for amphibole to crystallize, which would be > 4 wt percent H_2O at 2 kbar (Gardner et al., 1995). Therefore, it is plausible to postulate that the depleted lavas contained a lower concentration of H_2O and that the enriched sites contained higher concentrations of water in the magma prior to eruption.

Petrogenetic Model

It has been hypothesized that the andesitic lavas flows and their inclusions are hybrid lavas formed by the mixing of mafic and silicic magmas, which is based on both chemical and petrographic observations as well as chemical modeling. Furthermore, the andesitic lava flows and their inclusions were formed predominately by magma mixing and crystal fractionation, while assimilation fractionation crystallization (AFC) plays a negligible role as petrogenetic process.

Magma mixing is a complex process that involves more than physical or mechanical mixing of two magmas, it also involves chemical diffusion between the

85

mixing magmas and thermal re-equilibration (Bacon, 1986; Thomas and Tait, 1997; Blake and Fink, 2000). Thermal re-equilibration occurring during hybridization of the mixing magmas is the process by which the temperature of the mafic magma will cool and the silicic magma will increase until some intermediate temperature is achieved. Once thermal re-equilibration has been achieved, the inclusion groundmass will have crystallized to a greater degree than that of the host groundmass (Coombs et al, 2002). The presence of inclusions indicates that complete mixing did not occur. During the mixing process pieces or blobs of the warmer hybrid magma that contained higher proportions of the mafic end member were undercooled or quenched against the hybrid containing more of the silicic end member, which is cooler. This resulted in the blobs to become rigid bodies, thereby preventing the complete homogenization of the mixing magmas. The textural features of the host lava/inclusion interface (rim), inclusion groundmass and various phenocrysts (host lava and inclusion) record thermal re-equilibration of mixing magmas.

Rims of the inclusions are usually crenulated and convex toward the host, which is a result of the temperature difference between the host and inclusion. Crenulation indicates a liquid/liquid interaction, and is best observed when there is a relatively large temperature difference (Bacon, 1986). Further evidence that the inclusions and host lavas underwent a liquid/liquid interaction is the spheriodal to ellipsoidal shape; however they may become distorted due to the exertion of stress by flowing or mixing lava giving the inclusions a stretched or swirled appearance (Perugini et al., 2003b). On the contrary, if an inclusion has a planar boundary it is an indication that the inclusion was solid at the time of incorporation (Bacon, 1986;

86

Blake and Fink, 2000). Upon formation, extensive crystallization in the inclusion will cause the volatile concentration in the remaining melt to be driven above saturation, thus forcing exsolution and vesiculation resulting in a vesicular to porous texture of the groundmass (Bacon, 1986; Coombs et al., 2002).

Phenocrysts in both inclusions and host lavas exhibit several examples of disequilibrium textures that are characteristic for magma mixing, such as sieved textures (plagioclase), resorption rims (orthopyroxene), secondary mineral overgrowths (clinopyroxene rim on orthopyroxene phenocrysts) and skeletal or spiky phenocrysts (amphibole). Disequilibrium textures observed are not homogeneously distributed throughout the entire volume of magma, for example samples from the same site may have varying amounts of disequilibrium textures present. Variation can occur over small distances, for example, within a single thin section (3-4 cm), and was observed in the Mount Hood lavas and is also reported by other investigators (i.e. Clynne, 1999; Perugini et al., 2003a). Reverse zoning (plagioclase, orthopyroxene and amphibole) is also indicative of magma mixing, and as well as complicated crystallization histories (plagioclase).

Resorption rims and sieved textures are formed when the phenocryst experiences an increase in temperature, whether its magma is heated or the phenocryst was incorporated into warmer magma (i.e. into a forming inclusion). Sieved textures arise when compositional zones, whose solidus is at a lower temperature than other compositional zones, will begin to melt when exposed to an elevated temperature (Hibbard, 1995). Resorption rims are formed when the phenocryst experiences a rise in temperature that is above the solidus for that mineral and the phenocryst begins to

melt along the rim or it may occur by dissolution. Another indication that there was an elevation in temperature can be postulated by finding a mineral with an early (inner) part that originated from silicic magma overgrown by a later (outer) portion that crystallized from more mafic magma (Perugini et al., 2003a). Figure 15 shows an orthopyroxene phenocryst with an outer rim of clinopyroxene. My interpretation is that the orthopyroxene grew from more silicic magma, and was resorbed during mixing before crystallization from the inclusion magma (i.e. the more mafic hybrid caused clinopyroxene instead of orthopyroxene to grow). The last type of disequilibrium texture that is observed in both Mount Hood host lavas and inclusions are the skeletal and spiky amphibole phenocrysts. Unlike the previous textures that indicate an elevation in temperature, the amphiboles record a sudden decrease in temperature leading to quenching effects. In addition to the skeletal or spiky amphibole crystals, the presence of interstitial glass as reported by Bacon (1986) is an important characteristic in identifying whether or not a portion of the magma was undercooled.

The reverse zoning in the orthopyroxene and amphibole phenocrysts, as observed by the increase in Mg# from core to rim, attests that the phenocrysts experienced growth from a more mafic thus hotter magma. Similarly with disequilibrim textures, an elevation in temperature could be caused by an influx of more mafic magma mixing with more silicic magma (Perugini et al., 2003a). The plagioclase phenocrysts in both inclusions and host lavas have alternating zones of anorthite and albite rich plagioclase (optically observed as oscillatory zoning), and in many cases an overall trend of reverse zoning (increasing anorthite content) towards

the rim. The strongest compositional effect to induce an increase in anorthite content leading to the generation of reversely zoned plagioclase are higher temperatures and higher Ca/Na content and that both are achieved at the same time by an influx of more mafic magma (Grogan and Reavy, 2002; Landi et al., 2004).

The inclusions are relatively phenocryst poor, whereas the host lavas are phenocryst rich; yet there is evidence that a number of the phenocrysts found in the inclusions may have originated from the host lavas. Table 2 shows that there is a number of plagioclase phenocrysts that have sieved textures found both in the inclusions and the host lavas. Similar observations regarding sieved plagioclase has been observed in other volcanic systems and it is generally presumed that the mafic mixing end member would contain very few phenocrysts, while the silicic mixing end member would be a crystal mush, and during the mixing process phenocrysts from the silicic host become incorporated into the inclusions (Clynne, 1999).

Mafic magma can be either injected into the magma chamber from another source of magma deeper within the continental crust or by density currents resulting in convection of the magma chamber. Due to the time constraints of this study, I was not able to determine the mechanism by which mafic magma was introduced into a more silicic magma, but it lends to an area for future work.

Chemical Comparison among Neighboring Cascade Volcanoes

Comparison of the Mount Hood lavas to lavas erupted from neighboring Cascade volcanoes was investigated to determine how similar and/or different the compositions of Mount Hood are to compositions of its neighbors. I chose to compare

89

the average composition of the most depleted site (0203, U.S. Highway 26) and the most enriched site (0210, Laurence Lake) to comparable samples from four neighboring volcanoes, which are Mount Rainier (Stockstill et al., 2002) and Mount St. Helens (Smith and Lehman, 1993) in Washington and Mount Jefferson (Conrey et al., 2001) and Mount Mazama (Crater Lake) (Bacon and Druitt, 1988) in Oregon. Magma mixing is also the dominating petrogenic process for lavas of these four neighboring volcanoes (Bacon and Druitt, 1988; Conrey et al., 2001; Smith and Leeman, 1993; Stockstill et al., 2002). Samples for comparison were chosen based on silica content. The average silica content for the Mount Hood inclusions is 58.6 wt% and for the host lavas is 61.7 wt %, therefore when selecting samples from other studies I chose two samples, where applicable, an inclusion and a host lava with similar silica contents to the average values of Mount Hood. Studies at Mount Rainier and Crater Lake identified samples as inclusion and host lava, while studies are Mount St. Helens and Mount Jefferson investigated only lavas. In the latter case, I chose samples that have similar silica contents to the average values of both inclusion and host material for Mount Hood.

Figure 49, is a spiderdiagram illustrating the relationship among the host lavas of Mount Hood to comparable samples from the neighboring volcanoes. The plot shows a typical subduction zone signature (see section on Geochemistry in Chapter 3). The (most) depleted host lavas (site 0203) fall in the mid-range, in that no single (or multiple) trace element(s) appear to be neither enriched nor depleted, however, the behavior of the average (most) enriched host lavas (site 0210) is different. The pattern for the enriched host lavas are slightly above the median of all samples plotted, and is

enriched in comparison to other Cascade volcanoes in the following incompatible trace elements: Nd, Zr, Hf, Sm, and Eu.
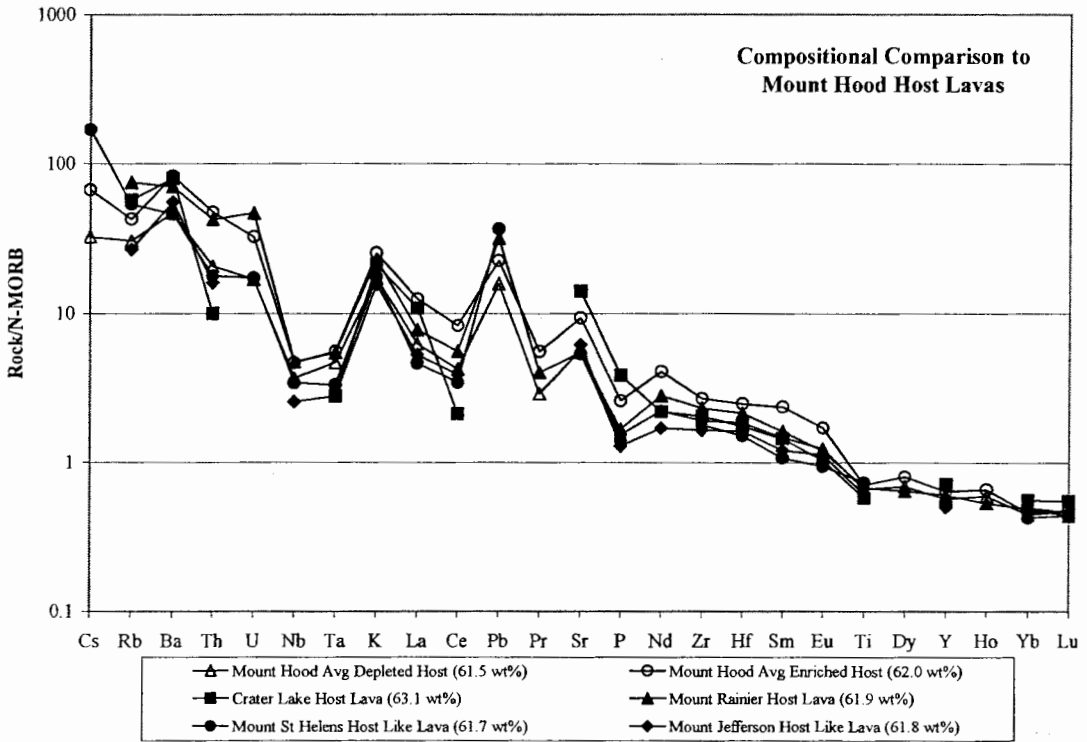
Figure 49 – Spiderdiagrams illustrating the compositional relationship between Mount Hood host lavas and comparable samples from neighboring Cascade volcanoes. Silica contents indicated in parentheses.

Figure 50 is a similar spider diagram that illustrates the compositional relationship between Mount Hood mafic inclusions and comparable samples from neighboring volcanoes. This spiderdiagram also shows that the lavas erupted exhibit a typical subduction zone signature. The average depleted Mount Hood inclusions follow the same trend as in Figure 49, in that they lie in the median of all samples plotted. The Laurence Lake average enriched inclusions from Mount Hood are enriched in comparison to the other volcanoes (except Cs and Pb).

91
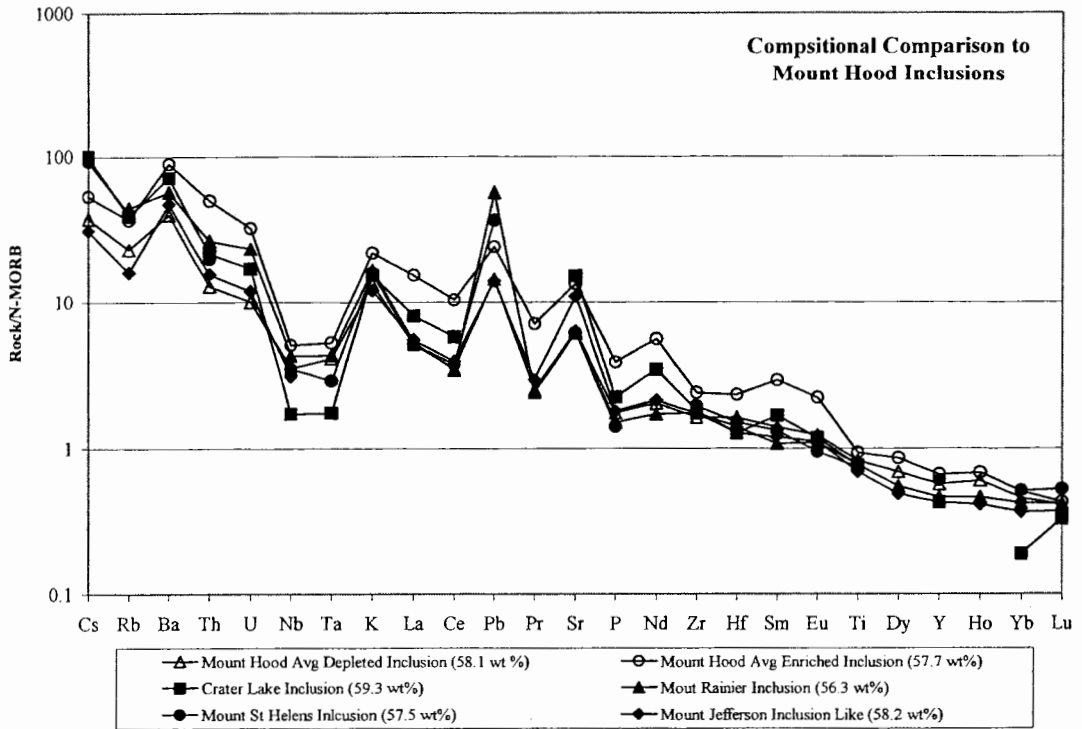
Figure 50 – Spiderdiagrams illustrating the compositional relationship between Mount Hood inclusions and comparable samples from neighboring Cascade volcanoes. Silica contents indicated in parentheses.

On a regional scale, Mount Hood andesites and their associated mafic magmatic inclusions are compositionally similar to comparable samples from neighboring volcanoes. The differences in enrichment and depletion of certain trace elements among the five volcanoes is influenced by differing compositions of mafic and silicic end members when mixing together form the hybrid magmas erupted at these volcanoes, including Mount Hood.

CHAPTER 5 – CONCLUSION

The andesitic lava flows of Mount Hood contain slightly more mafic magmatic inclusions in which both host lavas and inclusion are mineralogically and compositionally similar. The mineral assemblage of the host lavas and inclusions is plag + opx ± cpx ± amp + oxides. Flank lavas were also found to be mineralogically similar to the host lavas and inclusions, but they do not contain amphibole, and since they are compositionally more mafic they do not contain amphibole but do contain olivine. Compositionally, the average composition of the flank lavas (57.6 wt % SiO_2), inclusions (58.6 wt % SiO_2) and host lavas (61.7 wt % SiO_2) is narrow, but the incompatible element composition is quite variable. The degree of incompatible element enrichment is independent of silica content for both the inclusions and host lavas, but the degree of variability is greater at the lower silica contents and narrows toward the higher silica contents. In terms of the incompatible element composition, the inclusion bearing sites can be grouped as either depleted (containing no amphibole) or enriched (containing amphibole with a general absence of clinopryoxene).

The mineralogy and composition of the three lava types analyzed were used to model major petrogenetic processes; crystal fractionation, magma mixing and assimilation fractional crystallization (AFC process). The host lavas and inclusions, as well as many of the flank lavas, are porphyritic, therefore crystal fractionation was modeled. Two crystal fractionation scenarios were carried out; one scenario in which the parental magma was the most depleted flank lava sampled and the second scenario

parental magmas were the average composition of inclusions at each site. Reproduction of the observed compositions of the host lavas was more successful when the parental magma was equivalent to the depleted flank lava.

A magma mixing model was constructed since there is abundant petrographic and geochemical evidence such as disequilibrium textures and reversely zoned phenocrysts suggesting that magma mixing is an important petrogenic process. Models assumed host lavas and inclusions as mixed products, and compositional constraints between inclusions and host lavas were used to calculate hypothetical silicic and mafic end members. The calculated mafic and silicic end members were plotted on Harker diagrams with data points of mafic and silicic lavas erupted during the Pliocene (Figures 42, 43). It was found that the calculated end members correlate to what has been erupted in the past indicating that the compositions of the hypothetical end members could exist. Mixing models largely required a compositional variable mafic imput most clearly expressed in the wide range in incompatible elements required. On the other hand, a single silicic end member is mostly sufficient for models. A second set of Harker diagrams plot the Pliocene mafic and silicic lavas along with all of the Mount Hood samples shows that the Mount Hood samples not only plot between the mafic and silicic lavas as expected but in a linear trend that implies that magma mixing is indeed a feasible petrogenic process.

Assimilation fractional crystallization was modeled since it is probable that assimilation of the wall rock into residing magma may be accountable for the variability in incompatible trace element compositions at each site. The model yielded no less than three possible scenarios in reproducing observed host lava and inclusion

94

compositions. The most probable scenario was assuming the most depleted flank lava as the parental lava and the host lavas or hypothetical silicic end member as the daughter lava, but overall this model does not work as a viable petrogenic model because is fails to account for the variability of the incompatible trace element concentrations among the sites sampled.

Therefore, I conclude that Mount Hood andesites were formed by a combination of crystal fractionation and magma mixing. The phenocrysts probably formed in each of the end members prior to the mixing, and the andesite and inclusions were formed upon magma mixing.

REFERENCES

Bacon, C.R., 1986, Magmatic Inclusions In Silicic and Intermediate Volcanic Rocks: Journal of Geophysical Research, V. 91, p. 6091-6112.

Bacon, C.R. and Druitt, T. H., 1988, Compositional Evolution of The Zoned Calc-Alkaline Magma Chamber of Mount Mazama, Crater Lake, Oregon: Contributions To Mineralogy and Petrology, V. 98.

Blake, S. and Fink, J. H., 2000, On The Deformation and Freezing of Enclaves During Magma Mixing: Journal of Volcanology and Geothermal Research, V. 95, p. 1-8.

Blakely, R.J. and Jachens, R. C., 1990, Volcanism, Isostatic Residual Gravity, and Regional Tectonic Setting of The Cascade Volcanic Province: Journal of Geophysical Research, V. 95, p. 19,439-19,451.

Blundy, J. and Wood, B., 2003, Partitioning of Trace Elements Between Crystals and Melts: Earth and Planetary Science Letters, V. 210, p. 383-397.

Clynne, M.A., 1999, A Complex Magma Mixing Origin For Rocks Erupted In 1915, Lassen Peak, California: Journal of Petrology, V. 40, p. 105-132.

Conrey, R.M., Hooper, P.R., Larson, P.B., Chelsey, J. and Ruiz, J., 2001, Trace Element and Isotopic Evidence For Two Types of Crustal Melting Beneath A High Cascade Volcanic Center, Mt. Jefferson, Oregon: Contributions To Mineralogy and Petrology, V. 141, p. 710-732.

Conrey, R.M., Sherrod, D. R., Uto, K. and Uchiumi, S., 1996, Potassium-Argon Ages from Mount Hood Are of Cascade Range, Northern Oregon: Isochron/West, V. 63, p. 10-20.

Conrey, R.M., Sherrod, D.R., Hooper, P.R. and Swanson, D.A, 1997, Diverse Primitive Magmas In The Cascade Arc, Northern Oregon and Southern Washington: The Canadian Mineralogist, V. 35, p. 367-396.

Coombs, M.L., Eichelberger, J.C. and Rutherford, M.J., 2000, Magma Storage and Mixing Conditions For The 1953-1974 Eruptions of The Southwest Trident Volcano, Katmai National Park, Alaska: Contributions To Mineralogy and Petrology, V. 140, p. 99-118.

Coombs, M.L., Eichelberger, J.C. and Rutherford, M.J., 2002, Experimental and Textural Constraints On Mafic Enclave Formation In Volcanic Rocks: Journal of Volcanology and Geothermal Research, V. 119, p. 125-144.

Crandell, D.R., 1980, Recent Eruptive History of Mount Hood, Oregon, and Potential Hazards from Future Eruptions, Us Geological Survey Bulletin, 1492, 81 p.

Cribb, J.W. and Barton, M., 1997, Significance of Crustal and Source Region Processes On The Evolution of Compositionally Similar Calc-Alkaline Lavas, Mt. Hood, Oregon: Journal of Volcanology and Geothermal Research, V. 76, p. 229-249.

Deer, W.A., Howie, R.A. and Zussman, J., 1992, An Introduction To The Rock Forming Minerals: Edinburgh, Pearson Education Limited, 696 p.

Gardner, J.E., Carey, S., Rutherford, M.J. and Sigurdsson, H., 1995, Petrologic Diversity In Mount St. Helens Dacites During The Last 4,000 Years: Implications For Magma Mixing: Contributions To Mineralogy and Petrology, V. 119, p. 224-238.

Gray, L.B., Sherrod, D.R. and Conrey, R.M., 1996, Potassium-Argon Ages from The Northern Oregon Cascade Range: Isochron/West, V. 63, p. 21-28.

Grogan, S.E., and Reavy, R.J., 2002, Disequilibrium Textures In The Leinster Granite Complex Se Ireland: Evidence For Acid-Acid Magma Mixing: Mineralogical Magazine, V. 66, p. 929-939.

Hawthorne, F.C., 1983, The Crystal Chemistry of Amphiboles: The Canadian Mineralogist, V. 21, p. 173-480.

Hess, P.C., 1989, Origins of Igneous Rocks: Cambridge, Ma, Harvard University Press, 336 p.

Hibbard, M.J., 1995, Petrography to Petrogenesis, Prentice Hall, 587 p.

Knaack, C. Cornelius, S., and Hooper, P., 1994, Trace Element Analysis of Rocks and Minerals By ICP-MS, GeoAnalytical Labaoratory, Washington State Unoversity, Pullman, WA,

Landi, P., Metrich, N., Bertagnini, A., and Rosi, M., 2004, Dynamics of Magma Mixing and Degassing Recorded In Plagioclase At Stromboli (Aeolian Archipelago, Italy): Contributions To Mineralogy and Petrology, V. 147, p. 213-227.

Le Maitre, R.W., 2002, Igneous Rocks: A Classification and Glossary of Terms, Cambridge University Press, 236 p.

McBirney, A.R., 1978, Volcanic Evolution of The Cascade Range: Earth and Planetary Science Letters, V. 6, p. 437-456.

McBirney, A.R., 1993, Igneous Petrology: Boston, Jones and Bartlett Publishers, Inc., 508 p.

Perugini, D., Busa, T., Poli, G. and, Nazzareni, S., 2003a, The Role of Chaotic Dynamics and Flow Fields In The Development of Disequilibrium Textures In Volcanic Rocks: Journal of Petrology, V. 44, p. 733-756.

Perugini, D., Poli, G. and, Mazzuoli, R., 2003b, Chaotic Advection, Fractals and Diffusion During Mixing of Magmas: Evidence from Lava Flows: Journal of Volcanology and Geothermal Research, V. 124, p. 255-279.

Priest, G.R., 1990, Volcanic and Tectonic Evolution of The Cascade Volcanic Arc, Central Oregon: Journal of Geophysical Research, V. 95, p. 19,583-19,599.

Rogers, G.C., 1985, Variation In Cascade Volcanism With Margin Orientation: Geology, V. 13, p. 495-498.

Rollinson, H., 1993, Using Geochemical Data: San Francisco, Prentice Hill, 352 p.

Russell, J.K., 1990, Magma Mixing Process: Insights and Constraints from Thermodynamic Calculations, *In* Nicholls, J.R., J.K., Ed., Modern Methods of Igneous Petrology: Understanding Magmatic Process, Volume 24: Reviews In Mineralogy: Washington, D.C., Mineralogical Society of America, p. 153-190.

Scott, W.E., Gardner, C. A., Sherrod, D. R., Tilling, R. I., Lanphere, M. A. and Conrey, R. M., 1997, Geological History of Mount Hood Volcano, Oregon - A Field Trip Guidebook: Unites States Geological Survey Open File Report 97-263, p. 1-38.

Scott, W.E., Gardner, C.A., Tilling, R.I. and Lanphere, M.A., 2003, Geologic History of Mount Hood Volcano, Oregon - A Field Trip Guide: State of The Arc Meeting, Timberline Lodge, Oregon, p. 1-39.

Sisson, T.W. and Bacon, C. R., 1999, Gas-Driven Filter Pressing In Magmas: Geology, V. 27, p. 613-616.

Smith, D.R. and Leeman, W.P., 1993, The Origin of Mount St. Helens andesites: Journal of Volcanology and Geothermal Research, V. 55, p. 271-303.

Stockstill, K.R., Vogel, T.A. and Sisson, T.W., 2002, Origin and Emplacement of The andesite of Burroughs Mountain, A Zoned, Large-Volume Lava Flow At Mount Rainier, Washington, Usa: Journal of Volcanology and Geothermal Research, V. 119, p. 275-296.

Streck, M.J., Dungan, M. A., Malavassi, E., Reagan, M.K. and Bussy, F., 2002, The Role of Basalt Replenishment on the Generation of Basaltic Andesites of the Ongoing Activity at Arenal Volcano, Costa Rica: Evidence from Clinopyroxene and Spinel, Bulletin of Volcanology, V. 64, p. 316-327.

Taylor, E.M., 1990, Volcanic History and Tectonic Development of The Central High Cascade Range, Oregon: Journal of Geophysical Research, V. 95, p. 19611-19622.

Tepper, J.H. and Keuhner, S.M., 2004, Geochemistry of Mafic Enclaves and Host Granitoids from The Chilliwack Batholith, Washington: Chemical Exchanges Processes Between Coexisting Mafic and Felsic Magmas and Implications For The Interpretation of Enclave Chemical Traits: Journal of Geology, V. 112, p. 349-367.

Thomas, N. and Tait, S. R., 1997, The Dimensions of Magmatic Inclusions As A Constraint On The Physical Mechanism of Mixing: Journal of Volcanology and Geothermal Research, V. 75, p. 167-178.

Trimble, D.E., 1963, Geology of Portland and Adjacent Areas: United States Geological Survey Bulletin, No. 1119, p. 1-116.

Wells, R.E., 1990, Paleomagnetic Rotations and The Cenozoic Tectonics of The Cascade Arc, Washington, Oregon and California: Journal of Geophysical Research, V. 95.

White, C., 1980, Geology and Geochemistry of Mt. Hood Volcano: Oregon Department of Geology and Mineral Industries Special Paper, V. 8, p. 1-26.

Wiebe, R.A.,Smith, D., Sturm, M., King, E.M. and Seckler, M.S., 1997, Enclaves In The Cadillac Mountain Granite (Coastal Maine): Samples of Hybrid Magma from The Base of The Chamber: Journal of Petrology, V. 38, p. 393-423.

Williams, H., Turner, F.J. and Gilbert, C.M., 1982, Petrography: An Introduction To The Study of Rocks In Thin Sections: San Francisco, W.H. Freeman and Company, 626 p.

Wilson, M., 1989, Igneous Petrogenesis: A Global Tectonic Approach: Boston, Kluwer Academic Publishers, 466 p.

Winter, J.D., 2001, An Introduction To Igneous and Metamorphic Petrology, Prentice Hall, 699 p.

Wise, W.S., 1969, Geology and Petrology of The Mt. Hood Area: A Study of High Cascade Volcanism: Geological Society of America Bulletin, V. 80, p. 969-1,006.

APPENDIX A

COMPILED CHEMICAL DATA

FLANK LAVAS

XRF wt%

	0201	0202	0204	0206	0208	0209
SiO_2	56.89	59.76	55.77	59.00	56.02	58.11
Al_2O_3	18.38	18.09	18.53	18.00	18.57	18.26
TiO_2	1.20	0.88	1.21	0.98	1.13	1.15
FeO^*	7.78	5.84	7.26	6.07	7.31	6.61
MnO	0.14	0.10	0.12	0.11	0.13	0.11
CaO	7.17	6.47	7.46	6.84	7.43	6.86
MgO	3.56	3.38	4.42	3.54	4.43	3.46
K_2O	0.71	1.34	0.67	1.01	0.92	0.86
Na_2O	3.91	3.96	4.32	4.23	3.84	4.32
P_2O_5	0.26	0.19	0.23	0.23	0.21	0.27

XRF ppm

	0201	0202	0204	0206	0208	0209
Ni	27	24	55	35	42	31
Cr	28	25	78	57	72	48
Sc	19	15	16	16	19	14
V	127	111	136	106	133	116
Ba	204	259	216	316	189	279
Rb	4	13	6	15	7	11
Sr	533	705	617	542	560	625
Zr	166	145	115	160	124	139
Y	25	15	18	19	18	17
Nb	11.0	7.4	8.0	10.6	7.8	9.9
Ga	22	21	21	22	22	20
Cu	46	37	49	49	49	41
Zn	96	64	82	76	76	87
Pb	10	12	12	10	11	12
La	21	16	21	15	0	1
Ce	46	38	32	43	36	38
Th	2	3	2	4	3	2

FLANK LAVAS

ICPMS ppm

	0201	0202	0204	0206	0208	0209
La	12.68	15.84	11.72	17.49	10.50	14.04
Ce	28.23	32.51	23.67	34.63	23.39	29.73
Pr	3.80	3.98	3.21	4.21	3.08	3.78
Nd	17.61	16.74	14.83	17.85	14.21	16.66
Sm	4.79	3.83	3.81	4.31	3.85	4.15
Eu	1.68	1.24	1.40	1.42	1.42	1.46
Gd	4.83	3.32	3.77	4.05	3.85	4.00
Tb	0.76	0.50	0.58	0.64	0.62	0.61
Dy	4.56	2.84	3.32	3.73	3.67	3.45
Ho	0.89	0.56	0.64	0.71	0.73	0.65
Er	2.35	1.41	1.61	1.94	1.94	1.68
Tm	0.32	0.20	0.22	0.27	0.27	0.23
Yb	1.95	1.21	1.32	1.64	1.61	1.39
Lu	0.30	0.19	0.20	0.25	0.26	0.21
Ba	197	244	216	308	176	274
Th	0.73	2.68	0.77	1.94	1.35	1.12
Nb	9.77	6.68	7.51	9.76	6.57	9.16
Y	23.45	14.46	17.58	19.17	19.04	17.20
Hf	4.22	3.61	2.94	3.99	3.26	3.50
Ta	0.61	0.43	0.47	0.65	0.43	0.58
U	0.26	0.72	0.24	0.60	0.43	0.38
Pb	3.83	4.81	3.17	4.58	4.37	4.27
Rb	4.8	12.3	5.9	15.3	6.8	9.1
Cs	0.07	0.10	0.05	0.41	0.14	0.20
Sr	525	698	625	555	567	637
Sc	19.2	15.3	17.6	17.1	19.6	15.5
Zr	155	132	107	154	115	131

FLANK LAVAS

INAA ppm

	0201	0202	0204	0206	0208	0209
Na (wt%)	3.68	3.66	4.03	3.91	3.74	4.03
Fe (wt%)	12.09	9.52	6.84	6.08	7.16	6.10
Sc	14.83	11.59	15.25	14.46	17.37	13.23
Cr	29.79	25.00	93.79	64.09	97.48	60.75
Co	23.01	19.14	24.92	20.06	25.76	20.21
Zn	0.99	1.35	79.26	74.23	82.80	75.26
As	0.40	0.38	0.43	0.57	0.73	0.57
Sb	0.07	0.10	0.11	0.10	0.11	0.08
Rb	0.20	0.33	9.84	16.14	11.98	10.51
Cs	0.13	0.12	0.09	0.44	0.17	0.26
Ba	234.80	268.04	241.46	309.81	219.27	279.75
La	12.28	15.20	11.50	16.29	10.73	13.11
Ce	12.49	12.10	23.89	35.88	25.36	29.65
Nd	16.85	16.40	14.44	17.32	14.70	15.47
Sm	4.00	3.17	3.26	3.91	3.69	3.72
Eu	0.38	0.26	1.26	1.27	1.36	1.33
Tb	0.95	0.60	0.53	0.55	0.56	0.54
Yb	1.91	1.38	1.26	1.52	1.69	1.35
Lu	0.29	0.18	0.20	0.23	0.25	0.19
Hf	3.66	3.16	2.83	3.97	3.27	3.45
Ta	0.94	0.54	0.48	0.70	0.48	0.62
Th	0.00	0.00	0.70	1.79	1.30	1.02
U	0.70	1.03	0.23	0.32	0.31	0.25

HOST LAVAS

XRF wt%

	0203-1	0203-2	0203-3	0205-1	0205-2	0205-3	0205-4	0210-1	0210-2	0211-1	0211-2	0212-1	0212-2	0213-1	0213-2
SiO_2	61.56	61.55	61.51	60.54	60.44	60.64	60.69	61.96	62.09	61.12	62.34	63.31	63.54	62.21	62.32
Al_2O_3	17.39	17.29	17.24	17.23	17.57	17.64	17.58	17.06	16.90	17.27	17.38	17.06	16.79	17.66	17.70
TiO_2	0.83	0.84	0.84	0.97	0.97	0.97	0.95	0.88	0.91	0.94	0.82	0.75	0.75	0.82	0.83
FeO^*	5.36	5.60	5.58	6.15	5.84	5.51	5.75	5.35	5.21	5.52	5.30	4.78	4.95	5.21	5.34
MnO	0.09	0.10	0.10	0.11	0.11	0.11	0.10	0.09	0.09	0.10	0.10	0.09	0.09	0.09	0.09
CaO	5.97	5.80	5.79	6.03	6.17	6.16	6.10	5.70	5.77	5.97	5.45	5.50	5.40	5.77	5.55
MgO	3.07	3.14	3.21	3.14	3.13	3.16	3.05	2.56	2.57	2.75	2.66	2.58	2.56	2.57	2.65
K_2O	1.23	1.26	1.27	1.42	1.41	1.40	1.40	1.81	1.85	1.65	1.54	1.49	1.49	1.31	1.35
Na_2O	4.33	4.24	4.27	4.18	4.12	4.18	4.14	4.28	4.30	4.39	4.23	4.26	4.26	4.19	4.01
P_2O_5	0.18	0.18	0.18	0.23	0.24	0.23	0.23	0.30	0.31	0.30	0.18	0.17	0.16	0.17	0.17

XRF ppm

	0203-1	0203-2	0203-3	0205-1	0205-2	0205-3	0205-4	0210-1	0210-2	0211-1	0211-2	0212-1	0212-2	0213-1	0213-2
Ni	35	39	41	32	29	30	28	20	22	22	25	22	23	22	25
Cr	50	49	50	32	31	31	29	16	19	22	26	20	22	23	23
Sc	16	9	9	21	13	18	18	12	11	16	16	13	12	12	12
V	90	96	98	102	107	103	97	88	82	99	98	85	84	92	86
Ba	297	284	302	335	343	342	334	523	520	444	425	329	338	307	287
Rb	18	18	18	20	18	20	20	24	25	24	23	22	22	17	20
Sr	504	499	495	550	548	545	546	829	835	834	555	541	531	557	539
Zr	139	143	144	177	179	177	181	203	198	186	162	153	153	146	147
Y	16	15	17	20	20	19	20	18	18	17	18	15	15	18	15
Nb	9.1	8.9	8.6	10.9	10.2	10.7	11.0	10.2	11.5	10.8	12.0	8.6	9.4	8.6	7.8
Ga	17	20	19	21	23	20	20	19	23	19	18	21	21	19	18
Cu	50	44	43	39	27	45	27	32	36	28	35	24	35	32	34
Zn	68	71	66	72	72	73	68	78	79	76	66	62	63	68	69
Pb	10	8	7	11	12	9	10	12	14	13	9	11	11	10	11
La	7	25	7	16	20	18	19	25	20	34	20	8	13	23	12
Ce	31	35	26	24	34	39	39	73	65	72	35	35	47	26	27
Th	3	3	3	3	5	3	6	4	7	5	4	3	4	5	4

HOST LAVAS

ICPMS ppm

	0203-1	0203-2	0203-3	0205-1	0205-2	0205-3	0205-4	0210-1	0210-2	0211-1	0211-2	0212-1	0212-2	0213-1	0213-2
La	15.33	15.98	15.66	21.47	19.99	20.99	20.90	30.31	31.95	26.37	21.78	17.38	17.75	17.69	14.46
Ce	30.77	32.37	31.79	43.01	39.72	41.85	41.56	61.00	63.04	52.20	41.44	33.75	34.69	32.34	28.67
Pr	3.74	3.94	3.80	5.07	4.78	4.99	4.94	7.21	7.48	6.17	4.81	3.90	4.03	4.07	3.42
Nd	15.90	16.57	16.29	21.14	19.49	20.42	20.50	29.28	30.37	25.00	19.42	15.97	16.43	17.03	14.15
Sm	3.81	3.97	3.89	4.84	4.60	4.76	4.77	6.13	6.31	5.10	4.15	3.65	3.71	4.01	3.38
Eu	1.24	1.28	1.26	1.52	1.47	1.47	1.44	1.74	1.75	1.55	1.30	1.17	1.15	1.22	1.14
Gd	3.56	3.66	3.71	4.55	4.18	4.31	4.37	4.81	4.96	4.11	3.77	3.31	3.26	3.61	3.11
Tb	0.54	0.57	0.56	0.70	0.64	0.68	0.67	0.67	0.69	0.59	0.56	0.51	0.51	0.57	0.49
Dy	3.08	3.24	3.15	4.11	3.68	3.89	3.91	3.61	3.68	3.33	3.31	2.93	2.96	3.30	2.89
Ho	0.58	0.61	0.61	0.78	0.71	0.75	0.77	0.65	0.68	0.63	0.62	0.56	0.56	0.62	0.55
Er	1.57	1.65	1.57	2.05	1.91	2.02	2.02	1.64	1.71	1.61	1.64	1.46	1.47	1.67	1.43
Tm	0.22	0.22	0.23	0.29	0.27	0.28	0.28	0.23	0.23	0.22	0.23	0.21	0.21	0.23	0.20
Yb	1.34	1.36	1.36	1.77	1.62	1.72	1.74	1.37	1.43	1.36	1.45	1.29	1.31	1.43	1.26
Lu	0.21	0.22	0.21	0.28	0.26	0.27	0.27	0.22	0.22	0.21	0.23	0.21	0.20	0.22	0.20
Ba	296	306	305	358	333	347	343	502	515	438	397	330	340	295	271
Th	2.42	2.50	2.50	3.44	3.00	3.08	3.23	5.59	5.80	4.02	3.51	3.23	3.29	2.85	2.75
Nb	8.37	8.71	8.67	10.78	9.52	10.01	10.06	10.80	11.01	10.57	10.97	8.20	8.51	8.06	7.87
Y	15.88	16.62	16.38	20.99	18.79	19.87	20.03	17.61	18.04	16.34	17.07	14.82	15.13	17.23	14.51
Hf	3.75	3.80	3.87	4.66	4.34	4.50	4.60	5.02	5.17	4.57	4.04	4.10	4.05	3.72	3.61
Ta	0.60	0.62	0.63	0.74	0.66	0.69	0.69	0.71	0.75	0.74	0.71	0.62	0.64	0.59	0.58
U	0.78	0.80	0.81	1.02	0.87	0.90	0.94	1.49	1.55	1.04	1.06	0.96	0.97	0.88	0.87
Pb	4.99	4.75	4.41	4.33	5.40	5.16	2.54	6.46	7.00	5.22	5.71	5.16	5.73	5.28	5.31
Rb	16.6	17.4	17.1	20.0	17.9	18.5	18.0	23.0	24.7	19.8	20.5	20.9	20.2	15.6	16.9
Cs	0.18	0.24	0.26	0.21	0.38	0.37	0.35	0.46	0.47	0.26	0.30	0.50	0.47	0.38	0.41
Sr	503	517	514	604	530	562	551	833	844	804	544	538	543	557	520
Sc	13.9	14.1	14.2	14.8	14.1	15.1	15.2	12.3	12.3	12.4	13.0	11.8	11.8	12.6	12.7
Zr	135	138	139	181	162	169	171	187	192	167	146	144	146	136	132

HOST LAVAS

INAA ppm

	0203-1	0203-2	0203-3	0205-1	0205-2	0205-3	0205-4	0210-1	0210-2	0211-1	0211-2	0212-1	0212-2	0213-1	0213-2
Na (wt%)	3.99	3.95	3.96	3.98	3.96	3.93	3.83	4.12	4.03	4.17	3.91	4.02	4.03	3.91	3.82
Fe (wt%)	8.67	5.05	5.08	5.67	5.73	5.84	5.53	4.88	4.90	5.23	5.07	4.42	4.37	5.13	4.89
Sc	10.62	11.75	11.76	12.55	13.00	13.24	12.88	10.60	10.42	10.94	11.65	10.15	9.98	10.91	11.08
Cr	22.73	68.68	62.50	44.10	68.18	45.70	54.08	41.63	50.27	36.79	54.88	41.98	54.17	39.39	48.44
Co	17.27	17.21	17.27	17.50	18.54	18.18	18.02	15.55	15.76	16.54	16.27	14.16	14.09	15.20	15.52
Zn	2.13	64.58	64.50	65.22	64.20	69.45	65.76	67.88	66.10	66.42	62.44	53.86	51.18	57.91	60.70
As	0.68	0.41	1.33	0.65	0.69	0.74	0.92	1.17	1.03	0.74	0.81	0.92	0.75	1.55	0.97
Sb	0.08	0.07	0.15	0.14	0.16	0.08	0.11	0.22	0.15	0.11	0.18	0.17	0.08	0.11	0.14
Rb	0.52	18.04	17.09	18.95	18.58	22.61	21.22	18.92	24.75	28.54	18.77	22.20	19.82	16.59	19.73
Cs	0.31	0.23	0.27	0.22	0.41	0.43	0.31	0.49	0.46	0.27	0.39	0.53	0.45	0.45	0.35
Ba	282.70	310.19	303.95	349.56	346.21	357.49	316.89	502.67	508.82	439.99	400.04	334.71	338.39	325.68	305.52
La	14.07	14.13	13.33	19.07	19.25	19.68	18.94	30.35	30.41	25.78	21.85	15.68	16.65	17.31	14.70
Ce	11.35	31.26	30.73	41.34	41.58	42.12	40.74	65.03	64.50	54.66	44.55	34.76	34.59	33.76	31.86
Nd	15.01	15.91	15.18	18.47	20.43	20.61	19.32	30.88	31.20	26.07	21.08	15.91	16.65	17.26	15.43
Sm	3.13	3.21	3.19	4.02	4.17	4.26	4.13	5.83	5.74	4.92	4.13	3.37	3.42	3.76	3.35
Eu	0.27	1.11	1.10	1.29	1.32	1.31	1.28	1.63	1.57	1.47	1.21	1.01	1.07	1.14	1.05
Tb	0.67	0.47	0.47	0.60	0.61	0.59	0.62	0.60	0.62	0.57	0.54	0.44	0.45	0.51	0.45
Yb	1.34	1.43	1.23	1.56	1.90	1.80	1.52	1.53	1.48	1.38	1.44	1.48	1.38	1.34	1.43
Lu	0.20	0.21	0.19	0.25	0.24	0.28	0.28	0.22	0.18	0.21	0.24	0.21	0.21	0.22	0.21
Hf	3.09	3.65	3.60	4.40	4.47	4.39	4.33	5.14	5.07	4.70	4.24	3.97	3.86	3.71	3.70
Ta	0.68	0.61	0.60	0.68	0.71	0.75	0.69	0.77	0.75	0.82	0.79	0.67	0.69	0.67	0.65
Th	0.00	2.24	2.27	3.06	2.96	3.05	3.06	5.29	5.33	4.07	3.53	3.13	3.09	2.84	2.79
U	1.06	0.96	0.29	1.09	1.25	1.30	1.22	1.59	1.79	1.34	1.29	1.09	1.14	1.44	0.87

INCLUSIONS

XRF wt%

	0203A	0203C	0203G	0203I	0205LE	0205RT	0205B	0205E	0205L	0205M	0210B	0210C
SiO_2	59.36	55.39	58.48	59.31	57.94	57.91	58.73	59.10	58.44	57.39	57.83	57.39
Al_2O_3	17.92	18.22	17.85	17.86	18.01	17.91	17.73	17.88	17.99	17.99	17.29	17.47
TiO_2	0.92	1.17	1.10	1.03	1.06	1.07	1.03	1.04	1.06	1.10	1.23	1.21
$FeO*$	5.94	6.70	7.02	6.09	6.79	6.78	6.64	6.19	6.51	7.07	6.32	6.59
MnO	0.10	0.11	0.14	0.11	0.12	0.12	0.11	0.11	0.12	0.12	0.10	0.10
CaO	6.57	8.21	6.39	6.75	6.93	6.84	6.66	6.66	6.73	6.85	7.26	7.42
MgO	3.79	5.59	3.53	3.78	3.72	3.69	3.50	3.42	3.67	3.72	3.44	3.52
K_2O	1.08	0.72	1.03	1.00	1.06	1.08	1.25	1.25	1.16	1.35	1.81	1.65
Na_2O	4.13	3.71	4.22	3.88	4.12	4.34	4.09	4.10	4.08	4.13	4.21	4.16
P_2O_5	0.19	0.19	0.23	0.20	0.25	0.26	0.24	0.25	0.25	0.27	0.51	0.48
XRF ppm												
Ni	44	94	31	47	37	36	34	34	36	37	28	30
Cr	68	130	40	64	43	37	40	38	42	44	31	28
Sc	12	18	15	20	17	22	19	15	18	13	15	12
V	110	164	104	119	105	93	121	124	126	102	135	134
Ba	264	201	302	244	302	305	320	317	308	314	675	605
Rb	13	10	15	14	10	10	14	15	15	19	24	21
Sr	527	559	631	557	553	545	548	543	546	532	1244	1583
Zr	130	106	79	131	170	175	172	173	174	185	227	195
Y	17	15	17	16	22	20	21	21	21	23	20	16
Nb	8.7	7.8	11.7	8.6	10.3	11.7	11.4	11.6	11.3	12.2	12.8	10.6
Ga	19	19	20	18	23	20	20	20	20	20	21	23
Cu	28	†179	111	61	29	75	33	42	38	93	46	55
Zn	81	82	133	87	82	96	79	85	86	85	96	94
Pb	7	11	16	10	12	13	8	9	8	10	11	12
La	15	16	19	24	21	26	0	21	3	10	29	42
Ce	20	31	50	44	42	37	45	60	55	38	103	74
Th	1	2	5	2	2	2	4	4	5	4	7	8

INCLUSIONS

ICPMS ppm

	0203A	0203C	0203G	0203I	0205LE	0205RT	0205B	0205E	0205L	0205M	0210B	0210C
La	13.74	10.59	12.94	13.89	18.21	19.76	18.76	19.07	18.64	20.21	45.22	38.70
Ce	27.92	22.46	25.63	28.14	36.16	39.31	37.26	37.94	38.00	40.49	91.04	78.38
Pr	3.49	2.93	3.24	3.48	4.35	4.75	4.43	4.50	4.49	4.83	10.81	9.53
Nd	14.92	13.54	14.18	15.27	18.35	19.76	18.50	18.92	18.77	20.41	44.19	39.75
Sm	3.76	3.62	3.61	3.74	4.32	4.72	4.45	4.50	4.44	4.90	8.74	7.55
Eu	1.32	1.32	1.13	1.25	1.50	1.56	1.53	1.54	1.52	1.57	2.47	2.25
Gd	3.54	3.56	3.51	3.56	4.14	4.44	4.20	4.28	4.14	4.66	6.34	5.34
Tb	0.54	0.55	0.54	0.56	0.65	0.69	0.66	0.67	0.65	0.73	0.84	0.69
Dy	3.08	3.21	3.10	3.21	3.83	4.05	3.88	3.89	3.85	4.36	4.22	3.61
Ho	0.60	0.62	0.60	0.62	0.74	0.79	0.74	0.75	0.75	0.82	0.75	0.64
Er	1.53	1.54	1.52	1.61	1.98	2.10	2.00	2.01	1.98	2.24	1.83	1.61
Tm	0.21	0.21	0.22	0.22	0.27	0.30	0.28	0.28	0.27	0.31	0.24	0.21
Yb	1.29	1.25	1.35	1.36	1.75	1.81	1.71	1.75	1.69	1.92	1.45	1.25
Lu	0.21	0.19	0.21	0.21	0.27	0.29	0.28	0.27	0.27	0.29	0.21	0.19
Ba	266	200	249	254	300	318	314	314	301	303	655	587
Th	1.87	0.89	1.80	1.80	2.44	2.63	2.64	2.72	2.56	2.64	8.03	6.55
Nb	8.37	7.21	8.45	8.55	10.30	10.80	10.62	10.58	9.99	11.04	12.53	11.16
Y	15.74	15.74	15.87	16.51	19.41	20.79	19.93	19.96	19.64	22.10	20.28	17.37
Hf	3.36	2.83	3.51	3.60	4.12	4.41	4.14	4.26	4.17	4.54	5.65	4.95
Ta	0.56	0.46	0.56	0.58	0.67	0.70	0.68	0.70	0.65	0.70	0.72	0.65
U	0.59	0.31	0.57	0.57	0.69	0.71	0.74	0.76	0.75	0.75	1.99	1.52
Pb	4.19	4.36	4.17	4.57	5.96	7.49	3.90	4.36	4.16	4.45	6.54	6.11
Rb	13.5	8.8	12.5	14.6	10.4	10.0	14.4	13.8	14.0	17.4	24.8	19.3
Cs	0.30	0.11	0.21	0.26	0.15	0.12	0.17	0.15	0.21	0.30	0.42	0.28
Sr	562	592	585	551	569	571	570	566	555	544	1239	1576
Sc	16.3	23.8	16.8	16.9	17.1	17.3	16.9	16.7	16.8	18.0	16.2	15.7
Zr	123	102	125	132	156	168	158	160	160	177	219	185

INCLUSIONS

INAA ppm

	0203A	0203C	0203G	0203I	0205LE	0205RT	0205B	0205E	0205L	0205M	0210B	0210C
Na (wt%)	4.14	3.58	3.64	3.89	3.97	4.15	4.01	3.83	3.79	3.99	4.06	4.08
Fe (wt%)	5.98	6.96	5.97	6.08	6.14	6.39	6.29	6.07	6.21	6.72	5.76	5.99
Sc	14.44	20.69	14.25	14.63	15.36	15.20	15.14	14.23	14.62	15.81	13.10	13.85
Cr	72.18	133.40	62.53	77.76	40.04	37.79	35.28	34.88	35.77	39.56	25.16	29.18
Co	21.17	28.17	20.76	21.38	20.71	21.49	20.67	19.85	20.79	22.22	20.16	21.33
Zn	78.83	87.74	77.45	75.20	74.76	82.49	72.70	81.44	79.45	80.93	80.37	83.17
As	0.79	0.49	0.34	0.63	0.49	0.42	0.87	0.39	0.48	0.65	0.50	0.98
Sb	0.14	0.08	0.06	0.10	0.08	0.07	0.12	0.09	0.09	0.08	0.10	0.15
Rb	2.82	9.06	15.65	17.14	7.84	11.34	18.79	19.11	14.16	20.97	23.63	25.43
Cs	0.34	0.13	0.23	0.36	0.19	0.18	0.17	0.17	0.27	0.34	0.45	0.37
Ba	274.79	243.83	261.65	285.85	330.08	324.16	365.27	334.81	326.34	338.82	670.05	602.29
La	13.93	10.41	12.53	13.75	18.67	19.48	19.69	18.81	18.74	20.28	44.92	38.84
Ce	29.80	22.81	26.35	29.68	38.19	41.54	41.82	39.70	39.76	43.41	93.08	84.67
Nd	14.97	14.09	15.25	14.76	20.12	20.49	19.74	21.15	19.59	22.36	44.45	43.25
Sm	3.23	3.13	3.06	3.42	4.07	4.20	4.39	4.07	4.05	4.75	7.95	7.13
Eu	1.19	1.19	1.02	1.15	1.36	1.44	1.48	1.40	1.37	1.46	2.19	2.06
Tb	0.52	0.51	0.47	0.51	0.58	0.64	0.62	0.61	0.61	0.71	0.78	0.68
Yb	1.25	1.47	1.25	1.62	1.79	2.05	2.10	1.53	1.87	1.85	1.77	1.54
Lu	0.20	0.17	0.19	0.19	0.28	0.27	0.25	0.24	0.25	0.31	0.20	0.19
Hf	3.57	2.73	3.42	3.63	4.01	4.36	4.37	4.23	4.12	4.60	5.51	5.01
Ta	0.56	0.39	0.53	0.54	0.68	0.67	0.71	0.68	0.63	0.76	0.72	0.63
Th	1.86	0.85	1.70	1.78	2.48	2.57	2.77	2.57	2.49	2.55	7.21	6.29
U	0.74	0.23	0.19	0.73	0.81	0.23	0.76	0.87	0.69	0.64	1.76	1.55

110

INCLUSIONS

XRF wt%

	0210E	0210F	0210L	0211A	0211B	0211H	0212A	0212D	0212E	0213C	0213F
SiO_2	56.83	59.21	57.05	59.50	59.18	59.84	58.78	60.14	59.37	60.39	59.97
Al_2O_3	17.21	17.73	17.67	17.93	17.97	18.01	17.96	17.78	18.08	18.22	18.38
TiO_2	1.28	0.97	1.23	0.94	0.96	0.97	0.86	0.85	0.96	0.91	0.89
FeO^*	6.63	6.05	6.28	6.27	6.39	6.03	5.71	5.60	6.30	6.15	5.81
MnO	0.10	0.10	0.10	0.10	0.11	0.11	0.10	0.09	0.11	0.11	0.10
CaO	7.82	6.52	7.63	6.37	6.58	6.25	7.39	6.72	6.68	6.19	6.39
MgO	3.79	4.01	3.56	3.29	3.43	3.21	4.02	3.30	3.10	2.76	3.23
K_2O	1.66	1.18	1.62	1.46	1.25	1.38	1.16	1.41	1.17	1.18	1.14
Na_2O	4.13	4.05	4.33	3.92	3.92	3.98	3.89	3.93	3.98	3.89	3.92
P_2O_5	0.55	0.19	0.53	0.21	0.21	0.22	0.13	0.16	0.24	0.20	0.17

XRF ppm

	0210E	0210F	0210L	0211A	0211B	0211H	0212A	0212D	0212E	0213C	0213F
Ni	33	51	28	31	32	30	39	27	24	21	32
Cr	30	76	29	40	46	41	40	32	25	24	30
Sc	12	12	13	11	14	14	17	16	12	13	16
V	144	111	131	89	92	107	117	106	105	86	91
Ba	633	255	644	349	340	372	242	308	268	223	231
Rb	21	15	23	20	18	21	17	19	16	12	14
Sr	1360	537	1308	590	539	518	643	602	612	598	572
Zr	214	138	212	152	158	166	108	134	144	132	129
Y	18	17	18	17	18	20	16	15	19	18	13
Nb	11.7	8.4	11.0	11.2	12.3	12.3	6.4	7.1	9.1	8.6	7.3
Ga	24	20	21	20	20	20	17	21	18	22	20
Cu	61	32	90	62	37	22	62	82	35	39	39
Zn	88	82	97	73	77	74	65	72	77	82	85
Pb	11	8	18	10	14	7	9	12	10	9	8
La	49	19	50	12	15	25	18	5	12	11	9
Ce	102	20	80	40	47	51	41	32	39	35	38
Th	6	3	7	2	3	1	2	5	1	0	2

INCLUSIONS

ICPMS ppm

	0210E	0210F	0210L	0211A	0211B	0211H	0212A	0212D	0212E	0213C	0213F
_La_	44.56	17.42	46.64	19.39	19.39	21.14	13.24	14.97	16.51	12.86	10.57
_Ce_	89.90	35.59	93.60	37.36	37.11	40.01	27.06	30.02	33.98	27.17	21.13
_Pr_	10.80	4.39	11.25	4.25	4.15	4.69	3.34	3.58	4.19	3.39	2.57
_Nd_	44.97	19.06	45.68	17.34	16.91	19.36	14.51	14.98	17.99	14.98	10.94
_Sm_	8.85	4.40	8.89	3.96	3.88	4.34	3.51	3.50	4.35	3.73	2.73
_Eu_	2.46	1.51	2.56	1.28	1.33	1.36	1.23	1.18	1.52	1.35	1.15
_Gd_	6.41	3.87	6.67	3.53	3.65	4.00	3.41	3.22	3.93	3.49	2.58
_Tb_	0.83	0.59	0.83	0.56	0.57	0.64	0.51	0.50	0.62	0.54	0.41
_Dy_	4.11	3.33	4.28	3.28	3.30	3.63	3.01	2.92	3.63	3.12	2.42
_Ho_	0.71	0.61	0.75	0.63	0.64	0.72	0.59	0.57	0.69	0.59	0.47
_Er_	1.74	1.54	1.81	1.64	1.65	1.86	1.48	1.45	1.75	1.49	1.27
_Tm_	0.23	0.21	0.24	0.24	0.24	0.26	0.21	0.21	0.26	0.21	0.18
_Yb_	1.37	1.31	1.47	1.49	1.49	1.62	1.27	1.30	1.54	1.26	1.15
_Lu_	0.21	0.20	0.22	0.23	0.23	0.25	0.20	0.20	0.24	0.20	0.19
_Ba_	607	293	676	349	341	353	245	296	272	220	227
_Th_	7.74	2.37	7.32	2.91	2.90	3.04	1.96	2.57	2.01	1.80	1.82
_Nb_	11.52	12.12	11.69	11.13	11.94	12.11	6.68	7.23	9.52	7.72	7.35
_Y_	19.26	16.60	19.78	16.50	16.84	18.90	15.28	15.06	18.45	15.70	12.71
_Hf_	5.42	2.21	5.48	3.77	3.97	4.09	2.86	3.47	3.70	3.36	3.31
_Ta_	0.66	0.73	0.70	0.68	0.73	0.74	0.46	0.52	0.63	0.52	0.52
_U_	1.92	0.68	1.77	0.80	0.83	0.89	0.59	0.76	0.60	0.62	0.59
_Pb_	7.31	7.45	8.91	5.61	5.67	3.49	4.63	5.73	5.59	4.67	4.88
_Rb_	21.0	13.2	21.7	18.4	17.4	18.6	16.0	17.8	14.6	12.3	13.8
_Cs_	0.35	0.28	0.39	0.45	0.38	0.27	0.32	0.33	0.33	0.27	0.32
_Sr_	1375	637	1336	583	540	515	646	605	630	622	592
_Sc_	17.1	15.3	16.4	15.1	16.5	16.3	18.3	15.2	14.3	12.9	15.1
_Zr_	207	71	205	139	148	150	99	126	134	122	123

INCLUSIONS

INAA ppm

	0210E	0210F	0210L	0211A	0211B	0211H	0212A	0212D	0212E	0213C	0213F
Na (wt%)	3.90	4.08	4.22	3.85	3.76	3.85	3.72	3.74	3.91	3.71	3.76
Fe (wt%)	6.07	6.53	6.17	5.58	5.76	5.54	5.40	5.29	6.11	5.87	5.71
Sc	14.57	13.12	14.44	13.76	14.48	13.50	15.78	12.91	12.71	11.20	12.83
Cr	30.50	39.40	30.13	38.44	42.75	38.33	40.04	29.83	27.78	19.98	29.72
Co	22.11	20.66	21.73	18.98	19.75	18.48	21.90	18.79	18.39	16.36	18.25
Zn	80.22	95.30	81.21	68.05	67.57	64.33	71.70	64.99	71.16	69.64	67.57
As	1.12	0.60	0.62	1.95	0.71	0.62	1.10	0.77	0.64	0.65	2.80
Sb	0.15	0.89	0.10	0.11	0.10	0.10	0.09	0.09	0.11	0.14	0.11
Rb	23.97	15.06	25.74	20.02	16.43	20.54	19.84	20.08	24.10	17.88	19.54
Cs	0.46	0.25	0.35	0.49	0.41	0.26	0.31	0.38	0.39	0.32	0.36
Ba	604.07	335.23	700.03	376.99	344.76	380.67	241.18	316.18	331.77	274.68	252.34
La	43.46	18.20	43.88	19.22	18.99	21.70	12.97	15.19	16.41	12.61	10.35
Ce	93.07	39.46	93.78	39.17	38.71	42.24	28.57	31.02	36.25	28.63	21.51
Nd	47.80	21.08	46.38	18.31	18.49	20.11	16.72	15.54	19.36	16.75	10.73
Sm	8.05	4.42	8.33	3.86	3.70	4.28	3.29	3.43	4.07	3.54	2.61
Eu	2.29	1.45	2.36	1.26	1.26	1.29	1.13	1.08	1.38	1.24	1.09
Tb	0.74	0.55	0.76	0.51	0.52	0.52	0.47	0.46	0.59	0.53	0.34
Yb	1.47	1.58	1.40	1.62	1.49	1.75	1.28	1.41	1.60	1.24	1.09
Lu	0.19	0.20	0.19	0.24	0.22	0.25	0.17	0.19	0.22	0.21	0.20
Hf	5.28	2.23	5.51	3.87	3.88	4.01	2.84	3.43	3.71	3.31	3.22
Ta	0.65	0.77	0.69	0.74	0.72	0.79	0.46	0.53	0.65	0.53	0.52
Th	7.08	2.28	7.26	3.00	2.81	3.10	1.90	2.47	1.96	1.74	1.78
U	1.58	1.00	1.78	0.93	1.04	0.98	0.22	0.92	0.83	0.79	0.69

APPENDIX B

MODAL PROPORTIONS

FLANK LAVAS

	plag	opx	cpx	amp	ol	ox
0201	65%	2%	2%	0%	0%	31%
0202	56%	9%	18%	0%	1%	16%
0204	69%	3%	9%	0%	12%	7%
0206	77%	3%	8%	0%	0%	12%
0208	74%	2%	4%	0%	8%	12%
0209	63%	1%	10%	0%	7%	18%

HOST LAVAS

	plag	opx	cpx	amp	ol	ox
0203-1	65%	12%	8%	0%	1%	14%
0203-2	68%	9%	8%	0%	0%	15%
0203-3	69%	8%	9%	0%	0%	13%
0205-1	74%	7%	5%	0%	0%	13%
0205-2	75%	8%	6%	0%	0%	12%
0205-3	72%	5%	4%	0%	0%	19%
0205-4	76%	4%	2%	0%	0%	19%
0210-1	59%	20%	0%	15%	0%	7%
0210-2	58%	19%	0%	19%	0%	4%
0211-1	50%	27%	0%	13%	0%	10%
0211-2	52%	18%	0%	20%	0%	11%
0212-1	53%	18%	0%	16%	0%	14%
0212-2	56%	16%	0%	19%	0%	8%
0213-1	49%	29%	0%	8%	0%	14%
0213-2	51%	30%	0%	7%	0%	13%

INCLUSIONS

	plag	opx	cpx	amp	ol	ox
0203A	65%	13%	6%	0%	0%	17%
0203C	62%	13%	7%	0%	0%	17%
0203G	61%	13%	9%	0%	0%	17%
0203I	61%	15%	11%	0%	0%	13%
0205B	60%	13%	9%	0%	0%	17%
0205E	63%	14%	5%	0%	0%	18%
0205L	60%	16%	9%	0%	0%	16%
0205LE	64%	11%	8%	1%	0%	17%
0205M	65%	12%	3%	0%	0%	19%
0205RT	60%	19%	8%	0%	0%	12%
0210B	25%	25%	6%	31%	0%	13%
0210C	41%	13%	0%	38%	0%	9%
0210E	45%	0%	0%	36%	0%	18%
0210F	38%	31%	0%	31%	0%	0%
0210L	31%	21%	5%	18%	0%	26%
0211A	44%	31%	0%	16%	0%	10%
0211B	41%	37%	0%	13%	0%	9%
0211H	36%	36%	5%	9%	0%	14%
0212A	38%	31%	0%	25%	0%	6%
0212D	41%	27%	0%	24%	0%	8%
0212E	40%	29%	2%	21%	0%	7%
0213C	39%	25%	3%	14%	0%	19%
0213F	38%	25%	8%	17%	0%	13%

APPENDIX C

FRACTIONATION MODELS

The horizontal lines on each graph represent the observed concentration of element in the host lava.

Fractionation Model Site 0203, U.S. Highway 26

118
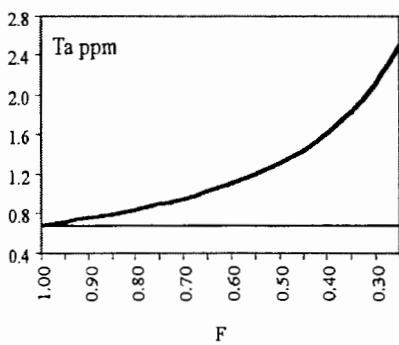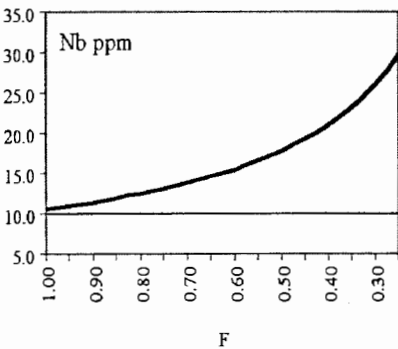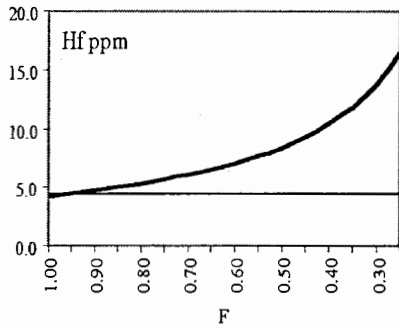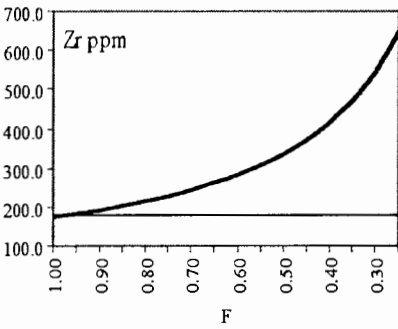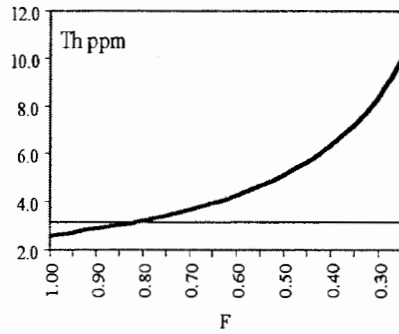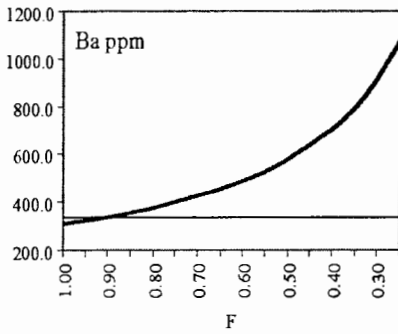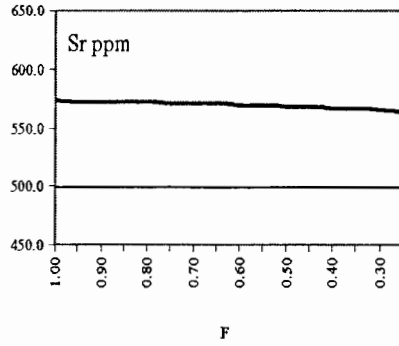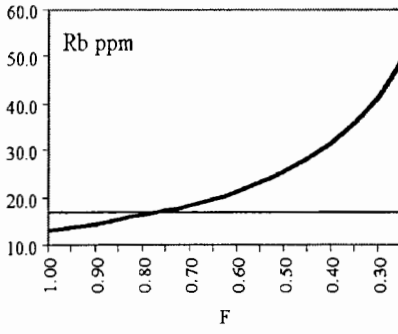
Fractionation Model Site 0203, U.S. Highway 26 (con't.)
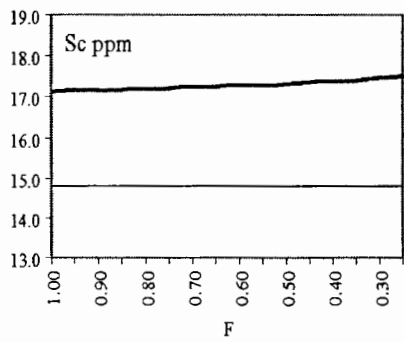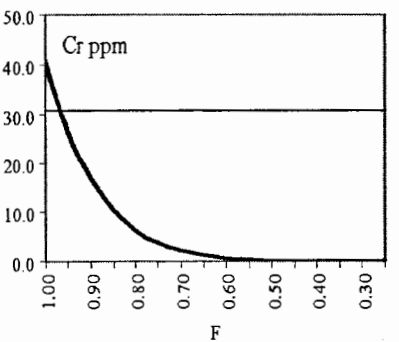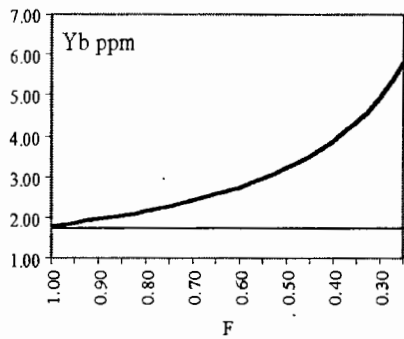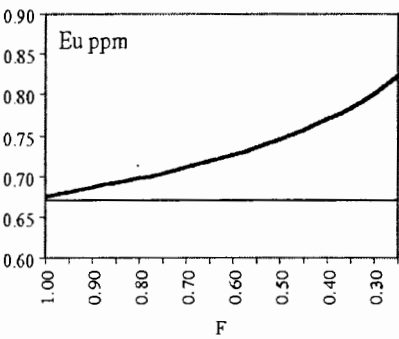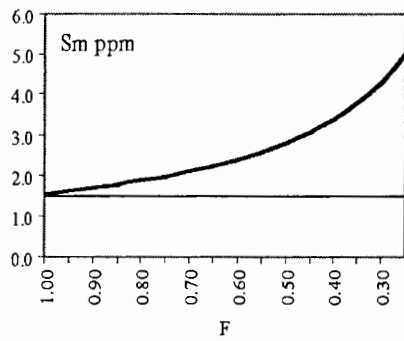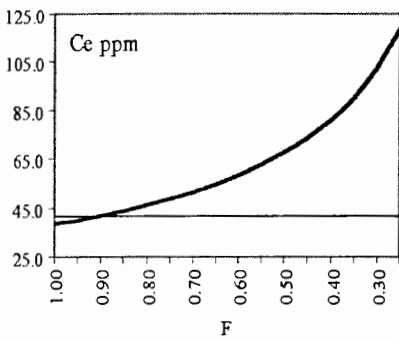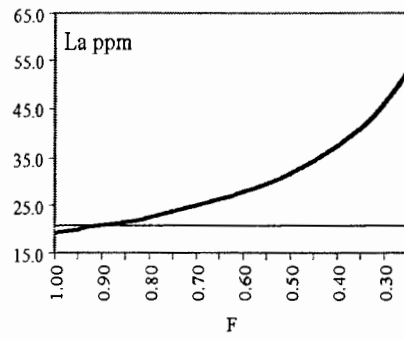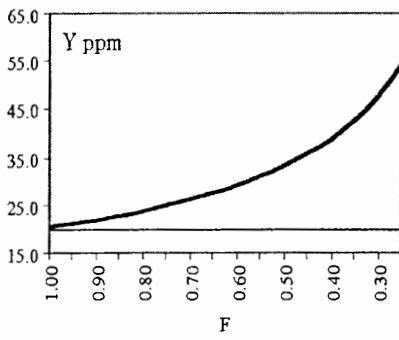
Fractionation Model Site 0205, Mount HoodMeadows Ski Resort
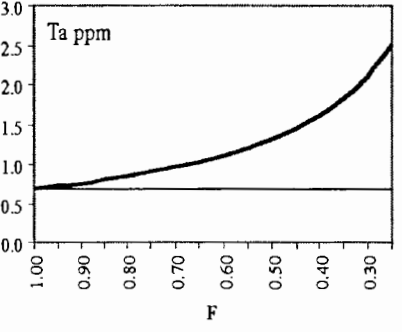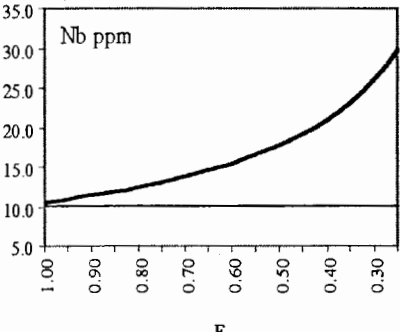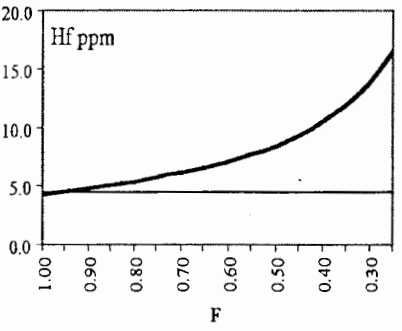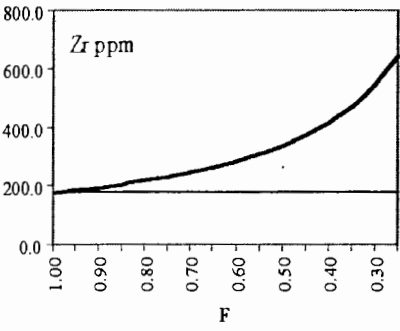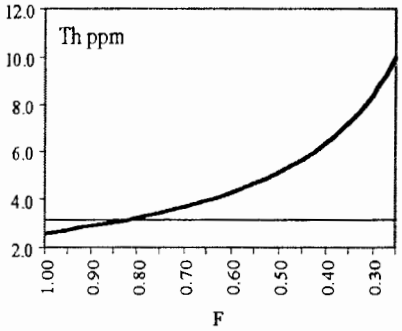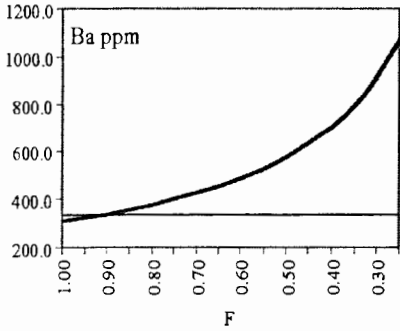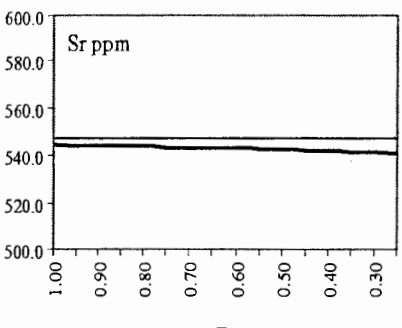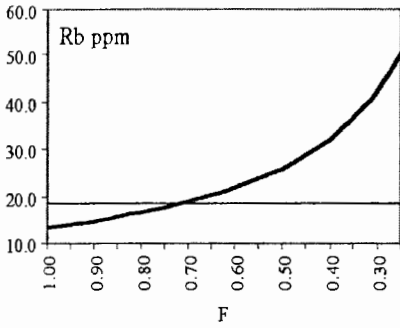
Fractionation Model Site 0205, Mount HoodMeadows Ski Resort (con't.)
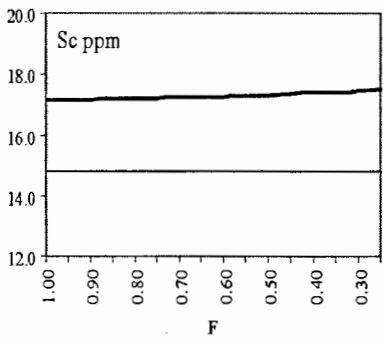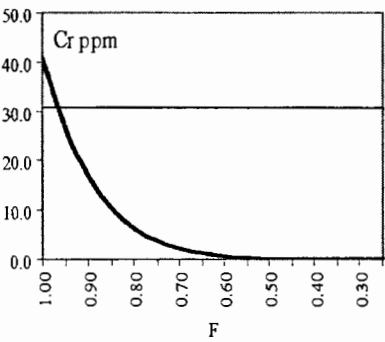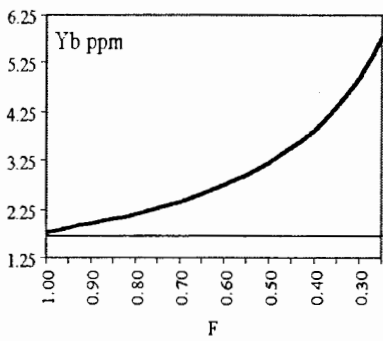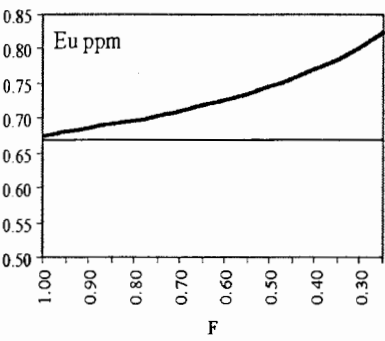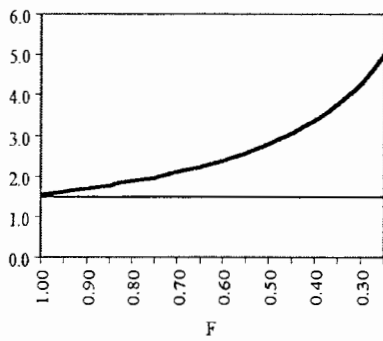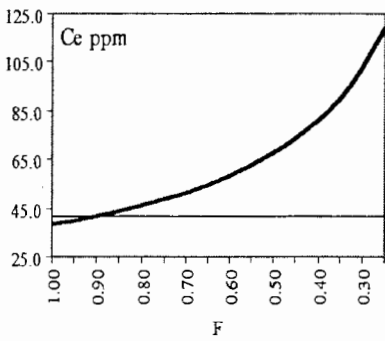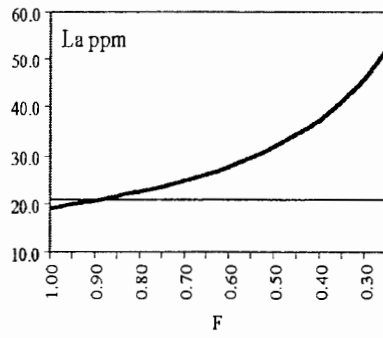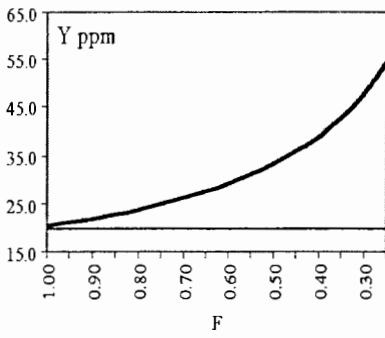
Fractionation Model Site 0210, Laurence Lake
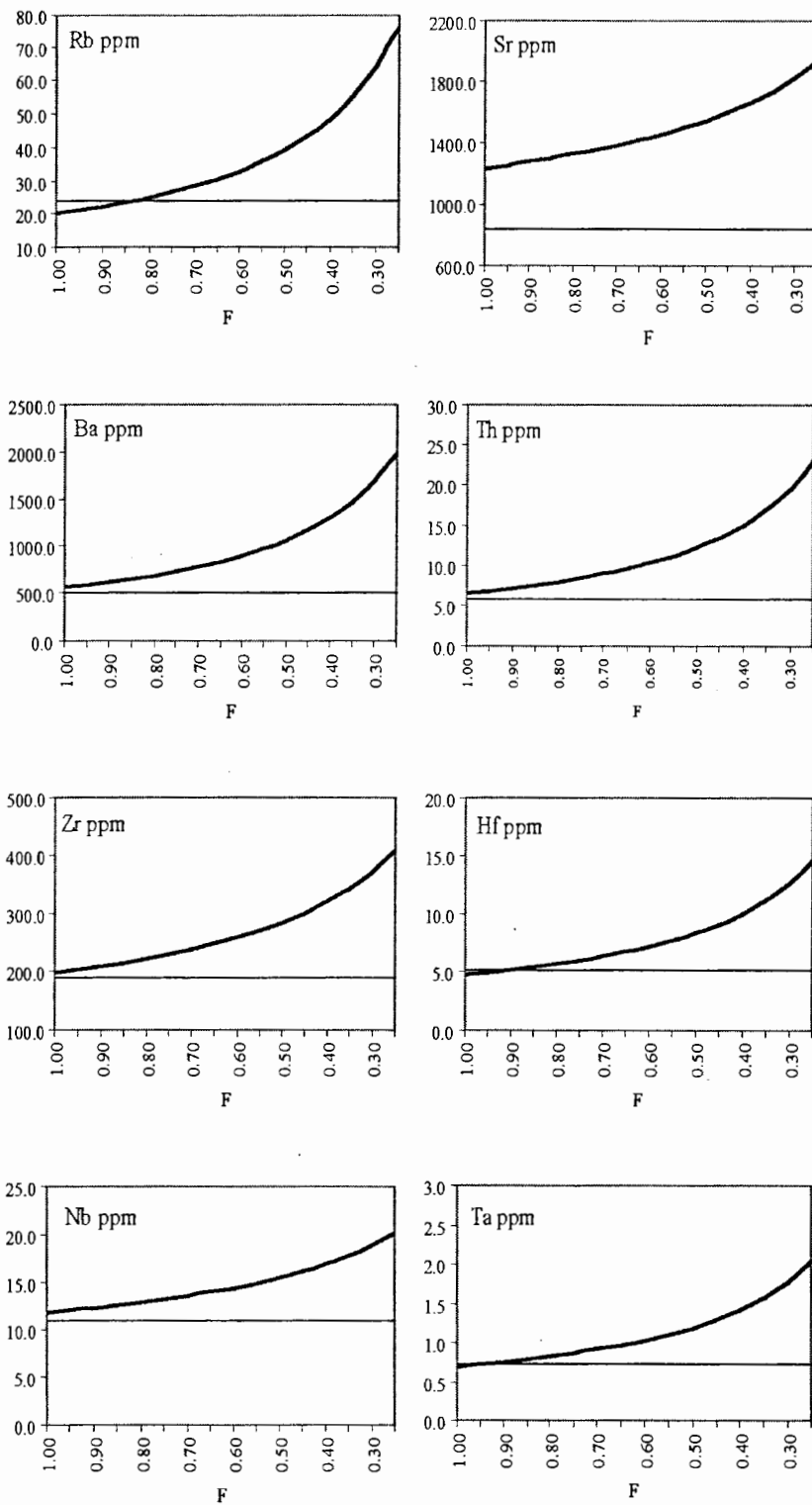
Fractionation Model Site 0210, Laurence Lake (con't.)
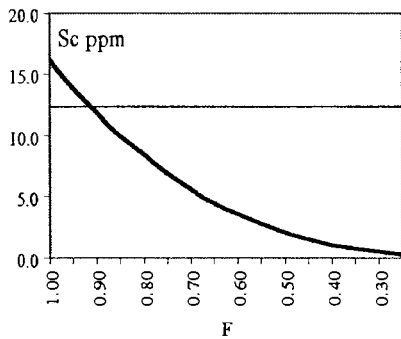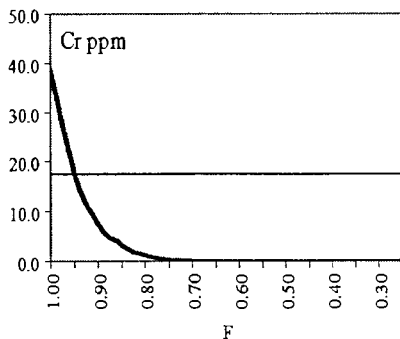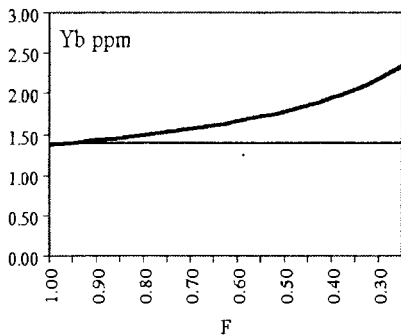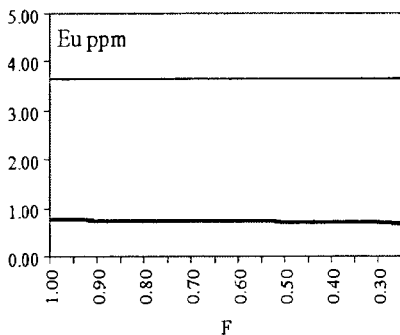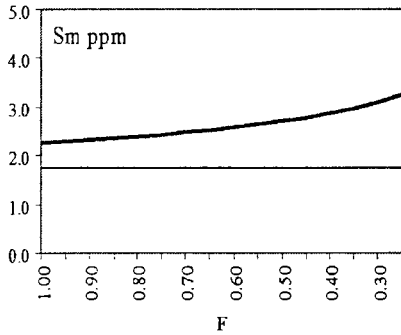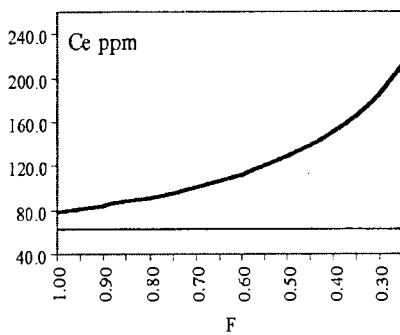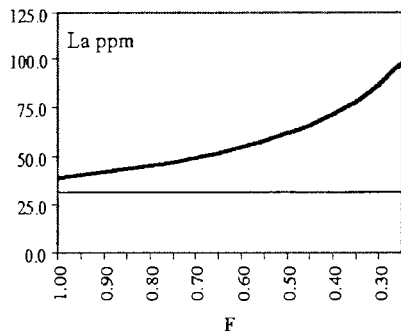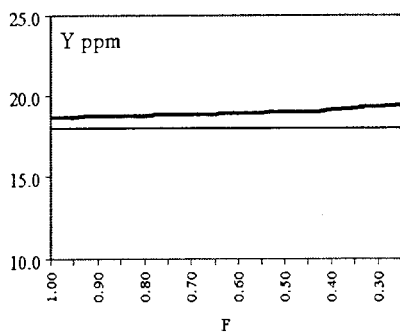
Fractionation Model Site 0211, Compass Creek

124
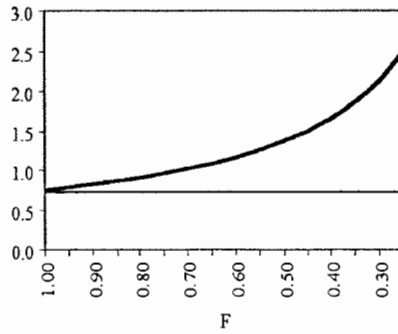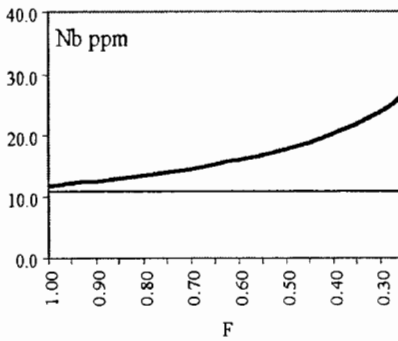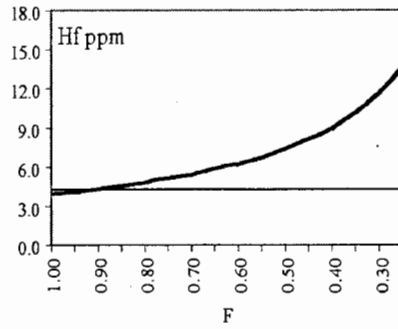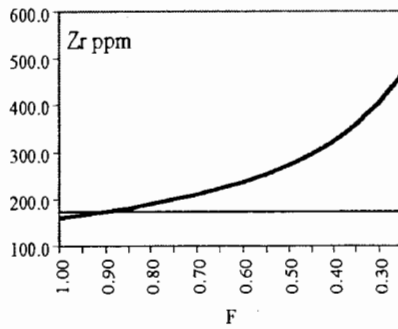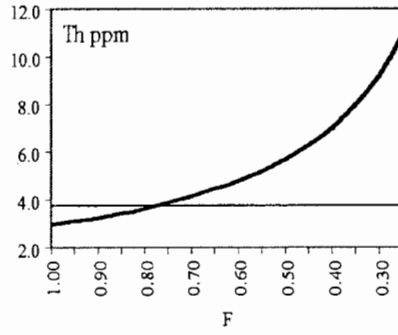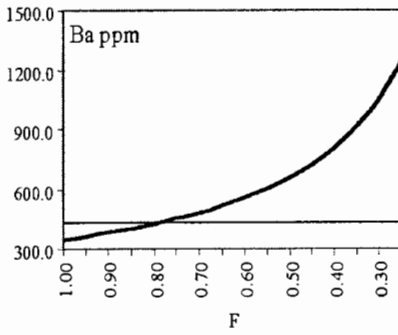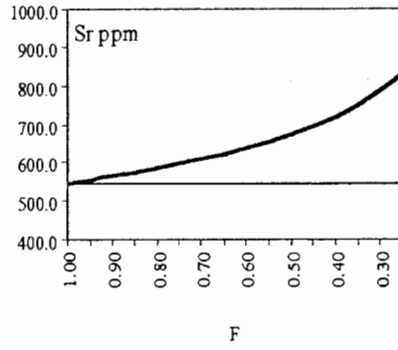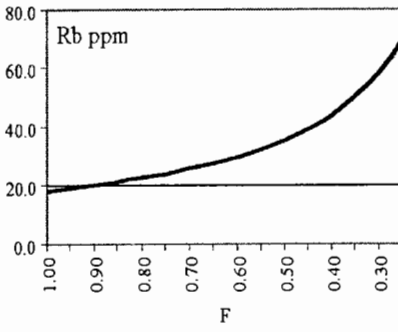
Fractionation Model Site 0211, Compass Creek (con't.)
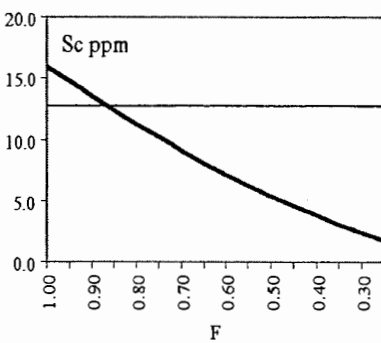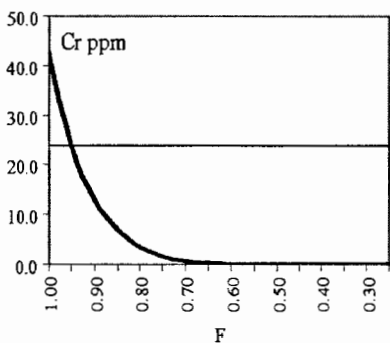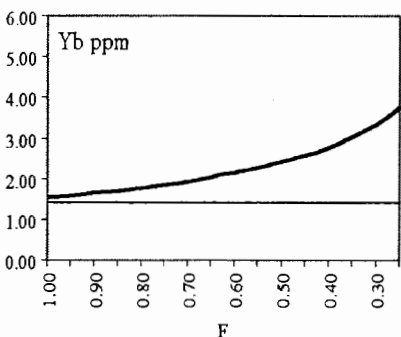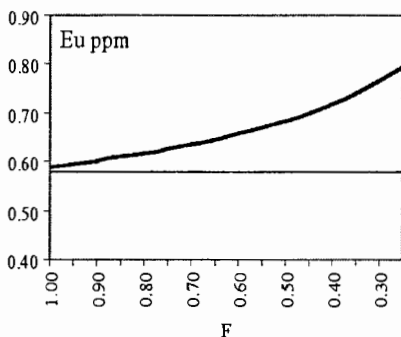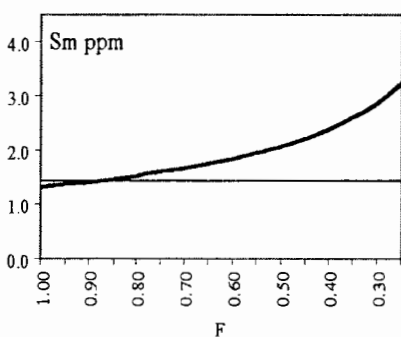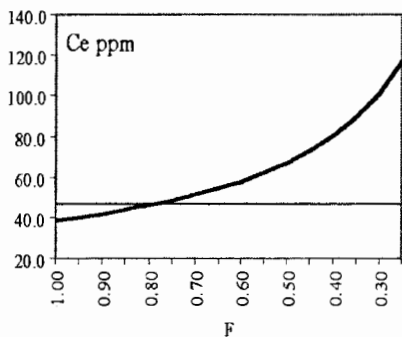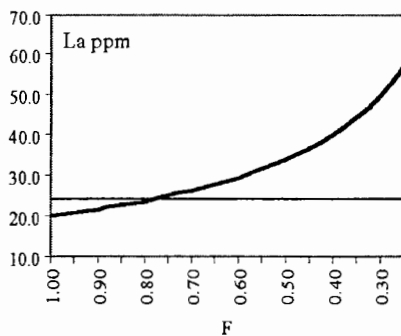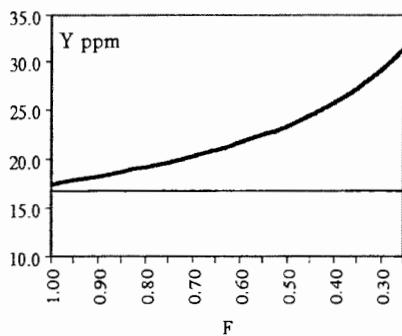
Fractionation Model Site 0212, Timberline Lodge
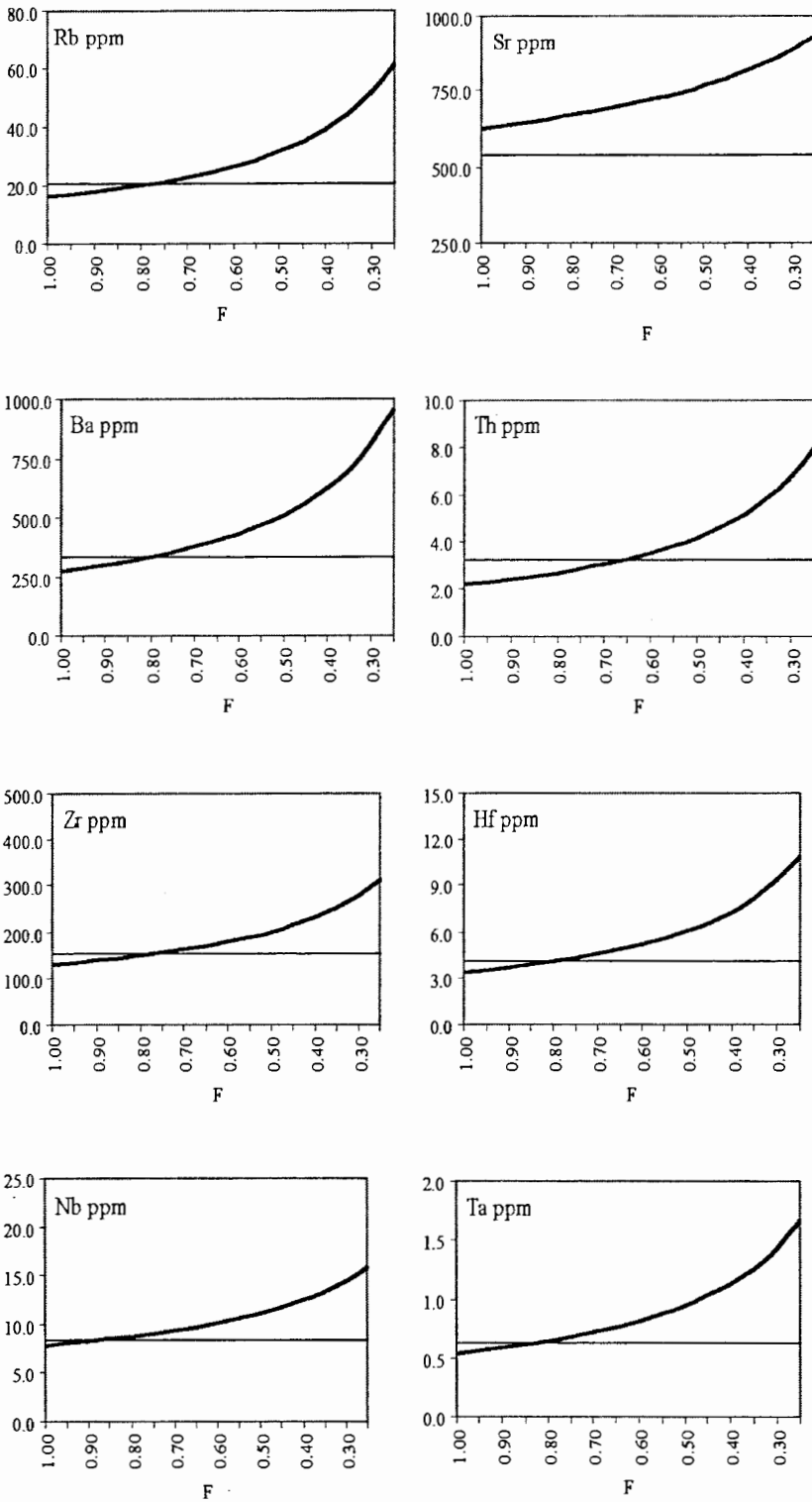
Fractionation Model Site 0212, Timberline Lodge (con't.)
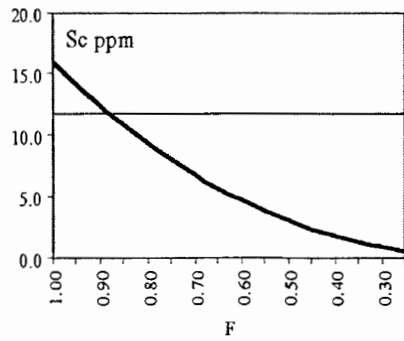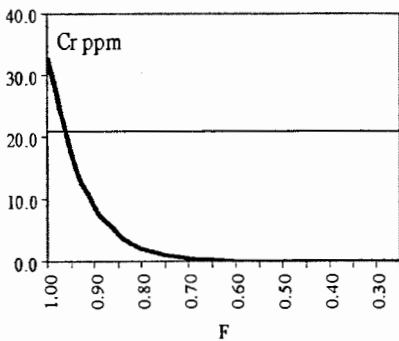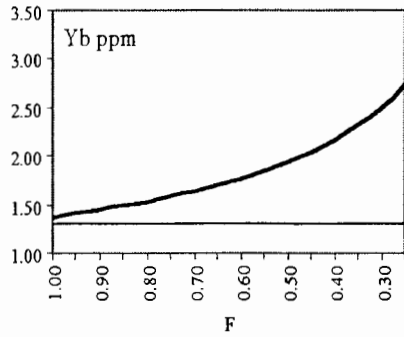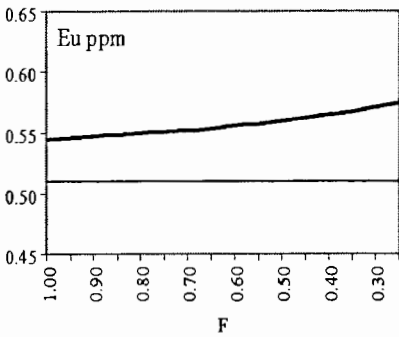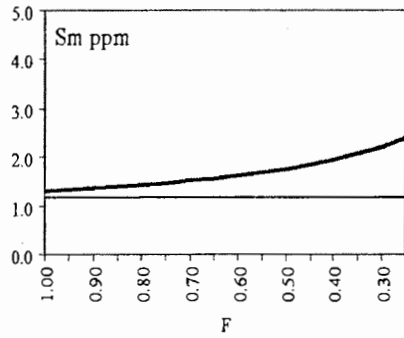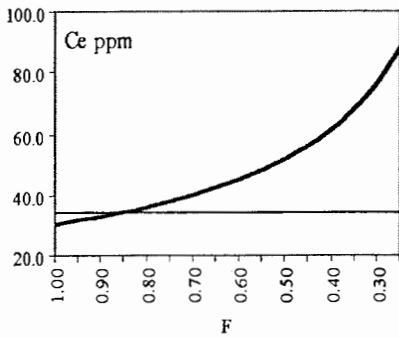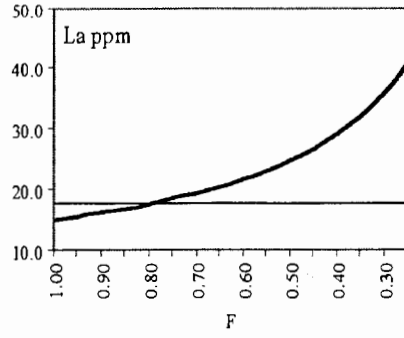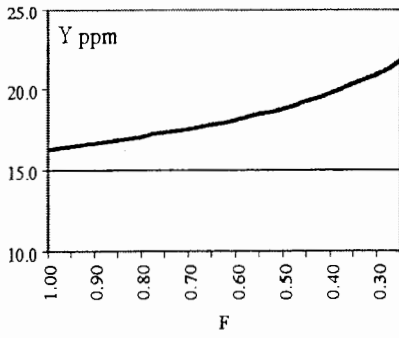
Fractionation Model Site 0213, Cathedral Ridge
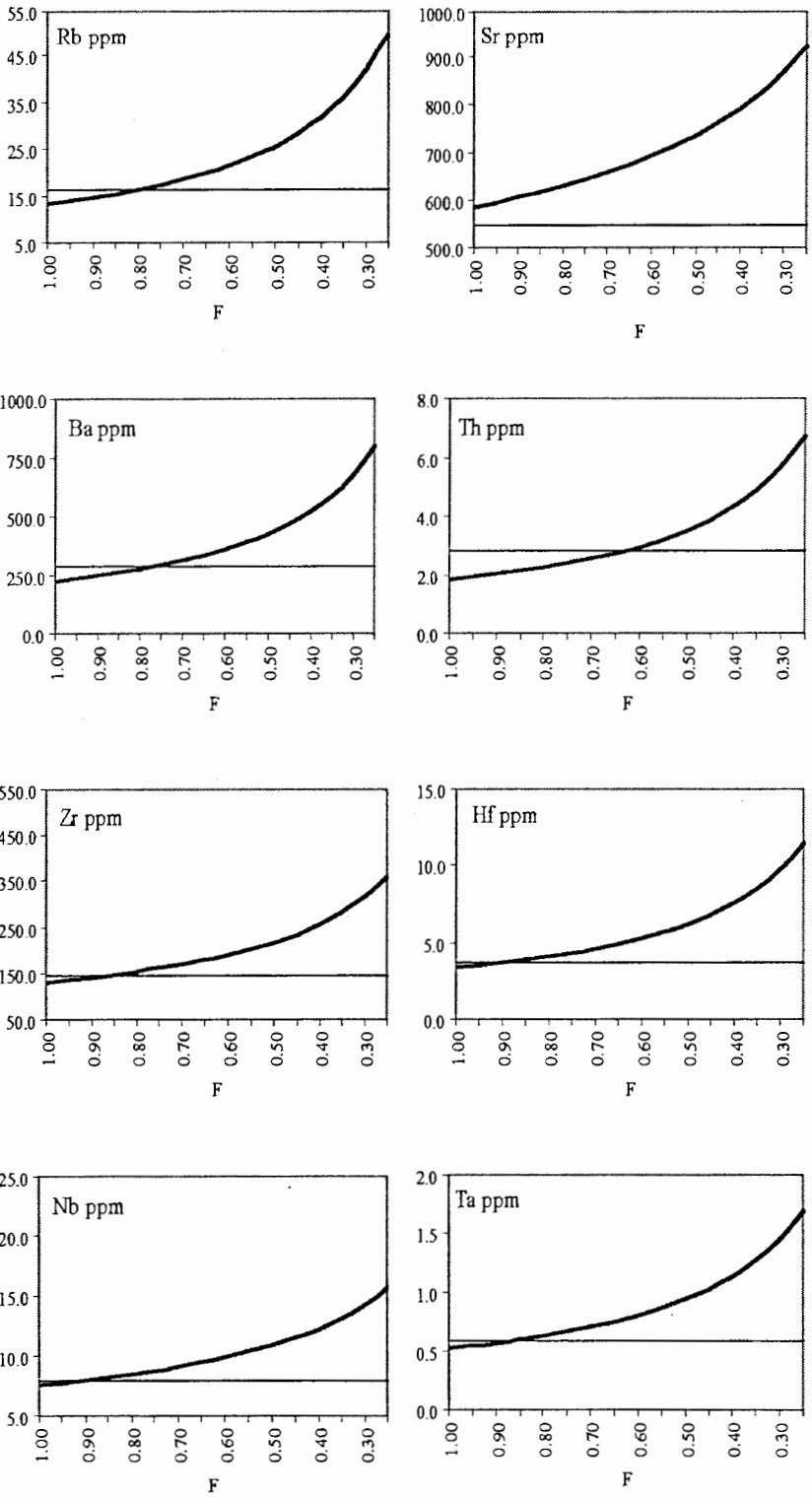
Fractionation Model Site 0213, Cathedral Ridge (con't.)
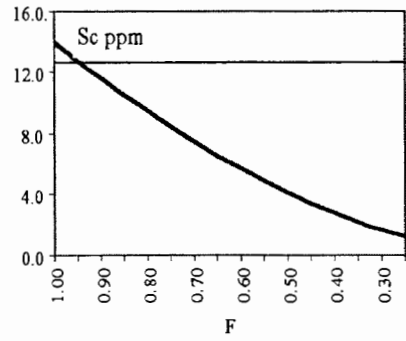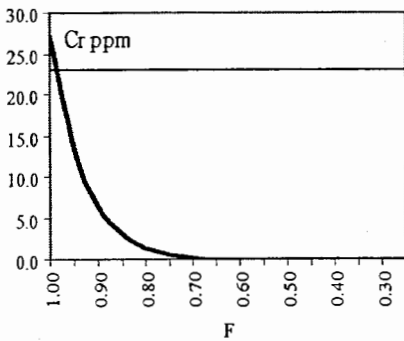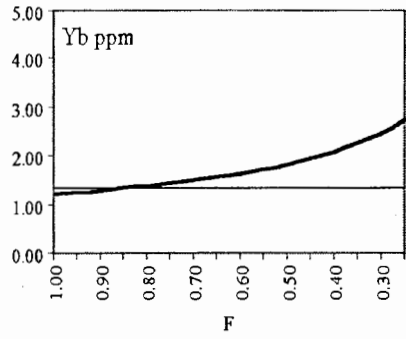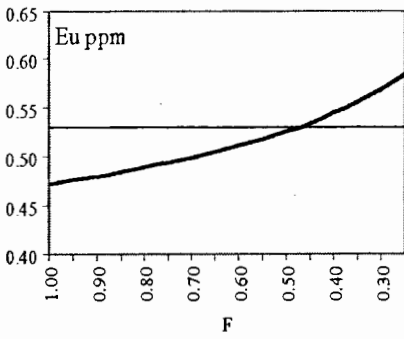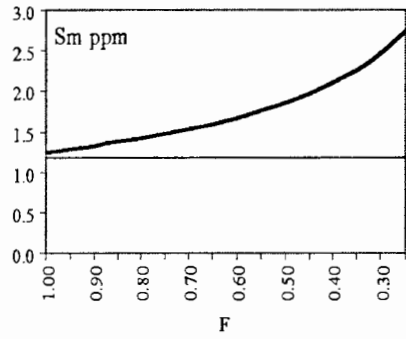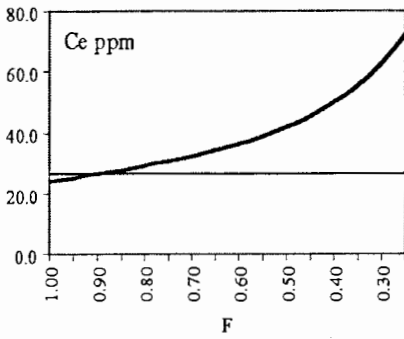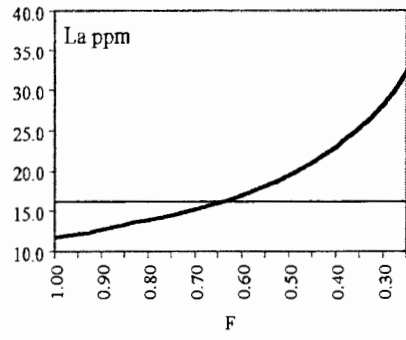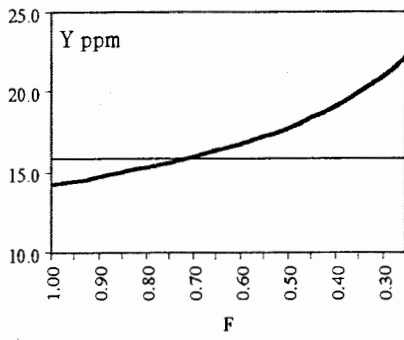
APPENDIX D

MAGMA MIXING:

CALCULATION OF THE HYPOTHETICAL SILICIC END MEMBER

133

135

137
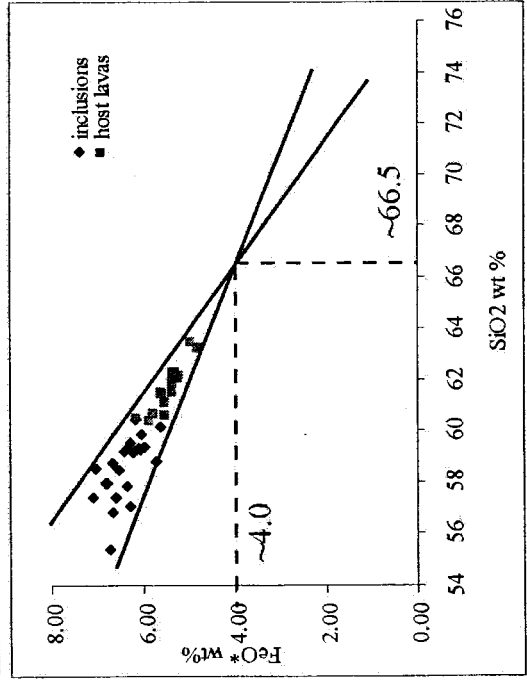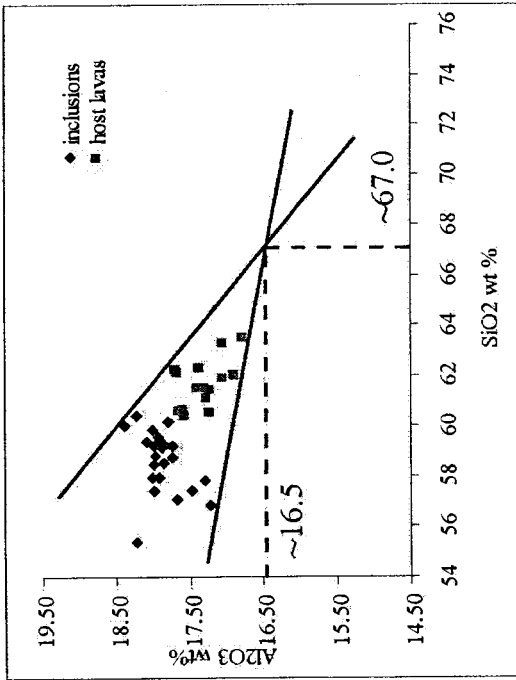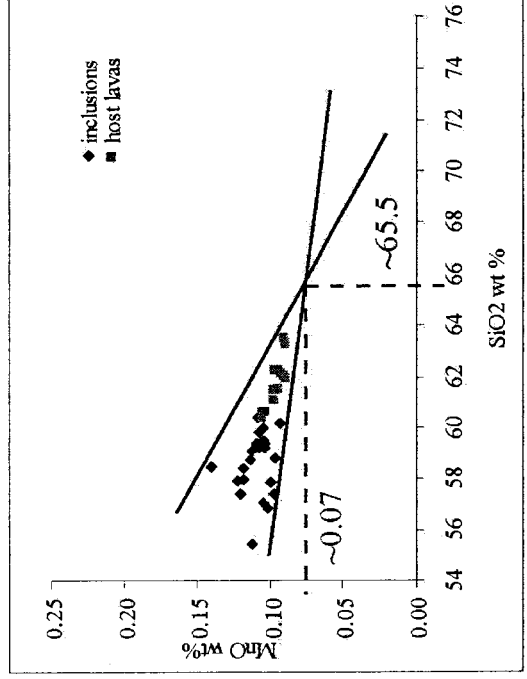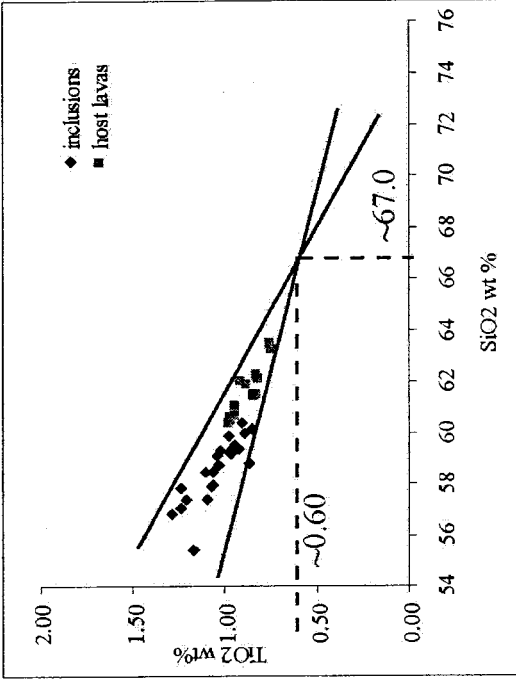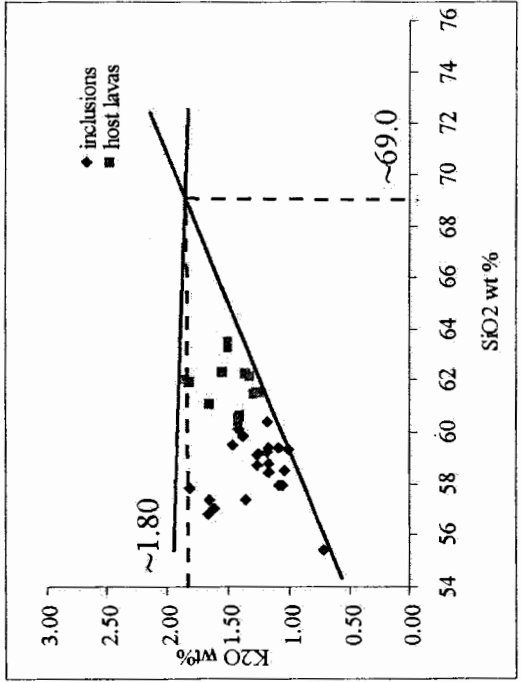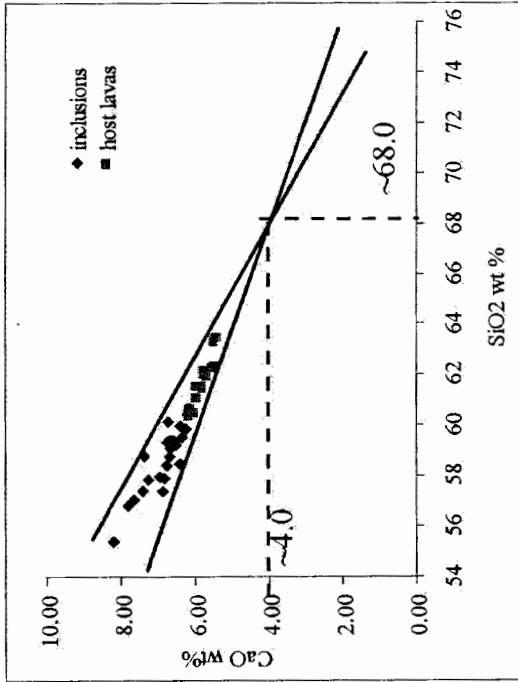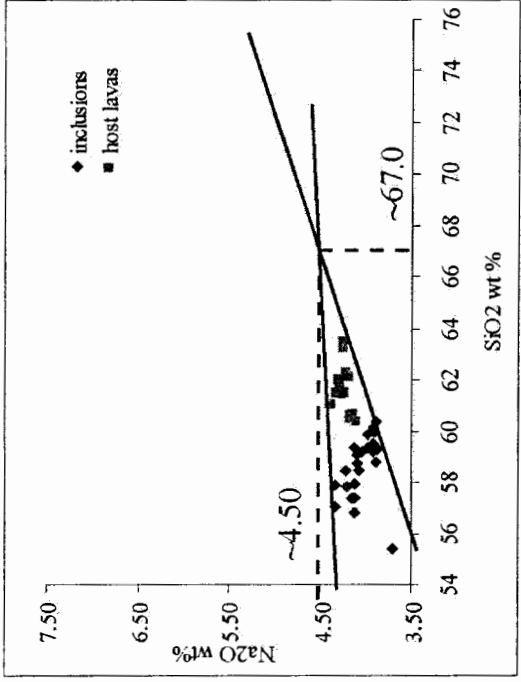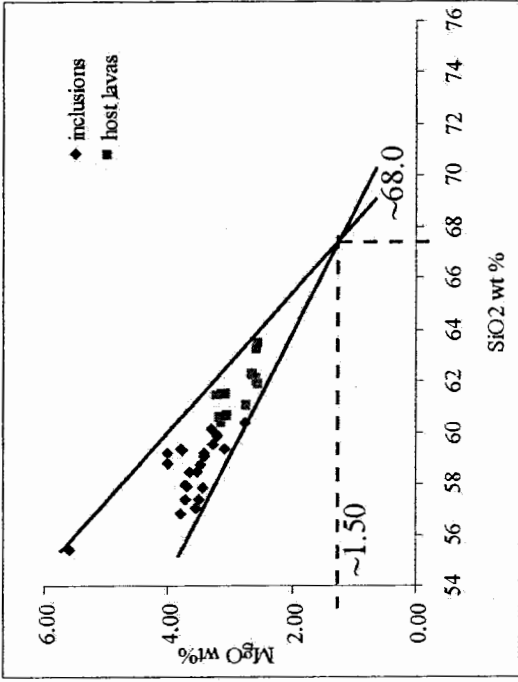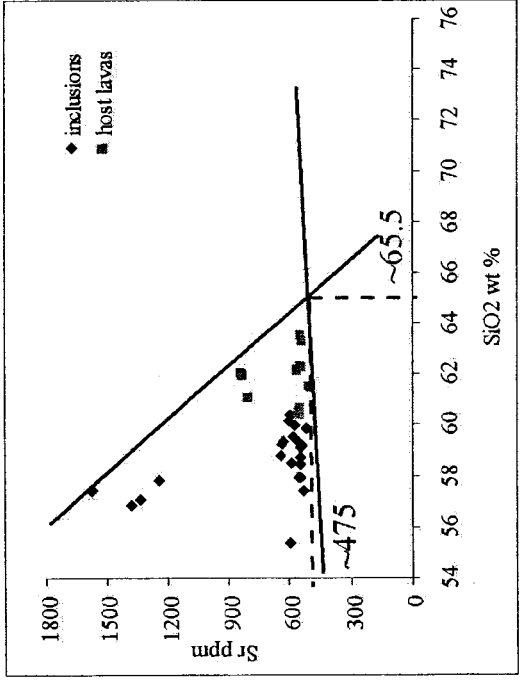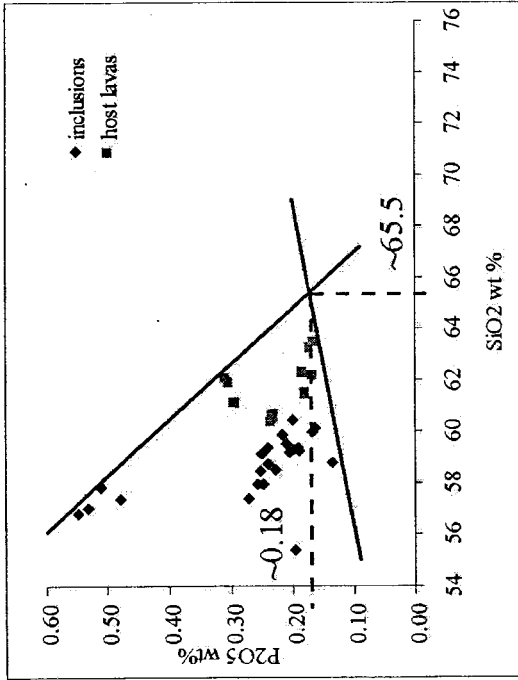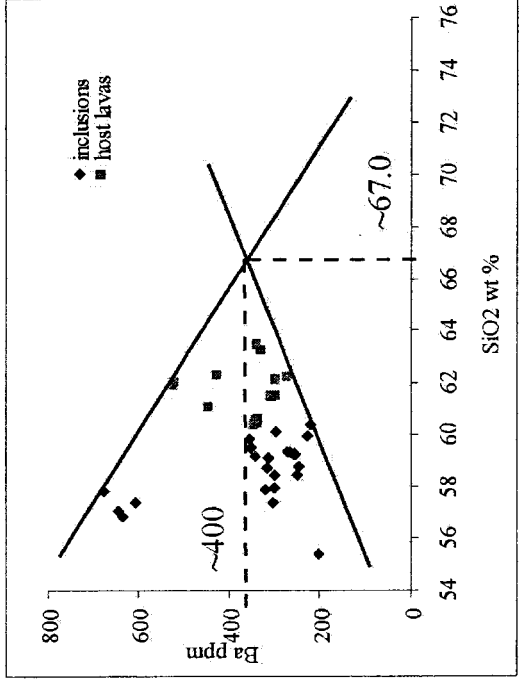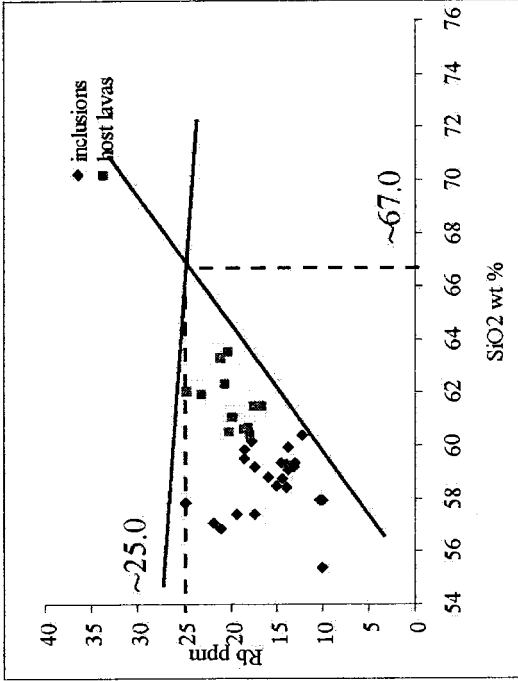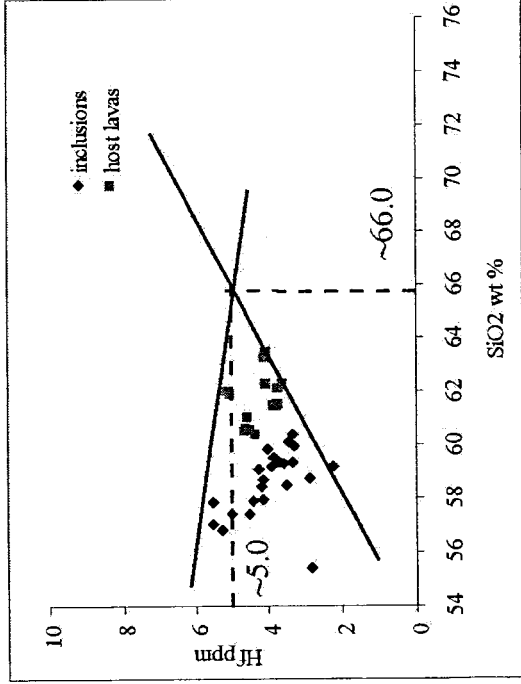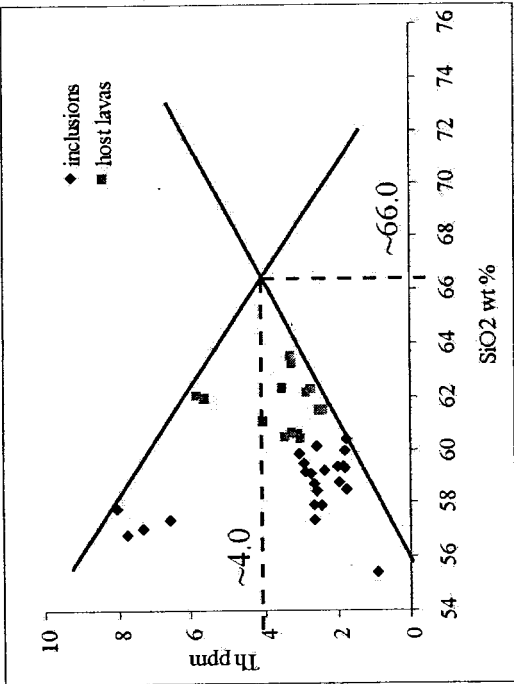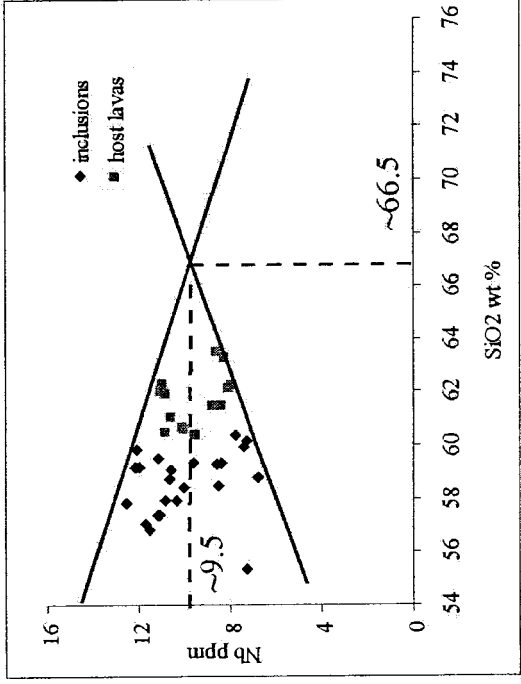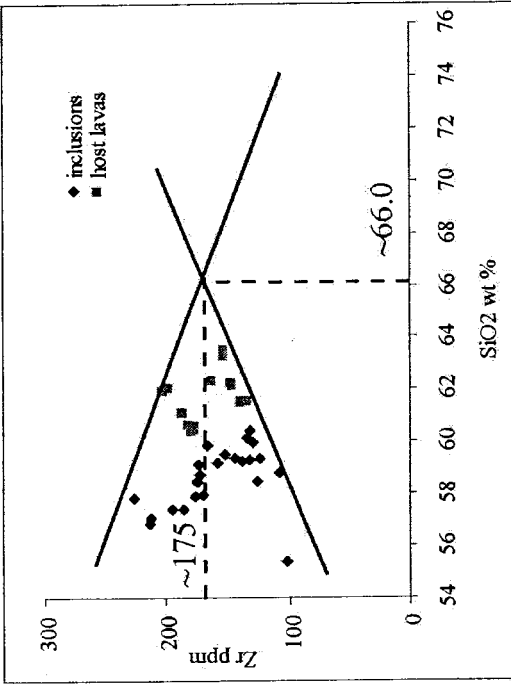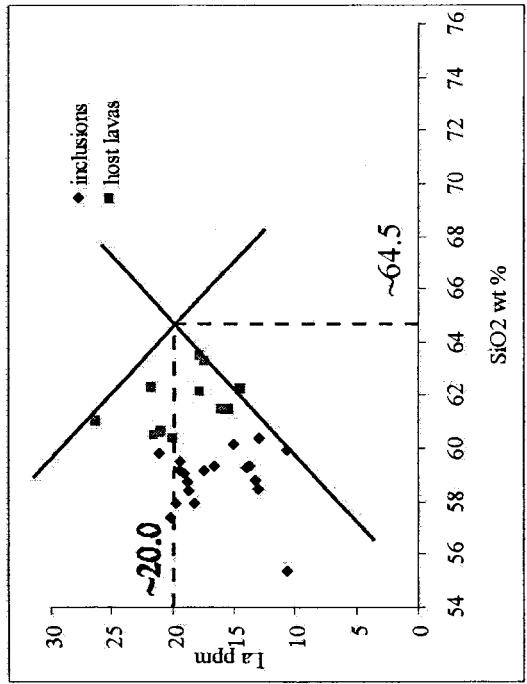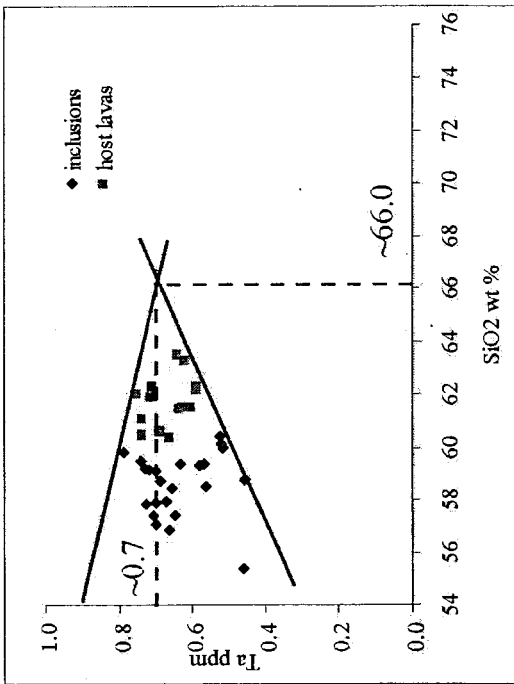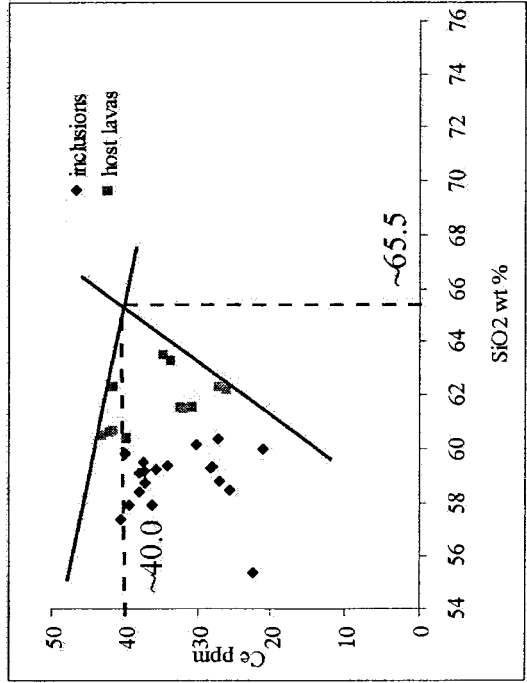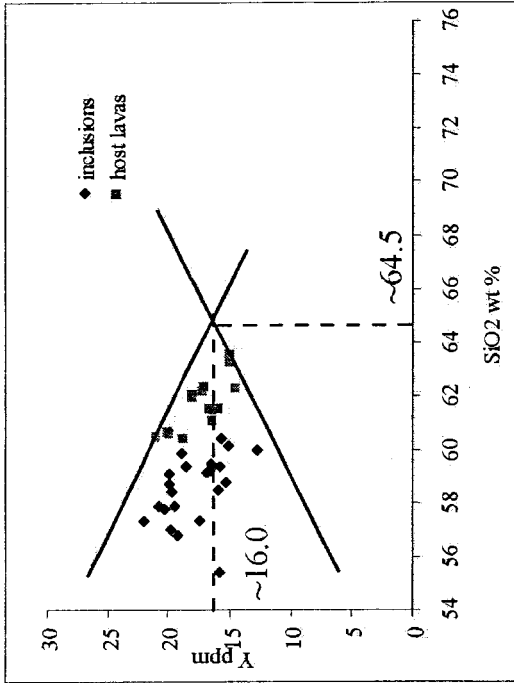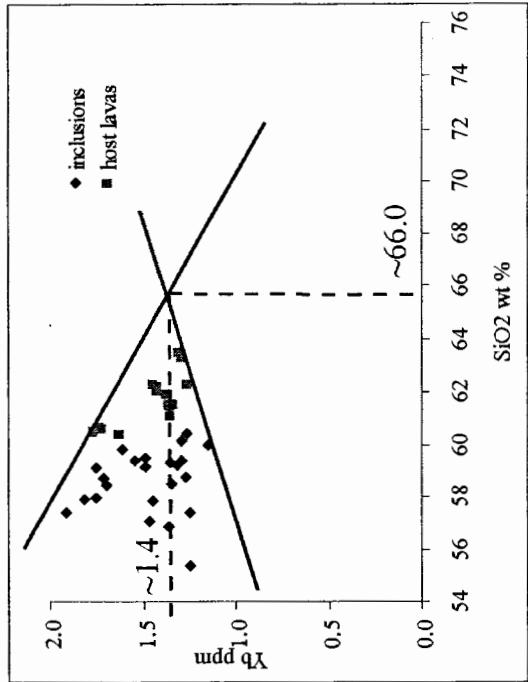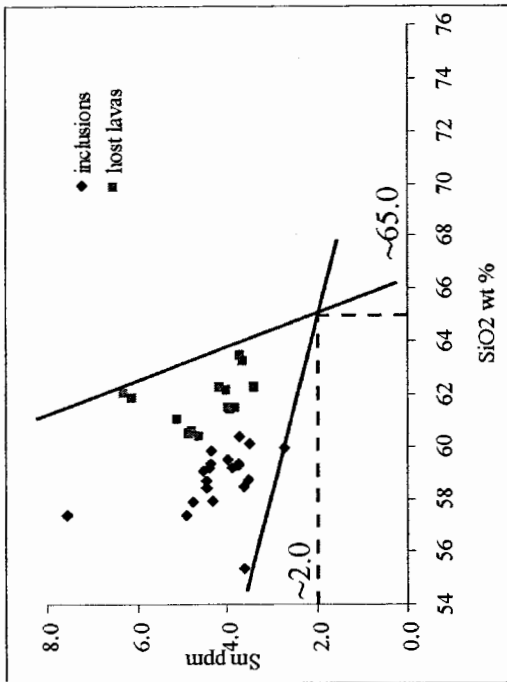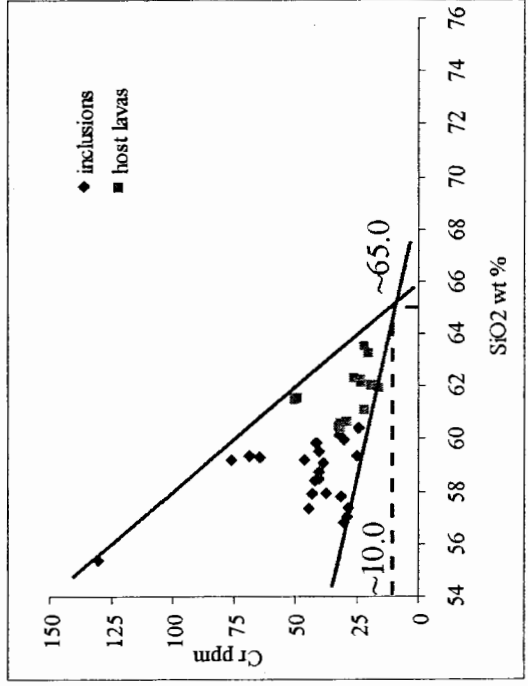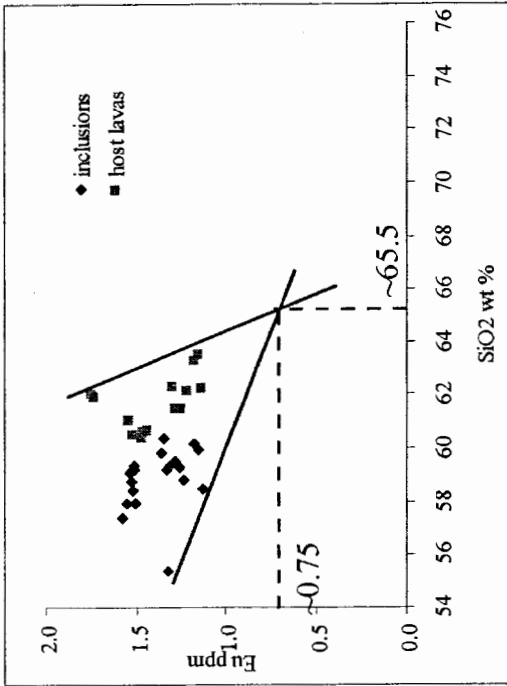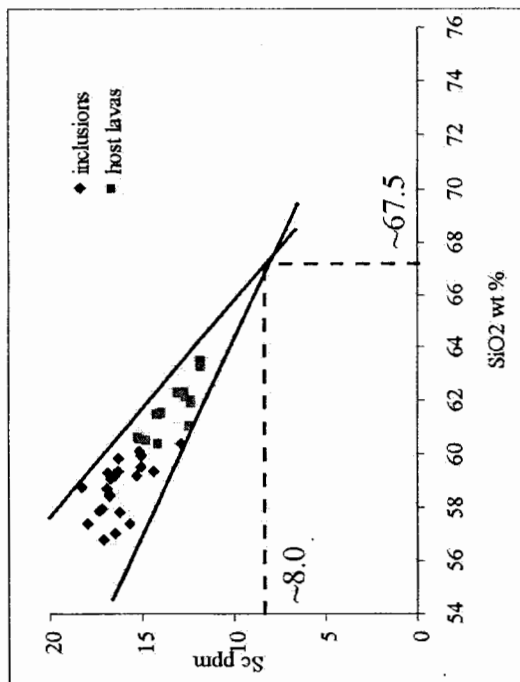
APPENDIX E

MAGMA MIXING:

CALCULATION OF THE HYPOTHETICAL MAFIC END MEMBERS

Equation $C_{HL}=C_{HSEM}X+C_{HMEM}(1-X)$

solve for C_{HMEM}

$C_{HMEM}=(C_{HL}-C_{HSEM}X)/(1-X)$, $X = amount\ of\ HSEM$

Site 0203 - Roadcut along US Hwy 26

Xa	0.90	0.85	0.80	0.75	0.72	0.65	0.61	0.55	0.50	0.45
SiO_2	18.1	34.2	42.2	47.1	48.9	52.6	54.0	55.6	56.7	57.6
Al_2O_3	23.7	21.3	20.1	69.2	19.2	18.6	18.4	18.2	18.0	17.9
TiO_2	3.0	2.2	1.8	3.3	1.5	1.3	1.2	1.1	1.1	1.0
FeO*	19.1	14.1	11.6	22.1	9.5	8.3	7.9	7.4	7.0	6.8
MnO	0.3	0.2	0.2	0.4	0.2	0.1	0.1	0.1	0.1	0.1
CaO	22.5	16.3	13.3	23.4	10.7	9.3	8.8	8.1	7.7	7.4
MgO	17.9	12.4	9.7	12.6	7.4	6.2	5.7	5.1	4.8	4.5
K_2O	-3.7	-1.8	-0.9	5.0	-0.2	0.2	0.4	0.6	0.7	0.8
Na_2O	2.3	3.0	3.4	17.1	3.7	3.9	3.9	4.0	4.1	4.1
P_2O_5	0.2	0.2	0.2	0.7	0.2	0.2	0.2	0.2	0.2	0.2
Rb	-54.7	-28.1	-14.9	68.1	-3.8	2.2	4.5	7.3	9.1	10.5
Sr	718.3	637.2	596.7	1997.3	562.8	544.5	537.6	529.1	523.7	519.2
Ba	-579.1	-252.7	-89.5	1208.4	46.5	120.3	148.3	182.4	204.2	222.0
Th	-11.3	-6.2	-3.6	9.9	-1.5	-0.4	0.1	0.6	0.9	1.2
Zr	-201.9	-76.3	-13.5	549.2	38.9	67.3	78.1	91.2	99.6	106.5
Hf	-7.0	-3.0	-1.0	15.2	0.7	1.6	1.9	2.3	2.6	2.8
Nb	4.9	6.3	6.9	34.4	7.5	7.8	7.9	8.1	8.2	8.3
Ta	-0.1	0.2	0.3	2.5	0.4	0.5	0.5	0.5	0.5	0.6
Y	18.9	18.0	17.5	65.2	17.1	16.8	16.8	16.7	16.6	16.5
La	-23.4	-8.9	-1.7	62.6	4.3	7.6	8.8	10.4	11.3	12.1
Ce	-43.5	-15.7	-1.8	126.6	9.8	16.1	18.5	21.4	23.3	24.8
Sm	20.9	14.6	11.4	15.6	8.8	7.4	6.9	6.2	5.8	5.4
Eu	5.9	4.2	3.3	2.5	2.6	2.2	2.1	1.9	1.8	1.7
Yb	4.5	3.3	2.8	-97.1	2.3	2.0	1.9	1.8	1.7	1.6
Cr	406.7	274.4	208.3	134.7	153.2	123.3	112.0	98.1	89.3	82.1
Sc	68.8	48.5	38.4	49.8	29.9	25.4	23.6	21.5	20.2	19.0

$$C_{HL}=C_{HSEM}X+C_{HMEM}(1-X)$$

Equation

Solve for C_{HMEM}

$C_{HMEM}=(C_{HL}-C_{HSEM}X)/(1-X),)$ $X = $ *amount of HSEM*

Site 0205 - Mount Hood Meadows Ski Resort

Xa	0.90	0.85	0.80	0.75	0.70	0.67	0.60	0.55	0.53	0.45
SiO_2	8.5	27.8	37.4	43.2	47.1	**48.9**	51.9	53.5	**54.0**	55.8
Al_2O_3	25.7	22.7	21.1	20.2	19.6	**19.3**	18.9	18.6	**18.5**	18.3
TiO_2	4.2	3.0	2.4	2.1	1.8	**1.7**	1.5	1.4	**1.4**	1.3
FeO*	22.1	16.1	13.1	11.3	10.0	**9.5**	8.5	8.0	**7.9**	7.3
MnO	0.4	0.3	0.2	0.2	0.2	**0.2**	0.2	0.1	**0.1**	0.1
CaO	25.2	18.1	14.6	12.5	11.1	**10.4**	9.3	8.7	**8.5**	7.8
MgO	17.7	12.3	9.6	8.0	6.9	**6.4**	5.6	5.1	**5.0**	4.4
K_2O	-2.1	-0.8	-0.2	0.2	0.5	**0.6**	0.8	0.9	**1.0**	1.1
Na_2O	1.0	2.2	2.8	3.1	3.3	**3.5**	3.6	3.7	**3.8**	3.9
P_2O_5	0.7	0.5	0.4	0.4	0.4	**0.3**	0.3	0.3	**0.3**	0.3
Rb	-39.0	-17.7	-7.0	-0.6	3.7	**5.7**	9.0	10.8	**11.3**	13.4
Sr	1197.5	956.7	836.3	764.0	715.8	**692.6**	655.6	635.6	**629.7**	606.4
Ba	-215.0	-10.0	92.5	154.0	195.0	**214.8**	246.3	263.3	**268.3**	288.2
Th	-4.1	-1.4	-0.1	0.7	1.3	**1.5**	2.0	2.2	**2.3**	2.5
Zr	210.0	198.3	192.5	189.0	186.7	**185.5**	183.8	182.8	**182.5**	181.4
Hf	0.2	1.8	2.6	3.1	3.4	**3.6**	3.8	3.9	**4.0**	4.1
Nb	19.9	16.3	14.5	13.4	12.6	**12.3**	11.7	11.4	**11.3**	11.0
Ta	0.7	0.7	0.7	0.7	0.7	**0.7**	0.7	0.7	**0.7**	0.7
Y	55.2	42.1	35.6	31.7	29.1	**27.8**	25.8	24.7	**24.4**	23.1
La	28.3	25.6	24.2	23.3	22.8	**22.5**	22.1	21.9	**21.8**	21.5
Ce	55.3	50.2	47.7	46.1	45.1	**44.6**	43.8	43.4	**43.3**	42.8
Sm	29.4	20.3	15.7	13.0	11.1	**10.3**	8.9	8.1	**7.9**	7.0
Eu	8.1	5.6	4.4	3.7	3.2	**2.9**	2.6	2.4	**2.3**	2.1
Yb	8.1	5.7	4.6	3.8	3.4	**3.1**	2.8	2.6	**2.5**	2.3
Cr	217.5	148.3	113.8	93.0	79.2	**72.5**	61.9	56.1	**54.4**	47.7
Sc	75.9	53.3	41.9	35.2	30.6	**28.4**	25.0	23.1	**22.5**	20.3

Equation $C_{HL}=C_{HSEM}X+C_{HMEM}(1-X)$

Solve for C_{HMEM}

$C_{HMEM}=(C_{HL}-C_{HSEM}X)/(1-X)$, X = amount of HSEM

Site 0210 - Laurence Lake

Xa	0.90	0.85	0.80	0.75	0.70	0.65	0.60	0.55	0.50	0.45
SiO_2	22.9	37.4	44.7	**48.9**	51.9	**54.0**	55.5	56.7	57.7	58.5
Al_2O_3	20.4	19.1	18.5	**18.1**	17.9	**17.7**	17.5	17.4	17.4	17.3
TiO_2	3.6	2.6	2.1	**1.8**	1.6	**1.4**	1.3	1.3	1.2	1.1
FeO*	16.8	12.5	10.4	**9.1**	8.3	**7.7**	7.2	6.8	6.6	6.3
MnO	0.2	0.2	0.2	**0.1**	0.1	**0.1**	0.1	0.1	0.1	0.1
CaO	21.3	15.6	12.7	**11.0**	9.8	**9.0**	8.3	7.9	7.5	7.2
MgO	12.2	8.6	6.8	**5.8**	5.1	**4.5**	4.2	3.9	3.6	3.4
K_2O	2.1	2.0	2.0	**1.9**	1.9	**1.9**	1.9	1.9	1.9	1.9
Na_2O	2.4	3.1	3.5	**3.7**	3.8	**3.9**	4.0	4.0	4.1	4.1
P_2O_5	1.4	1.0	0.8	**0.7**	0.6	**0.5**	0.5	0.5	0.4	0.4
Rb	14	17	19	**20**	21	**22**	22	22	23	23
Sr	4045	2855	2260	**1909**	1665	**1495**	1368	1268	1189	1124
Ba	1615	1210	1008	**888**	805	**747**	704	670	643	621
Th	21	15	12	**11**	10	**9**	8	8	7	7
Zr	430	345	303	**277**	260	**248**	239	232	226	221
Hf	6	6	5	**5**	5	**5**	5	5	5	5
Nb	28	22	19	**17**	15	**14**	14	13	13	12
Ta	1	1	1	**1**	1	**1**	1	1	1	1
Y	36	29	26	**24**	23	**22**	21	20	20	20
La	131	94	76	**65**	57	**52.**	48	45	42	40
Ce	260	187	150	**128**	113	**103**	95	89	84	80
Sm	44	30	23	**19**	16	**14**	13	11	10	10
Eu	11	7	6	**5**	4	**4**	3	3	3	3
Yb	5	4	3	**3**	2	**2**	2	2	2	2
Cr	85	60	48	**40**	35	**31**	29	27	25	24
Sc	51	37	30	**25**	22	**20**	19	18	17	16

Equation
$$C_{HL}=C_{HSEM}X+C_{HMEM}(1-X)$$

Solve for C_{HMEM}

$$C_{HMEM}=(C_{HL}-C_{HSEM}X)/(1-X),$$

X = amount of HSEM

Site 0211 - Compass Creek

Xa	0.90	0.85	0.80	0.75	0.73	0.65	0.63	0.55	0.50	0.45
SiO_2	20.0	35.5	43.2	47.8	48.9	53.1	54.0	56.1	57.1	57.9
Al_2O_3	23.8	21.4	20.2	19.5	19.3	18.7	18.5	18.2	18.0	17.9
TiO_2	3.4	2.5	2.0	1.7	1.7	1.4	1.4	1.2	1.2	1.1
FeO*	18.1	13.4	11.1	9.6	9.3	8.0	7.8	7.1	6.8	6.6
MnO	0.3	0.2	0.2	0.2	0.2	0.1	0.1	0.1	0.1	0.1
CaO	21.1	15.4	12.5	10.8	10.4	8.9	8.6	7.8	7.4	7.1
MgO	13.6	9.5	7.5	6.3	6.0	4.9	4.7	4.2	3.9	3.7
K_2O	-0.3	0.4	0.8	1.0	1.0	1.2	1.2	1.3	1.4	1.4
Na_2O	2.6	3.2	3.6	3.7	3.8	4.0	4.0	4.1	4.1	4.2
P_2O_5	0.8	0.6	0.5	0.4	0.4	0.3	0.3	0.3	0.3	0.3
Rb	-23.5	-7.3	0.7	5.6	6.8	11.1	12.0	14.2	15.3	16.2
Sr	1165.0	935.0	820.0	751.0	734.4	672.1	659.5	628.3	613.0	600.5
Ba	575.0	516.7	487.5	470.0	465.8	450.0	446.8	438.9	435.0	431.8
Th	1.7	2.4	2.8	3.1	3.1	3.3	3.4	3.5	3.5	3.6
Zr	165.0	168.3	170.0	171.0	171.2	172.1	172.3	172.8	173.0	173.2
Hf	-2.0	0.3	1.5	2.2	2.4	3.0	3.1	3.4	3.6	3.7
Nb	26.7	20.8	17.8	16.1	15.6	14.1	13.7	12.9	12.5	12.2
Ta	0.9	0.9	0.8	0.8	0.8	0.8	0.8	0.8	0.7	0.7
Y	23.0	20.7	19.5	18.8	18.6	18.0	17.9	17.6	17.4	17.3
La	60.8	47.2	40.4	36.3	35.3	31.6	30.9	29.1	28.2	27.4
Ce	108.2	85.4	74.1	67.3	65.6	59.5	58.2	55.1	53.6	52.4
Sm	28.2	19.5	15.1	12.5	11.9	9.5	9.0	7.8	7.2	6.8
Eu	7.5	5.2	4.1	3.4	3.3	2.7	2.5	2.2	2.1	2.0
Yb	5.0	3.7	3.0	2.6	2.5	2.1	2.1	1.9	1.8	1.7
Cr	150.0	103.3	80.0	66.0	62.6	50.0	47.4	41.1	38.0	35.5
Sc	55.2	39.5	31.6	26.9	25.7	21.5	20.6	18.5	17.4	16.6

$$C_{HL}=C_{HSEM}X+C_{HMEM}(1-X)$$

Equation

Solve for C_{HMEM}

$C_{HMEM}=(C_{HL}-C_{HSEM}X)/(1-X)$, $X = amount\ of\ HSEM$

Site 0212 - Timberline Lodge

Xa	0.90	0.85	0.80	0.75	0.72	0.65	0.60	0.55	0.50	0.45
SiO_2	30.9	42.8	48.9	52.2	53.9	56.2	57.5	58.5	59.3	59.9
Al_2O_3	22.8	20.7	19.6	19.1	18.8	18.4	18.1	18.0	17.8	17.7
TiO_2	2.5	1.8	1.5	1.3	1.3	1.1	1.1	1.0	1.0	0.9
FeO*	14.4	10.9	9.1	8.2	7.6	7.0	6.6	6.3	6.1	5.9
MnO	0.3	0.2	0.2	0.1	0.1	0.1	0.1	0.1	0.1	0.1
CaO	18.8	13.8	11.3	9.9	9.2	8.2	7.7	7.3	7.0	6.7
MgO	12.7	9.0	7.0	6.0	5.4	4.7	4.3	4.0	3.7	3.5
K_2O	-1.0	-0.1	0.4	0.7	0.8	1.0	1.1	1.2	1.2	1.3
Na_2O	2.0	2.8	3.3	3.5	3.6	3.8	3.9	3.9	4.0	4.0
P_2O_5	0.2	0.2	0.2	0.2	0.2	0.2	0.2	0.2	0.2	0.2
Rb	-19.5	-4.7	3.1	7.2	9.4	12.3	13.9	15.1	16.1	16.9
Sr	1135.3	915.2	800.3	739.1	706.7	663.7	640.1	621.7	607.1	595.1
Ba	170.0	246.7	286.7	308.0	319.3	334.3	342.5	348.9	354.0	358.2
Th	-3.4	-0.9	0.4	1.0	1.4	1.9	2.2	2.4	2.5	2.7
Zr	0.0	58.3	88.8	105.0	113.6	125.0	131.3	136.1	140.0	143.2
Hf	-4.3	-1.2	0.4	1.3	1.7	2.3	2.7	2.9	3.1	3.3
Nb	14.9	12.9	11.9	11.3	11.1	10.7	10.5	10.3	10.2	10.1
Ta	0.3	0.5	0.5	0.6	0.6	0.6	0.6	0.6	0.6	0.6
Y	16.3	16.2	16.2	16.1	16.1	16.1	16.1	16.1	16.1	16.1
La	15.8	17.2	17.9	18.3	18.5	18.8	19.0	19.1	19:2	19.2
Ce	16.0	24.0	28.2	30.4	31.6	33.1	34.0	34.7	35.2	35.6
Sm	18.8	13.2	10.3	8.7	7.9	6.8	6.2	5.7	5.4	5.1
Eu	4.9	3.5	2.8	2.4	2.2	1.9	1.8	1.7	1.6	1.5
Yb	4.0	3.0	2.5	2.2	2.1	1.9	1.8	1.7	1.6	1.5
Cr	140.0	96.7	74.0	62.0	55.6	47.1	42.5	38.9	36.0	33.6
Sc	52.2	37.4	29.7	25.7	23.5	20.6	19.0	17.8	16.8	16.0

$$C_{HL}=C_{HSEM}X+C_{HMEM}(1-X)$$

Equation

Solve for C_{HMEM}

$C_{HMEM}=(C_{HL}-C_{HSEM}X)/(1-X)$, $X = amount\ of\ HSEM$

Site 0213 - Cathedral Ridge

Xa	0.90	0.85	0.80	0.77	0.70	0.67	0.60	0.55	0.50	0.45
SiO_2	25.3	39.0	45.8	**48.9**	52.7	**54.0**	56.1	57.2	58.2	58.9
Al_2O_3	27.4	23.8	22.0	**21.2**	20.2	**19.9**	19.3	19.0	18.8	18.6
TiO_2	2.8	2.1	1.7	**1.6**	1.3	**1.3**	1.2	1.1	1.0	1.0
FeO*	16.7	12.5	10.4	**9.4**	8.2	**7.8**	7.2	6.8	6.5	6.3
MnO	0.3	0.2	0.2	**0.2**	0.1	**0.1**	0.1	0.1	0.1	0.1
CaO	20.6	15.1	12.3	**11.1**	9.5	**9.0**	8.1	7.7	7.3	7.0
MgO	12.6	8.9	7.0	**6.2**	5.2	**4.8**	4.3	4.0	3.7	3.5
K_2O	-2.9	-1.3	-0.5	**-0.2**	0.2	**0.4**	0.6	0.8	0.9	1.0
Na_2O	0.5	1.8	2.5	**2.8**	3.2	**3.3**	3.5	3.6	3.7	3.8
P_2O_5	0.1	0.1	0.1	**0.1**	0.1	**0.1**	0.2	0.2	0.2	0.2
Rb	-62.5	-33.3	-18.8	**-12.2**	-4.2	**-1.4**	3.1	5.6	7.5	9.1
Sr	1205.0	961.7	840.0	**785.6**	718.3	**695.5**	657.5	637.2	621.0	607.7
Ba	-768.7	-379.1	-184.4	**-97.3**	10.4	**46.9**	107.8	140.3	166.3	187.5
Th	-8.0	-4.0	-2.0	**-1.1**	0.0	**0.4**	1.0	1.3	1.6	1.8
Zr	-110.0	-15.0	32.5	**53.7**	80.0	**88.9**	103.8	111.7	118.0	123.2
Hf	-8.4	-3.9	-1.7	**-0.7**	0.5	**1.0**	1.7	2.0	2.3	2.6
Nb	-1.3	2.1	3.8	**4.6**	5.6	**5.9**	6.4	6.7	6.9	7.1
Ta	-0.4	-0.1	0.1	**0.2**	0.3	**0.4**	0.4	0.4	0.5	0.5
Y	14.7	15.1	15.3	**15.4**	15.6	**15.6**	15.7	15.7	15.7	15.8
La	-19.2	-6.2	0.4	**3.3**	6.9	**8.1**	10.2	11.3	12.2	12.9
Ce	-95.0	-50.0	-27.5	**-17.4**	-5.0	**-0.8**	6.3	10.0	13.0	15.5
Sm	19.0	13.3	10.5	**9.2**	7.7	**7.1**	6.2	5.8	5.4	5.1
Eu	5.1	3.6	2.9	**2.6**	2.2	**2.0**	1.8	1.7	1.6	1.5
Yb	4.5	3.3	2.8	**2.5**	2.2	**2.1**	1.9	1.8	1.7	1.6
Cr	140.0	96.7	75.0	**65.3**	53.3	**49.3**	42.5	38.9	36.0	33.6
Sc	54.5	39.0	31.3	**27.8**	23.5	**22.1**	19.6	18.3	17.3	16.5

APPENDIX F

MAGMA MIXING:

LINEAR CORRELATION PLOTS

Hwy 26

Mt Hood Meadows

Laurence Lake

Compass Creek

Timberline Lodge

Cathedral Ridge

◆ L-R, incl, host, HSEM
■ HMEM-B
▲ HMEM-BA

Mt Hood Meadows

Compass Creek

Cathedral Ridge

Hwy 26

Laurence Lake

Timberline Lodge

♦ L-R, incl, host, HSEM
■ HMEM-B
▲ HMEM-BA

Each panel plots Na2O (wt %) on the vertical axis (scale 2.00 to 7.00) against SiO2 (wt %) on the horizontal axis (scale 48 to 68). The six panels are labeled: Hwy 26, Mt Hood Meadows, Laurence Lake, Compass Creek, Timberline Lodge, and Cathedral Ridge. Legend: ◆ L-R, incl. host, HSEM; ▣ HMEM-B; ▲ HMEM-BA.

157

161

Mt Hood Meadows
Compass Creek
Cathedral Ridge
Hwy 26
Laurence Lake
Timberline Lodge

L.-R. incl, host, HSEM
HMEM-B
HMEM-BA

Hwy 26

Mt Hood Meadows

Laurence Lake

Compass Creek

Timberline Lodge

Cathedral Ridge

169

170